Design and Application of a Novel Driver Condition Monitoring Device - Smart Wheel

Hongjie Leng

A Thesis

in

The Department

of

Electrical and Computer Engineering

Present in Partial Fulfillment of the Requirements
for the Degree of Master of Applied Science(Electrical and Computer Engineering) at
Concordia University
Montreal, Quebec, Canada

December 2005

Your file Votre référence
ISBN: 0-494-14268-5
Our file Notre référence
ISBN: 0-494-14268-5

ABSTRACT

Design and application of a novel driver condition monitoring device - smart wheel

Hongjie Leng

People never stop pursuing safer and more comfortable driving. An important approach to that goal includes acquiring information about the driver's condition. The vehicle can then respond. However, most previous technologies are not suitable for a driver to use during daily driving. The present research investigates the technologies and sensors that can be utilized to assess a driver's condition, and then employs a polyvinylidene fluoride (PVDF) film sensor, a semiconductor temperature sensor and a piezo-resistive sensor to develop a smart wheel. The smart wheel can conveniently and reliably measure the driver's pulse wave, breathing wave, skin temperature and gripping force and does not influence the driver's normal behavior and condition. The driver's condition can be evaluated by using the output of the smart wheel. To verify the wheel's design and how effective it is at measuring the driver's pulse rate, the experimentation behind the present research paper involved thirty subjects to perform 120 experiments under four factorial combinations of gripping force and vibration. The result indicates that the smart wheel has good performance. The gripping force is the main factor that influences its accuracy. In addition, by utilizing the smart wheel and a virtual reality system, the present research investigates the relationship between the variance of a driver's pulse rate and different driving scenarios. Ten subjects were invited to perform 30 experiments based on a single line, a double line and a sinusoidal line. The results indicate that a more complicated scenario induces a larger standard deviation in the driver's pulse rate.

ACKNOWLEDGEMENTS

I wish to express my sincere thanks to my supervisor, Dr. Yingzi Lin. She has provided selfless and patient help to this research. Her profound knowledge, scientific spirit and keen discernment are strongly impressed on my memory.

I highly appreciate all friends and graduate students who have contributed to the research and experiments. Their kind support encourages me to face and overcome the challenges in the research.

I also like to thank the excellent faculty of Concordia University where I have enjoyed a memorable and fruitful time.

I finally wish to express my heartfelt thanks to my family, the origin of my happiness and power.

TABLE OF CONTENTS

LIST OF FIGURES

LIST OF TABLES

Chapter 1 Introduction

1.1 Driver's condition monitoring

The driver's condition plays an important role in a driving system. According to the report "Traffic Collision Statistics (British Columbia 2003)", 49,777 traffic collisions were reported in British Columbia in 2003. It is mentioned that 30,692 people were injured and 443 people were killed. In 2003, 19,875 reported casualty collisions involved 32,515 contributing factors. Among the contributing factors, 83.6% involved human action or condition, 14.8% belonged to environmental conditions, and 1.6% belonged to vehicle condition [Insurance Corporation of British Columbia, 2005]. If a driver's condition can be detected on line, then human-oriented subsystems can be developed to effectively prevent these collisions from taking place. For example, if it is detected that a driver's heart problem has abruptly taken place, the automatic driving system can be activated accordingly, and an emergency alarm can be send out. If a driver's body temperature is high, the air temperature in an inner vehicle can be lowered by using air conditioning. If it is detected that a driver is nervous, the volume of the audio system can be automatically decreased. These human-oriented subsystems can make driving safer, more comfortable and convenient. Such subsystems can help drivers control their emotions.

Hence, monitoring the driver's conditions in the driver-vehicle-environment system can substantially contribute to safer and more comfortable driving. However, the main

difficulty is how to develop a reliable and convenient system to ascertain a driver's conditions during driving.

1.2 Basic concepts concerning on a driver's physiology and psychology

A driver's condition consists of two aspects: physiology and psychology. The physiological condition refers to the state of the body or of the bodily functions such as fatigue. When a driver is healthy, his physiological condition depends on his physical workload (***The use of the masculine includes the feminine in this thesis***).The psychological condition refers to the mental or emotional state of the driver, such as his being sleepy, tense, or aggressive. When a driver is in a normal condition, his psychological condition is mainly influenced by his mental workload (MWL). The related terms and definitions are explained as follows.

- Mental workload (MWL) can be simply defined as the cost of a given task for the driver [Averty *et al.*, 2002]. It depends on the limited capacity of cognitive resources and the sequential processing of information [Lin, 2003]. Overload happens when information processing capacities make an excessive demand on the driver's perceptual and cognitive resources such as visual and auditory perception, memory and attention [Averty *et al.*, 2002, Noel *et al.*, 2005].
- The physiological parameter is the index reflecting the function or state of a living organism.
- The electrocardiogram (ECG or EKG) is the waveform representing the heart's bioelectric potential. It can be plotted by using an electrocardiography, which can

measure the electrical impulses moving through the heart muscle while the heart contracts and relaxes.

- The electroencephalogram (EEG) records the bioelectric potentials produced by the neuronal activity of the brain. It can be obtained by using electroencephalography.
- The electromyogram (EMG) is produced by the bioelectric potentials associated with muscle activity. It can be ascertained by using electromyography.
- Galvanic skin response (GSR) refers to a change in the ability of human skin to conduct electricity. It refers to moment-to-moment changes in perspiration and the related activities of the autonomic nervous system. It can be measured by attaching electrodes to human skin.
- The heart rate is the number of heart beats per time unit, usually per minute.
- The heart rate variability (HRV) is the variation of beat-to-beat intervals. This phenomenon occurs because the heart rate fluctuates over time. It is modified by thermoregulation, changes in the blood pressure system, and respiration [Hampson *et al.*, 2005].
- The respiration frequency is the number of times that a human breathes in and out per time unit, usually measured as one minute.

1.2 Literature review

1.2.1 Driver condition monitoring

How can one access a driver's condition? The methods of evaluating human's physiological condition or psychological condition have often been investigated. A human's physiological condition is evaluated by using physiological parameters.

Likewise, a human's psychological condition can also be inferred from physiological signals. Greater accuracy in the evaluation of the results requires more physiological parameters [Cacioppo et al., 1990, Picard, 1997]. This statement is supported by many research studies, some of which are described as follows.

The ECG is influenced by the driver's physiological condition and psychological condition. It is important for monitoring the condition of high-risk cardiac/respiratory patients [Anliker *et al.*, 2004]. In addition, it can indicate the changes in the driver's status. It can also be used to predict the degree of driving impairment [Brookhuis and De Waard, 1993]. When the driver is fatigued, the ECG is an effective indicator because it can be used as a physiological index of the workload especially during driving [Lal *et al.*, 2001]. Thus, the ECG is important in evaluating the driver's condition. However, measuring driver's ECG influences his normal action because it requires attaching some electrodes to the body skin.

The EEG can reflect the activities of the human brain, which processes the received information and responds. The EEG can provide psychophysiological information about the driver's emotional reaction [Kim *et al.*, 2000]. When a driver frequently changes the speed of his vehicle, his slow EEG activity is significantly higher than the ECG activity while remaining at a constant speed [Tejero and Choliz, 2002]. The real-time analysis of the delta (0–4 Hz), theta (4–8 Hz), alpha (8–13 Hz), and beta (13–20 Hz) of a driver's EEG can be achieved by using a discrete Fourier transform (FFT). The result can be utilized to evaluate the driver's condition such as alertness, transition to fatigue,

transitional–posttransitional, and posttransitional phases [Lal, *et al.*, 2003]. For example, if a driver has higher arousal levels, his electroencephalogram has lower spectral activity in the theta (4-7.75 Hz), alpha (8-11.75 Hz) and fast theta-slow alpha (6-9.75 Hz) frequency bands [Macchi *et al.*, 2002]. Thus, the EEG can provide information evaluating the driver's psychological condition. However, measuring the EEG requires attaching some electrodes to the head skin, thereby increasing a lack of comfort.

The EMG measures the activity of the muscles of certain parts of the human body. It is suitable for assessing the stress level of humans [Picard *et al.*, 1997]. Katsis *et al.* [2004] have compared several metrics of surface electromyograms (EMG), such as the mean frequency (MNF), the median frequency (MDF), and the signal RMS amplitude, all of which are employed to evaluate a driver's muscular fatigue during actual driving. Their experiments show that MDF and MNF decrease 9.5%-18.9% and 11.3%-18.4%, respectively, from their initial values. RMS increases 25.1%-47.7% from its initial value. These metrics are reliable fatigue indicators. Thus, the EMG can be utilized to evaluate the level of stress and fatigue. However, it is difficult to measure the driver's EMG during daily driving because it requires inserting electrodes into muscle or attaching them to the skin.

The measurement that we call 'facial expression' consists of the relative positions of the facial components, the eye movement, the eye blink, the mouth movement, etc. It can be analyzed by using image processing technologies. The analytic result has been employed to evaluate a driver's psychological condition [Eriksson and Papanikolopoulos, 2002], to

monitor the fatigue and distraction of a human being [Moreno *et al.*, 2003, Brandt *et al.*, 2004, Horng *et al.*, 2004, Ji *et al.*, 2004], to assess a driver's level of vigilance [Dikkers *et al.*, 2004]. Thus, analyzing facial expressions is an important method of evaluating a driver's psychological condition.

The galvanic skin response (GSR) and the skin conductivity are modified because of the activity of the human autonomic system and the psychological condition. For example, GSR values increase under frustration and anger [Nasoz *et al.*, 2002]. Skin conductivity has a close relationship with a driver's stress level and is useful in evaluating his stress level [Healey *et al.*, 2005]. However, the measurement requires attaching electrodes to the skin. It then may influence the measured subject's behavior.

The gripping force is the force the driver applies to the steering wheel. It has been utilized to evaluate real-time driver hypo-vigilance during driving [Polychronopoulos *et al.*, 2004]. In addition, it changes if driver's physiological condition is not normal. Thus, it is a useful parameter reflecting a driver's condition.

Heart rate (HR) and heart rate variability (HRV) are widespread parameters used in assessing a driver's condition. The autonomic nervous system, which consists of sympathetic and parasympathetic nervous systems, controls the cardiovascular system [Liu *et al.*, 2004]. A driver's heart rate and capillary pulse change under conditions and can help estimate the driver's internal state [Katayama and Sakai, 1994]. Some research has utilized the heart rate to monitor the driver's level of vigilance and stress [Rothkrantz

et al., 2004, Healey *et al.*, 2005]. Other research has found that the rate of the heart beat increases under anger and fear and decreases under sadness [Nasoz *et al.*, 2002]. Thus, the heart rate has a close relationship with the psychological condition and is one of the important parameters used in evaluating a driver's workload [Tanaka *et al.*, 2000, Backs *et al.*, 2003]. However, it is argued that the heart-beat rate changes with the mental workload, emotional strain, physical activity, and respiration. It is difficult to identify what it is that induces this change in the heart rate. Thus, heart rate variability (HRV) is recommended as a measure of mental effort [Jahn *et al.*, 2005]. The HRV should be employed to evaluate the mental workload (MWL) or to estimate the driver's mental stress [Kuriyagawa *et al.*, 2002, Liu *et al.*, 2004]. Jiao *et al.* [2005] have presented a method of evaluating driving fatigue by using the frequency domain indices of HRV heart rate variability (HRV). These researchers analyzed a subject's low frequency (0.04-0.15 Hz, LF), high frequency (0.15-0.4 Hz, HF), and LF/HF of HRV. Based on their experimental results, autonomic function indictors of HRV reflect the fatigue level and can be utilized to evaluate a driver's mental fatigue quantitatively. Hence, HR and HRV are both important in evaluating a driver's condition.

Respiration is influenced by a driver's physical and mental workloads. As the physical workload increases, more metabolic energy and oxygen are required and induce stronger respiration [Kroemer, 2001,]. In addition, respiration can indicate the activity of the autonomic nervous system in the condition of vigilance, emotional response and mental workload [Rada *et al.*, 1995]. It is also useful in studying a driver's reactions in a real

environment [Axisa *et al.*, 2003], and in recognizing a subject's underlying affective state [Picard *et al.*, 1997]. Thus, respiration is an important indicator of a driver's condition.

Temperature is an important physiological parameter of a human's condition. It is a critical indicator of health and disease. Measuring body temperature is a well-known diagnostic method in daily life and in medical care. A higher body temperature implies an infectious disease and fever, and it induces the accompanying feelings of illness [Levander, 2004]. While driving, it can reflect the autonomic responses and the activity of a human's autonomic nervous system [Rada *et al.*, 1995, Mina *et al.*, 2002, Axisa *et al.*, 2003]. However, it is argued that temperature does not show remarkable differences among certain emotions [Nasoz *et al.*, 2002]. Thus, temperature is important while evaluating driver's condition.

According to the review above, it is possible to evaluate a driver's condition by using the physiological information and the facial expression. Monitoring facial expression is suitable for evaluating a driver's psychological condition. On the other hand, it provides little information about the physiological condition. The present research is focused on utilizing physiological information to monitor driver's condition. The usual physiological parameters consists of ECG, EEG, EMG, GSR, heart rate (HR), heart rate variability (HRV), respiration, and body temperature. However, EEG, EMG, and GSR mainly reflect a driver's stress level or mental effort. Useful information can also be induced from the HR, HRV, respiration and body temperature. The ECG reflects the condition of the driver's heart and provides information about the HR and HRV. Thus, substantively,

the useful parameters are the heart rate (HR), heart rate variability (HRV), respiration, and body temperature. In addition, gripping force constitutes a useful referring parameter in evaluating a driver's condition. Hence, the present research pays more attention to the heart rate (HR), heart rate variability (HRV), respiration, body temperature and gripping force to establish a model to evaluate a driver's condition.

1.2.2 Current measuring technologies

Although a few people have studied the instrument or device that can be utilized to monitor a driver's condition during daily driving, there are some people who have studied other systems that can conveniently measure a human's physiological parameters. These methods and technologies are helpful to the field of monitoring a driver's condition.

(1) Technologies for measuring heart rate and heart rate variability

Zuckerwar *et al.* [1993] have developed a portable piezo-polymer pressure sensor to monitor fetal heart rate. They mounted several sensors in an array on a belt. When a mother wears it, the sensor can measure the features of the fetal heart tone such as the acoustic signature and the frequency spectrum. The system is portable and has good performance while measuring fetal tone. However, its performance in measuring adult heart rate has not been verified. Any other strong acoustic signal may add noise to its output. In addition, the driver has to wear it around the chest while the system is operating.

Fernando *et al.* [2003] have presented a new method for measuring heart rate variability (HRV) by using Doppler ultrasound techniques. The method utilizes the multiple signal characterization (MUSIC) algorithm to estimate the frequencies of sinusoidal signals involved in white noise. It has good performance under a variable angle of incidence of the ultrasound beam and the measurement noise and then permits a driver's natural activity. However, more research is required to verify the safety of the system if a driver uses it every day.

Hlimonenko *et al.* [2003] have analyzed the waveform of peripheral pulse waves detected in the fingertip with a photoplethysmographic sensor. The measurement system consists of a finger clip sensor, an amplifier, a data acquisition board and a computer. The system can reliably measure the pulse wave in a human finger, is portable, and is convenient to use. However, the finger clip sensor has to clip and fix on a driver's finger. It may influence a driver's normal behavior. In addition, the heat produced by the finger clip sensor may modify the condition of the measured tissue.

Konberg *et al.* [2003] have reported developing a system of monitoring the breathing and the heart rate of hockey players. The system utilizes a fiber-optic sensor to measure the respiratory rate and employs a sensing belt worn around the chest to measure the heart rate. Then, the data is transmitted by wireless module. The system does not influence the hockey player's behavior significantly. However, for the driver, wearing it is bothersome.

Korpasa *et al.* [2003] have developed a non-invasive, easy and mobile device for measuring and analyzing the pulse wave. The device includes a probe with a scanning membrane, a liquid and air component for transmitting pressure, a differential pressure sensor, a data acquisition card and a computer. The membrane of the probe must closely and in a stable manner contact the skin covering the artery. It is suitable for static measurement. However, a driver frequently moves while driving. Thus, it is difficult to utilize the device to monitor a driver's pulse wave.

Mack *et al.* [2003] have utilized a sensitive vibration sensor attached to an air-filled bladder to measure the pulsing generated through the blood vessels and the body movement related to respiration. The method provides an unconstrained method of measuring a driver's heart rate and respiratory frequency. However, the air-filled bladder induces an unstable feeling while a driver sits on it or leans against it. In addition, the vibration of vehicle may influence its accuracy. The same questions exist in the system presented by Ishikawa *et al.* [2004] and in the system developed by Jacobs *et al.* [2004] both of which monitor heart beat and respiration by measuring the pressure.

Takanobu *et al.* [2004] have employed strain gauges attached to a two-layer wrist band to count the heart beats. The device can measure the heart rate while the wearer is walking at 1.0-2.0m/s. It is portable and has little influence on the driver. However, more research is required to verify its performance under the strong vibrations that are common during driving.

Knoght *et al.* [2005] have designed a wearable system that utilizes a microphone and a pressure bulb strapped around the wrist to measure the pressure of the radial artery and then measures the heart rate. The system is easy to use and is portable. However, wearing the pressure bulb is uncomfortable. The strong external sound may influence the output of the system and decrease the accuracy.

(2) Technologies for measuring respiration

Putten *et al.* [1997] have developed an integrated silicon sensor with bi-directional flow for measuring respiratory flow. It is useful in the evaluation of the respiratory system. The sensor has wide input range and a quick response. However, the sensor has a nonlinear output and requires a fixed position relative to the driver's exhaling airflow.

Harada *et al.* [2000] have presented a sensor pillow system to monitor human respiration without restraint to humans. The system utilizes an array of pressure sensors under the pillow to measure the head pressure distribution from which the respiratory frequency can be calculated. However, it is not suitable for monitoring the driver during driving because the posture is different.

Jovanov *et al.* [2001] have designed a differential thermistor-based breathing sensor to measure the breathing amplitude, the breathing interval, and the breathing frequency. It does not influence the normal behavior of the people measured. However, the sensor is fixed on the bridge of the nose. It is not acceptable during daily driving.

Ong *et al.* [2002] have proposed a technique to monitor the human respiration rate. It emits a square-wave modulated electromagnetic impulse to the human body and then analyzes the time-amplitude spectrum of the reflected electromagnetic impulse. It is an un-invasive and unconstrained method. However, more research is required to verify the safety of continuously using the technique because it uses a microwave frequency pulse. The same question exists in the method presented by Ossberger et al. [2004]. It uses ultra wide-band (UWB) pulse radar to measure the thoracic displacement due to the respiratory movement.

Sato and Nakajima [2004] have developed a non-contact respiratory monitoring system that utilizes two charge-coupled devices (CCD) to monitor the movements of the infrared bright spots projected on the bodies of the people who are measured. The system is portable and non-constraining. However, while driving, the ambient light environment changes continuously. The vibration of the vehicle influences the movement of the infrared spots. Both factors may increase the measuring error. More research is required to verify its performance while monitoring a driver's respiration.

(3) Technologies for measuring body temperature

Betta *et al.* [1997] have investigated and compared three kinds of commercially available clinical thermometers that employ different thermal infrared sensors to obtain the human body temperature by measuring infrared radiation from the tympanic membrane. Their advantages consist of simplicity of use, rapid response and minimal distress to measured people. However, the probe of the sensor is inserted into the external auditory canal while

measuring the temperature. It is suitable for quick measurement, not for long-term monitoring. The same question exists in the method presented by Stec *et al.* [2004]. This method utilizes a multi-frequency microwave thermograph to measure temperature.

Vanoverschelde *et al.* [2001] have designed a temperature sensor that can measure spontaneous electromagnetic radiation from a human body. The sensor has a small size and little weight and provides a non-constrained method for measuring a driver's body temperature. However, the research only verified its performance while measuring the temperature of premature neonates. More research is required to test its performance while monitoring a driver because there are many sources of electromagnetic radiation in a vehicle.

Ballandras *et al.* [2002] have developed a wireless temperature sensor based on passive surface acoustic wave (SAW) resonators. It utilizes the large linear thermal dependence of the SAW frequency to measure the temperature. It is immersed in the measured tissue and transmits the data by wireless subsystem. However, it is an invasive method and is not suitable for monitoring a driver's condition. The same question arises in the case of the temperature sensor presented by Escudero *et al.* [2003], and in the case of the method developed by Liu and Bao [2003].

Jedrzejewska-Szczerska and Hypszer [2004] have designed a mono-mode and multimode fiber white-light interferometric temperature sensor based on a low-finesse Fabry-Perot interferometer that works in reflective mode. The sensor is compact and portable and has

good performance. However, it operates with light that shines on and reflects from the surface of the measured object or tissue. It is not suitable for measuring a driver's temperature.

Liess [2004] has developed an automatic climate-control system based on thermopile sensors that can measure the IR radiation of the measured objects or persons. The sensor is small, inexpensive, calibrated, and ambient temperature compensated. However, its accuracy is limited, and it requires a long response time.

(4) Technologies for measuring gripping force

Ding *et al.* [2000] have developed a type of tactile sensor based on a micro electromagnetic coil. The sensor has high reliability, compact sizes, high sensitivity and a wide frequency response. However, while measuring the gripping force, some improvement is required because the sensor is designed for fixing on the fingers of robots and measuring the contact force.

Mascaro and Asada [2001] have designed a touch sensor to measure the color change of human fingernails while the finger force changes. It then measures the contact pressures. The sensor is fixed on the fingernail rather than on the finger tip and does not impede the direct contact between the finger and the ambient environment. It is small and portable. However, it is not comfortable if a driver wears it during daily driving.

De silva *et al.* [2002] have presented a metallic strain gauge-based sensor for measuring finger force. It is suitable for attaching to the thumb and measuring thumb force and has a linear response, good repeatability and high sensitivity. However, the sensor prevents the direct contact between the driver's finger and the steering wheel and is not suitable for monitoring a driver's gripping force.

Chi and Shida [2003] have investigated a force sensor that has two coils, two media, and a multifunctional cylindrical tactile sensor structure. The sensor can measure the magnitude and direction of the force applied one by one. However, it induces a complicated structure and a high cost while the method is utilized to measure a driver's gripping force.

Shikida *et al.* [2003] have developed a force sensor that has a diaphragm over a mesa structure, a piezo-resistive displacement sensor on the diaphragm, and a chamber for pneumatic actuation. By using an array of these force sensors, the two-dimensional contribution of the contact force can be measured. The sensor has good performance. However, its structure is complex. In addition, its resolution and input range should be modified while measuring a driver's gripping force.

Cotton *et al.* [2004] have utilized a screen-printed piezo-resistive resistor and a piezoelectric dynamic transducer to design an integrated thick-film sensor for measuring the gripping force. The sensor has a low cost and compact sizes and achieves good

performance. However, its stability and performance in a vehicle has not been verified. The same question arises in the system proposed by Nikonovas *et al.* [2004].

Takao *et al.* [2004] have developed a silicon tactile image sensor that places a two-dimensional piezo-resistor array on its single silicon diaphragm and integrates the signal processing circuit. The sensor can measure the stress distribution of the deformed diaphragm while a force is applied to it. It has good performance, small sizes and an adjustable input range and a dynamic range. However, its structure and specifications require modification while utilizing it to measure a driver's gripping force.

All of these studies mentioned above present many types of technology for measuring physiological parameters and suggest that instruments for monitoring a driver's condition are technically feasible. However, most previous technologies or methods are not suitable for monitoring a driver's condition during daily driving. The ideal instrument would be a special application with particular requirements. It is necessary to develop new device or technologies to satisfy such an application.

1.2.3 Requirements for measuring the driver's condition

Up to the present day, medical instruments have usually been used to measure a driver's physiological parameters and then to evaluate his condition. However, few medical instruments are suitable for monitoring a driver's physiological condition during daily driving because of the special requirements in the application.

The first requirement is that the measurement should be non-invasive. Invasive technologies are not suitable for monitoring a driver's condition during driving. The second requirement is that the instrument should work well with the electrical power from a vehicle. Commonly, the engine of a vehicle can produce limited electrical power by using a generator. The power is direct-current electricity of 12volt or 24volt. However, some medical instruments, such as the electrocardiograph, are not suitable for use in a vehicle because they require strong and alternate-current power. Thus, it is necessary for instruments to be suitable for the vehicle supply power. The third requirement is that the instrument should allow real-time detection, which is necessary if the automatic subsystems of a vehicle are to respond quickly. Some instruments have a long response time lag before the final output is achieved. For example, the mercury sphygmomanometer requires almost 5 minutes until the final blood pressure is indicated. Hence, the instruments that can not produce real-time output can not be employed in monitoring a driver's condition. The fourth requirement is the digital output. However, some instruments can not satisfy this requirement. For example, a liquid-in-glass thermometer uses the height of liquid to indicate the measured temperature. This kind of signal can not be directly processed by a computer system. Thus, the instruments with non-digital output are not suitable for monitoring a driver's condition. The fifth requirement is the moderate accuracy. As the measurement during driving is used to evaluate the driver's condition and performance, it does not require the high accuracy that is necessary for a medical examination. Hence, an instrument used in a vehicle requires lower accuracy than that of medical instruments. The sixth requirement is the compact size and the light weight. HONDA Company suggests that Mini-machine-Max-space

(MM principle) is important for modern vehicles. In addition, a light instrument can decrease the load of a vehicle and increase the fuel efficiency. Hence, a smaller and lighter instrument would be much more popular. The seventh requirement is the operation convenience. Also it should not disturb the driver's daily work. Some medical instruments (e.g. ECG) require attaching many electrodes to a human's skin by using special glue. It is very uncomfortable for a driver to wear such electrodes during driving. The wire connecting to the electrodes would severely interrupt the driver's operation. Hence, few drivers would accept such kinds of instruments. The final requirement is the safety. Long-term safety would be a critical characteristic of any instrument used to monitor a driver's condition

Hence, an instrument utilized to monitor a driver's condition should (1) be non-invasive, (2) consume little direct-current electricity with 12volt or 24volt, (3) have a short response time lag, (4) produce digital outputs with moderate accuracy, (5) come in a small size, be light weight and have a low cost and (6) be safe, easy and convenient to use every day.

1.4 Research objectives and issues

A driver is a complicated biological system many details of which are still unknown. Moreover, differences between people are remarkable for all kinds of reasons: race, district, background, habit, etc. Thus, evaluating a driver's condition is a great challenge. Generally, a human body has three major systems: a cardiovascular system or circulatory system, a respiratory system and a metabolic system. The pulse wave, breathing wave,

and skin temperature are important indicators of the cardiovascular, respiratory, and metabolic systems, respectively. Thus, these parameters can be utilized to evaluate a driver's condition. In addition, the gripping force applied to the steering wheel is another useful parameter reflecting a driver's attention. All these important parameters are possibly measured by non-invasive technologies such as ECG, EEG. However, it is highly difficult for a driver to utilize these measuring technologies since they require that wired electrodes be attached to the driver's skin, thereby interrupting a driver's normal behavior. Such methods can not be employed to monitor a driver's condition during daily driving.

Usually during driving, a driver's hands are in direct contact with the steering wheel. If an innovative steering wheel, besides possessing its original functions, is capable of measuring a driver's physiological condition when a driver grips it, then it could be used to monitor a driver's condition. The present research focuses on developing such a kind of special steering wheel (named "smart wheel") that can be used to measure a driver's pulse wave, breathing wave, skin temperature and gripping force.

In addition, driving scenarios have a heavy influence on a driver's conditions. To describe such an influence in quantitative analysis, the key step is to measure the changes in the driver's conditions. Although measuring these changes during driving is a great challenge, the present research attempts to investigate the relationship between the variation of a driver's pulse rate and typical driving scenarios by using the smart wheel.

1.5 Organization of the thesis

After the introduction in Chapter 1, Chapter 2 describes the theoretical model of the smart wheel and the method of evaluating a driver's condition and provides overall knowledge about the smart wheel. Then, Chapter 3 presents the design of the electronic system of a smart wheel. Chapter 4 presents the mechanical design of the smart wheel. After presenting the design of the smart wheel, Chapter 5 proposes an application of the smart wheel to the monitoring of the driver's condition. The smart wheel is designed to monitor and compare changes in the driver's pulse rate in different driving scenarios. Chapter 6 presents the designs and the results of two groups of experiments to verify the performance of the smart wheel. Chapter 7 concludes the present research and suggests future work.

Chapter 2 Conceptual design of the smart wheel

2.1 Introduction

A smart wheel measures a driver's pulse wave, breathing wave, skin temperature, and gripping force. It also functions as a common steering wheel by controlling the moving direction of a vehicle. Based on the output of the smart wheel, the driver's condition can be evaluated. Before considering the detailed design, it is important to establish the theoretical approach of the smart wheel.

This chapter firstly introduces the methods of measuring a driver's pulse wave and breathing wave. Next, it explains how to measure a driver's skin temperature. Then, it describes the method of measuring a driver's gripping force. Finally, an overall model of evaluating a driver's condition is given.

2.2 A driver's pulse and respiration model

Heart rate (HR) and heart rate variability (HRV) are usually used to evaluate a driver's condition because his heart rate and heart rate variability are closely and significantly related to his physiological and psychological condition. The pulse wave, which is produced by the driver's heart, has a close relationship with his cardiovascular system. The pulse beat of course follows the heart beat. Thus, a driver's heart beat and heart beat variability can be accessed by using his pulse beat. In addition, the relationship of driving behavior to the cardiovascular system is remarkable. A complicated driving scenario can produce a change in the physiological parameters of a driver's cardiovascular system.

The change may induce some unexpected event such as the outbreak of a heart attack. Hence, the pulse wave is important in evaluating a driver's condition.

A driver's respiratory system, mainly reflecting respiratory frequency, respiratory volume, etc., provides oxygen for metabolism and dissipates metabolic products. The parameters always vary with the change of a driver's condition. For example, when the heart muscle does not obtain an adequate supply of blood, a shortness of breath will take place. This will signal the driver's poor condition. In addition, a driver commonly alters his normal respiratory rhythm while he is sick or sleepy. The same phenomenon may occur to a driver if he undergoes certain emotions such as excitement, nervousness, strain, etc. Hence, respiration is highly useful in evaluating a driver's condition. The breathing wave produced by the respiratory system is a good indicator of a driver's respiration. It can provide information about the rhythm of the respiration system. The information is useful in the evaluation of a driver's condition.

In the present research, the pulse wave and respiration wave are simultaneously measured by using sensors on the smart wheel (Figure 2.1). When a drive's palms contact the sensors, the sensors produce an output reflecting the pulse wave and the respiration wave. The output requires amplifying because it is weak. After that, compensation and filtering are performed to eliminate the influence of any disturbance and noise. Then, by using another filter, the processed signal will be separated into a pulse wave and a breathing wave by using the fact that a pulse wave and a breathing wave have different frequencies.

Finally, the pulse wave is used to calculate the heart rate, while the breathing wave is used to calculate the breathing frequency. The whole process is shown in Figure 2.1.

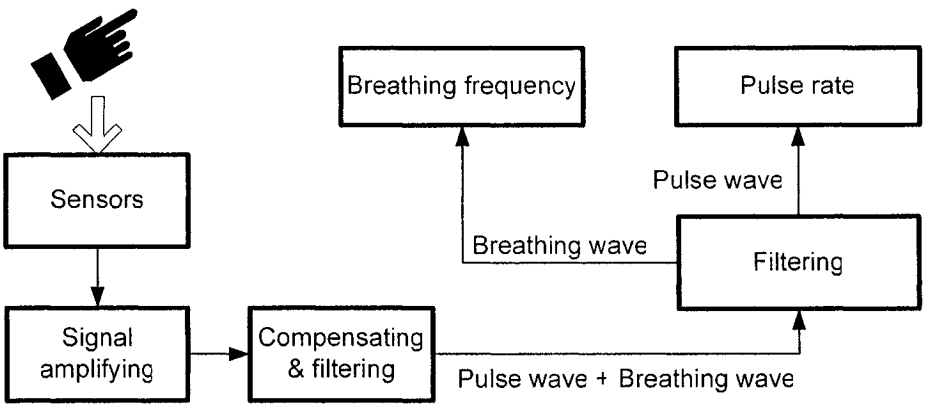

Figure 2.1 A driver's pulse and respiration model

2.3 A driver's skin temperature model

Generally, a driver's skin temperature changes due to the ambient temperature. When the ambient temperature increases, the driver's skin temperature increases, and vice versa. Next, the skin temperature is also influenced by driving behavior and by driving scenarios. A driver's skin temperature decreases as the speed of a vehicle increases both during the day and at night. In addition, a driver's skin temperature has a certain relation with his conditions. Thus, skin temperature is a required component in the model used to evaluate a driver's condition.

In the present research, while a driver's palms contact the sensors of the smart wheel, temperature sensors produce signals reflecting his skin temperature (Figure 2.2). The signal is firstly amplified and then sent to the circuit to compensate for the temperature

drift. After that, a linearization circuit depending on the type of sensors is selected to linearize the relation between the input and the output. At last, a digital signal for the skin temperature is obtained by using an analog/digital (A/D) converter.

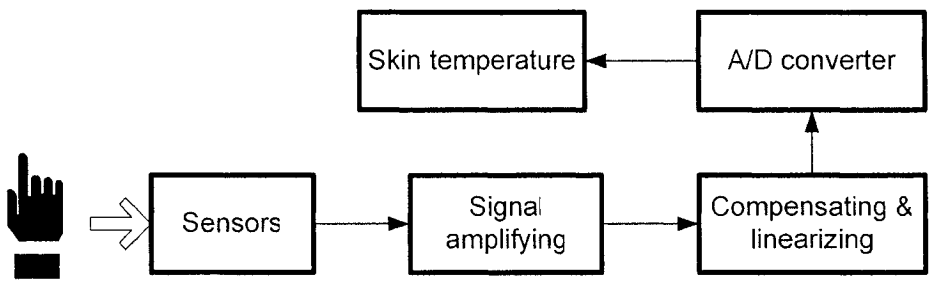

Figure 2.2 A driver's skin temperature model

2.4 A driver's gripping force model

A driver grips and rotates the steering wheel to control the direction of the motion of a vehicle. Commonly, a driver applies a moderate gripping force to the steering wheel. However, the driver may increase the gripping force when he is nervous or tense; while he may decrease the gripping force when his attention is distracted from driving. A driver's gripping force can also be used to determine whether the driver is drowsy. Hence, the gripping force is one of the main parameters used to evaluate a driver's condition. In the present research, a driver's gripping force can be measured by employing some force sensors on a smart wheel. The measuring model is shown in Figure 2.3.

2.5 The overall model of the smart wheel

According to the discussion above, an overall model of a smart wheel can be created as shown in Figure 2.4. The model consists of three components: the skin temperature sub-model, the gripping force sub-model, and the pulse and respiration sub-model, as shown in Figure 2.4. Finally, a driver's condition will be evaluated using this model.

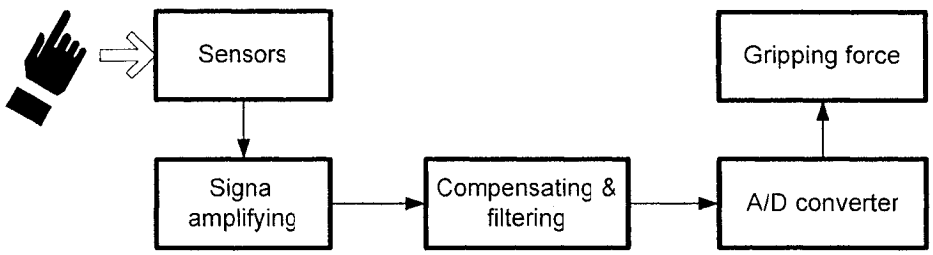

Figure 2.3 A driver's gripping force model

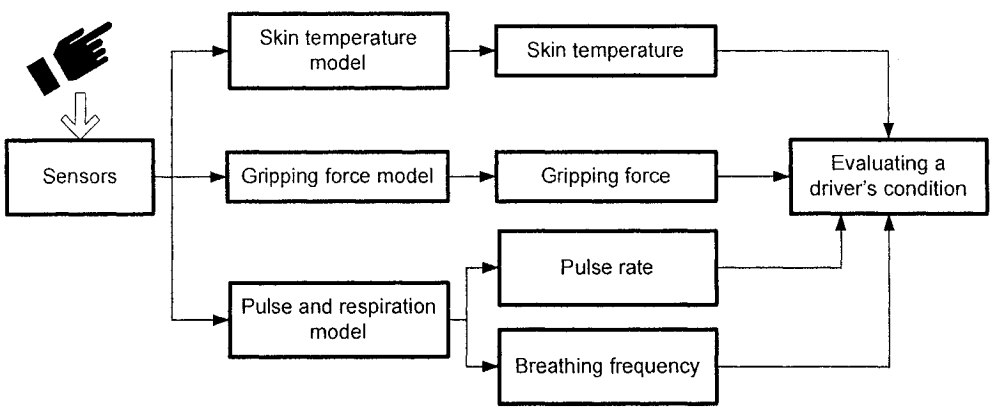

Figure 2.4 The overall model of the smart wheel

2.6 Summary

This chapter explains the proposed model to be used to evaluate a driver's condition. It employs the pulse wave, breathing wave, skin temperature, and gripping force, all three

of which can be measured by using the smart wheel. Thanks to the model, a driver's driving ability can be qualitatively analyzed and determined. The detailed design and analysis of a smart wheel will be presented in Chapter 3 (electronic subsystem), Chapter 4 (mechanical sub-system), and Chapter 5 (system integration and application).

Chapter 3 Electronic design of the smart wheel

3.1 Introduction

To measure a driver's pulse wave, breathing wave, skin temperature and gripping force, the smart wheel requires appropriate sensing methods and a special sensor structure. Moreover, collecting, conditioning and processing the output from the sensors require a professional data acquisition system. In the design of the hardware, great attention should be paid to the systemic speed because the system consists of many sensors and requires a high sampling frequency. In the design of the software, the challenges arise in the processing of the data and the implementing of the proposed model of smart wheel.

In this chapter the design of appropriate sensors is shown. They measure a driver's physiological parameters. Next, the functions of the data acquisition (DAQ) system of a smart wheel are analyzed. Then, after determining the main technological parameters of the DAQ system, its hardware and software is designed. Finally, this chapter verifies the power consumption of the electronic system of a smart wheel and then analyzes its cost.

3.2 Sensor selection

3.2.1 Basic requirements of the sensors

A smart wheel is installed in the same position as the common steering wheel of a vehicle. Its sensors operate in the inner space of a vehicle in which there is little dust, no corrosive gas, no radiation, and no strong light. There is a slight range of temperature (the typical range is 0°C~+60°C) which undergoes slow changes throughout the duration of

the driving. Thus, the work environment of the sensors of a smart wheel is good. However, the sensors themselves will come into close contact with the driver's palms, which are possibly bearing sweat, machine oil, soy sauce, coffee, etc. Thus, the sensors require good stability against chemical attack. In addition, a driver frequently grips the smart wheel during driving. The gripping force possibly changes in a range of 0N~390N [Edgren, 2004]. Thus, the sensors require the ability to withstand strong mechanical stress. These characteristics are important in designing and selecting the appropriate sensors for a smart wheel.

3.2.2 Measurement of the driver's pulse wave and breathing wave

3.2.2.1 Introduction of the pulse wave and breathing wave

The cardiovascular system of human beings consists of a heart and blood vessels. The heart pumps blood through the arteries, which are thick-walled, distensible tubes with a circular covering of yellow elastic fibers. An artery dilates or contracts according to whether the pressure in it increases or decreases. Then the pulse wave is transmitted along the arteries. In addition, the blood pressure of arteries is simultaneously influenced by breathing. During breathing, the blood volume in the lungs varies (the typical range is 200ml~1000ml) because they are compliant and can store a large amount of blood. During inhalation, the ascending pulmonary blood volume decreases the arterial blood pressure. During exhalation, the descending pulmonary blood volume increases the arterial blood pressure. Then, breathing naturally produces a breathing wave that represents a continuous variation in arterial blood pressure. Hence, the pulse wave and the breathing wave taken together represent continuously variable blood pressure and can

be measured by using a pressure sensor. In the present research, the pressure P is defined as a force F applied perpendicularly on a unit area A

$$P = \frac{F}{A} \tag{3.1}$$

3.2.2.2 The principles of the pressure sensor

Pressure can be measured by different kinds of pressure devices or sensors such as U-tube manometers, bourdon tubes, strain gauges, piezo-resistive sensors, optic sensors, piezoelectric sensors, etc. These sensors function according to different principles or effects.

Firstly, a U-tube manometer employs a tube in a U shape and a segment of fluid such as water or mercury. Both terminals of the U-tube are connected to a reference pressure and the measured pressure, respectively. The two pressures are separated by the segment of fluid. Similarly, a Bourdon tube is an oval cross-sectioned tube bent into a C shape or a spiral shape. One terminal is closed and is moveable. The other terminal is connected to the measured pressure and is fixed. The moveable terminal can produce a displacement proportional to the measured pressure. Thus, for measuring a pulse pressure, a U-tube manometer and Bourdon tube require a segment of air or fluid to follow the pressure. Both devices are difficult to apply to the smart wheel.

Secondly, a strain gauge is an elastic transducer the resistance of which changes when strained.

$$\frac{\Delta R}{R} = G_f \times Strain \text{ [Fraden, 1997]} \tag{3.2}$$

where ΔR is the change in the resistance, R is the initial resistance, G_f is the gauge factor of the strain gauge element. Usually, a strain gauge is used with a diaphragm that deflects while a pressure is applied. The deflection induces a strain in the strain gauge. Then, the pressure is measured by using the resistive change of the strain gauge. However, the sensitivity of this kind of sensor is finite. When small pressures are being measured, the deflection is too small for stain gauges stuck on or imbedded into the diaphragm to produce an acceptable output.

Thirdly, a piezo-resistive sensor is a resistor the resistance of which varies when stress is applied:

$$\frac{\Delta R}{R} = P_{R\_L} \times Stress_L + P_{R\_T} \times Stress_T \text{ [Fraden, 1997]} \tag{3.3}$$

where P_{R_L} and $Stress_L$ are the piezo-resistive coefficient and the stress in the longitudinal direction of the sensor, respectively. P_{R_T} and $Stress_T$ are the piezo-resistive coefficient and the stress in the transverse direction of the sensor. If a piezo-resistive sensor is used to measure the pulse pressure in a driver's palm, the input full scale (FS) will be small in order to obtain enough sensitivity because the input is very weak. Then, the upper limit of the input range is much less than an adult's gripping force the mean of which can achieve 192.8N for women and 331.9N for men [Edgren *et al.*, 2003]. As soon as a gripping force is applied, the sensor is overloaded. Hence, the piezo-resistive sensor is not suitable for measuring pulse pressure when gripping force is applied.

Fourth, an optic sensor uses an effect of photoplethysmography to measure pulse pressure. It consists of photo detectors [Cheang and Smith, 2003]. While light is applied to the skin, the optic sensor measures the amount of light reflected by the skin. The vessels under the light engorge when the pulse pressure increases. The engorgement induces a change in the amount of light going to the photo detector. Then, the change of the pulse pressure can be measured. However, the heat produced by the light induces dilatation of vessels and then alters their condition. Moreover, the surface and roughness of skin is not the same at different locations. The difference also changes the amount of light reflected to the photo detector. Thus, while the measured palm is moving relative to the sensor, it is difficult to identify the true reason for the change in the amount of light detected.

Finally, piezoelectric material, including natural crystals (e.g. quartz) and poled artificial ceramics and some polymers, can generate an electric charge when they are subjected to a stress. In describing the piezoelectric effect, people define two important coefficients: piezoelectric charge coefficient

$$d_{i\_j} = \frac{\text{electric charge density in direction } i \text{ } (coulomb/m^2)}{\text{stress in direction } j \text{ } (N/m^2)} \quad i,j = 1,2,3 \text{ [MSI, 1998]} \quad (3.4)$$

and piezoelectric voltage coefficient

$$g_{i\_j} = \frac{\text{electric field in direction } i \text{ } (voltage/m)}{\text{stress in direction } j \text{ } (N/m^2)} \quad i,j = 1,2,3 \text{ [MSI, 1998]} \quad (3.5)$$

The subscripts i and j indicate the perpendicular direction of the electrodes and the direction of stress, respectively. If there is a polyvinylidene fluoride (PVDF) film of

rectangle, directions 1, 2 and 3 are the length (or stretch) direction, the width (or transverse) direction and the thickness direction, respectively (Figure 3.1).

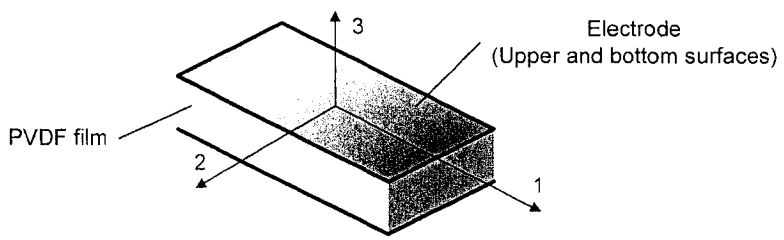

Figure 3.1 The structure and directions of a rectangle PVDF film

Theoretically, a piezoelectric sensor produces output only from dynamic stress. This means that a piezoelectric sensor can measure the pulse pressure while the gripping force is applied simultaneously. In available piezoelectric material, polyvinylidene fluoride (PVDF) is highly important because it has a remarkable piezoelectric effect, a low cost and good mechanical characteristics. In addition, PVDF film is a flexible, lightweight, tough and inexpensive engineering plastic with a wide frequency range (0.001Hz~10^9Hz), a vast dynamic range (10^{-8}~10^6 psi) and a high output. It can withstand strong electrical fields of up to 75V/μm and can resist the effect of moisture, most chemicals, and ultraviolet and nuclear radiation. Table 3.1 describes the typical characteristics of PVDF film. Hence, the present research selects PVDF film sensors to measure the pulse wave and the breathing wave of a driver's palms.

3.2.2.3 The design of a PVDF film sensor

Commonly, a PVDF film sensor is usually a micrometer in thickness, which is much smaller than its length and width, which are usually a millimeter. This suggests that the

electrodes should be attached to the upper and bottom surfaces of which the direction is 3 (Figure 3.1). Then, the sensor can work in the models 3-1 or 3-2 or 3-3 because the stress can be applied on directions 1, 2, and 3. If the input stress is the same, a sensor in model 3-3 can produce a larger output than that in the other models because the piezoelectric coefficient of model 3-3 is larger than that of models 3-1 and 3-2 (Table 3.1). However, the experiments undertaken in the present research indicate that the PVDF film sensor can not measure the pulse wave of a driver's palms under model 3-3 because the input stress is very weak. Thus, in the present research a structure is designed to transform a stress in direction 3 into a stress in directions 1 or 2.

Table 3.1 Typical properties of a PVDF film

Symbol	Description	Value	Units
d_{31}	Piezoelectric charge coefficient	23	$10^{-12}\frac{C/m^2}{N/m^2}$
d_{33}		-33	
g_{31}	Piezoelectric voltage coefficient	216	$10^{-3}\frac{V/m}{N/m^2}$
g_{33}		-330	
p	Pyroelectric Coefficient	30	$10^{-6}C/m^2{}^\circ K$
ε	Permittivity	106~113	$10^{-12}F/m$
$\varepsilon/\varepsilon_0$	Relative Permittivity	12-13	
E	Young's Modulus	2~4	$10^9 N/m^2$
υ	Passion's ratio	0.34	
	Yield strength	45~55	$10^6 N/m^2$ (stretch axis)

Assume that a PVDF film sensor covers a circular hole with a fixed boundary (Figure 3.2). In elastodynamics, the PVDF film is a clamped circular plate and has two stresses: radial stress σ_r and tangential stress σ_θ. They can be calculated as follows:

$$\sigma_r = \frac{3P}{8t^2}[(1+\upsilon)a^2 - (3+\upsilon)r^2] \text{ [Ugural,1981]} \tag{3.6}$$

$$\sigma_\theta = \frac{3P}{8t^2}[(1+\upsilon)a^2 - (1+3\upsilon)r^2] \text{ [Ugural,1981]} \tag{3.7}$$

where P is the pressure applied by a driver's palm, t is the thickness of the PVDF film, υ is the Passion's ratio of PVDF, a is the radius of the circular hole, r is a distance to the center of the film. While r = 0,

$$\sigma_r = \sigma_\theta = \frac{3Pa^2}{8t^2}(1+\upsilon) \text{ [Ugural,1981]} \tag{3.8}$$

While r = a,

$$\sigma_r = \frac{3Pa^2}{4t^2},\ \sigma_\theta = \frac{3\upsilon Pa^2}{4t^2} \text{ [Ugural,1981]} \tag{3.9}$$

Hence, the maximum stress is $\sigma_{\max} = \frac{3Pa^2}{4t^2}$ because $\upsilon = 0.34$ .The center of the film (i.e. $r = 0$) has the maximum displacement

$$z_{\max} = \frac{3P(1-\upsilon^2)a^4}{16Et^3} \text{ [Ugural,1981]} \tag{3.10}$$

where E is the Young's module of PVDF [Ugural,1981]. If $t = 100\mu m$, $a = 2mm$,

$$\sigma_{\max} = \frac{3Pa^2}{4t^2} = \frac{3\times P\times(2\times10^{-3})^2}{4\times(100\times10^{-6})^2} = 300\times P \tag{3.11}$$

To verify the theoretical result, the software package named FEMLAB is used to simulate this case. FEMLAB provides an interactive environment for modeling scientific and engineering applications based on partial differential equations and utilizes the finite element method to solve them. Figure 3.3 shows the simulated result while $P = 1N/m^2$.

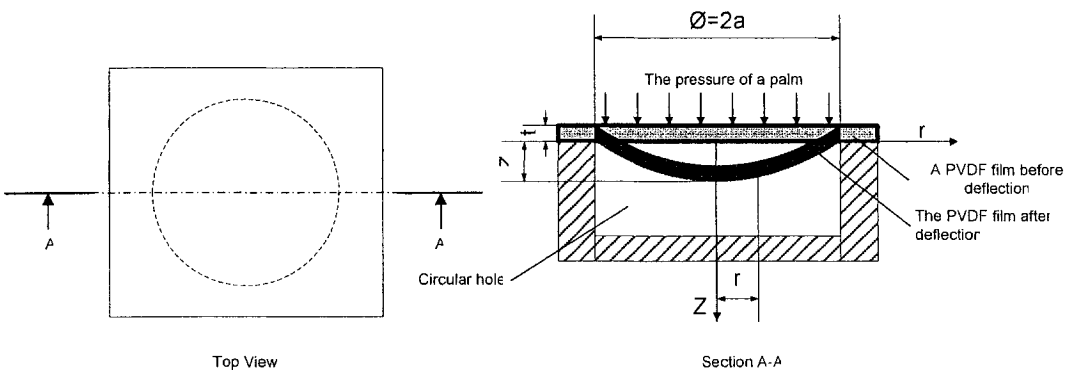

Figure 3.2 A PVDF film covering a circular hole

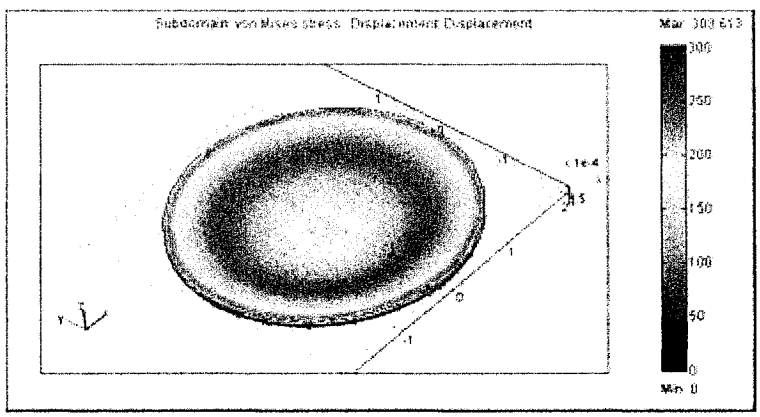

Figure 3.3 The stress in the PVDF film covering a circular hole while $P = 1N/m^2$

The maximum stress is $P = 304N/m^2$, and distributes along the circumference. The sensor output

$$\sigma_{max} \times g_{31} = (300 \times P) \times (\frac{216}{330} \times g_{33}) \approx 196 \times (P \times g_{33}) >> P \times g_{33} \quad (3.12)$$

In addition, assume that a PVDF film sensor covers a rectangular hole with fixed boundary (Figure 3.4). The rectangular hole has a length of c, a width of b, and a thickness of t. $c > 2b$. Its maximum stress occurs at the midpoint of both longer edges and

$$\sigma_{max} = 0.5 \times \frac{Pb^2}{t^2} \text{ [Ugural,1981].} \quad (3.13)$$

The maximum deflection occurs at the central point O and

$$z_{max} = 0.0284 \times \frac{Pb^4}{Et^2} \text{ [Ugural,1981].} \quad (3.14)$$

If $t = 100\mu m, b = 2a = 4mm$

$$\sigma_{max} = 0.5 \times \frac{Pb^2}{t^2} = \frac{0.5 \times P \times (4 \times 10^{-3})^2}{(100 \times 10^{-6})^2} = 800P \quad (3.15)$$

Figure 3.5 shows the result simulated by using FEMLAB while $P = 1N/m^2$. The maximum stress is $P = 760N/m^2$, and distributes at the middle segments of the long sides. The sensor output

$$\sigma_{max} \times g_{31} = (800 \times P) \times (\frac{216}{330} \times g_{33}) = 524 \times (P \times g_{33}) >> P \times g_{33} \quad (3.16)$$

Hence, by using the structures above, the output of a PVDF film sensor can be increased hundreds of times. The amplifying effect is very helpful in measuring the weak pulse pressure. Moreover, comparing the equations (3.12) and (3.16), the output of the sensor using a rectangular hole is much larger than that using a circular hole when the applied

pressure is same. Thus, the present research selects the PVDF film sensor with a structure of rectangular hole.

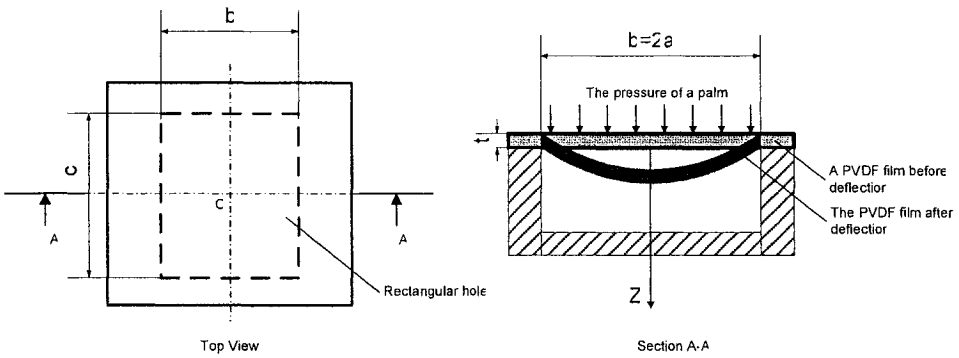

Figure 3.4 A PVDF film covering a rectangular hole

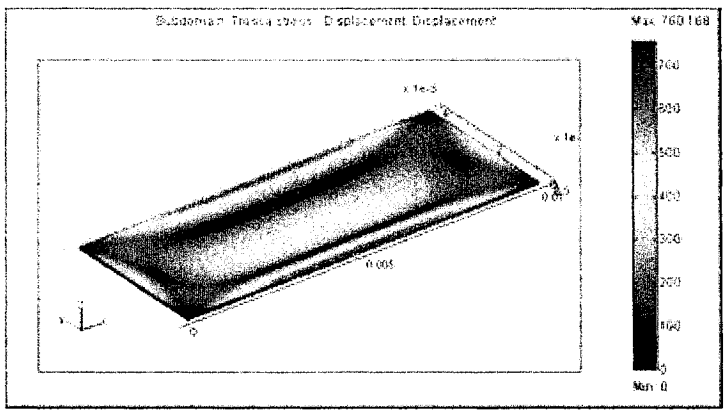

Figure 3.5 The stress in the PVDF film covering a rectangular hole while $P = 1N/m^2$

3.2.2.4 Checking the yield strength of a PVDF film sensor

A driver simultaneously applies pulse pressure and gripping force to the PVDF film sensor of a smart wheel. It is necessary to check whether the PVDF film sensor can withstand the total stress applied. However, compared to the gripping force, the pulse pressure is so small that it can be ignored. Thus, the stress of the gripping force can represent the total stress. Firstly, the maximum of a driver's gripping force is estimated.

Edgren *et al.* [2003] have measured the gripping force of people whose ages are 24~60. According to the experimental data, the males in the age group of 20~29 use the maximum mean gripping force. The mean and standard deviation (SD) are 274.7N and 40.6N when the handle diameter is 25.4mm, and are 331.9N and 31.5N when the handle diameter is 38.1mm, respectively. Thus, the maximum gripping force of 95% of the males in the age group of 20~29 can be calculated by using the percentile calculation of ergonomics. While the handle diameter is 25.4mm, the maximum gripping force

$$F_{D=25.4} = 274.7 + 1.64 \times 40.6 = 341.3\ (N) \tag{3.17}$$

While the handle diameter is 38.1mm, the maximum gripping force

$$F_{D=38.1} = 331.9 + 1.64 \times 31.5 = 383.6\ (N) \tag{3.18}$$

Thus, while the handle diameter D=34 mm, the gripping force can be calculated by using the linear interpolation formula as follows:

$$F_{D=34} = 341.3 + (D - 25.4) \times \frac{383.6 - 341.3}{38.1 - 25.4} = 369.9\ (N) \tag{3.19}$$

In addition, the mean hand breadth is 85.6mm for 95% of adult females, and 97.6mm for 95% adult males [Kroemer, 2001]. Then, while the handle diameter D=34 mm, the minimum gripping area for 95% of the adults can be calculated by 85.6mm multiplying the circumference of the handle. Thus, the maximum stress of a driver's gripping force can be calculated as follows:

$$P_{\max} = \frac{F_{D=34}}{mini\ gripping\ area} = \frac{369.9}{0.0856 \times (3.14159 \times 0.034)} \approx 40456(N/m^2) \quad (3.20)$$

Using equation (3.15),

$$\sigma_{\max} = 800 \times P = 800 \times 40456 \approx 32.4 \times 10^6 N/m^2 \quad (3.21)$$

Figure 3.6 shows the result simulated by using FEMLAB. The maximum stress is $P = 30.8 \times 10^6 N/m^2$, and is approximately equal to the result of equation (3.21). The typical yield strength of PVDF is $45 \sim 55 \times 10^6 N/m^2$. Thus, the PVDF film sensor can withstand the gripping force. Finally, the maximum deflection of the PVDF film sensor

$$z_{\max} = 0.0284 \times \frac{Pb^4}{Et^2} = \frac{0.0284 \times 40456 \times (4 \times 10^{-3})^4}{2 \times 10^9 \times (100 \times 10^{-6})^3} = 0.147(mm) \quad (3.22)$$

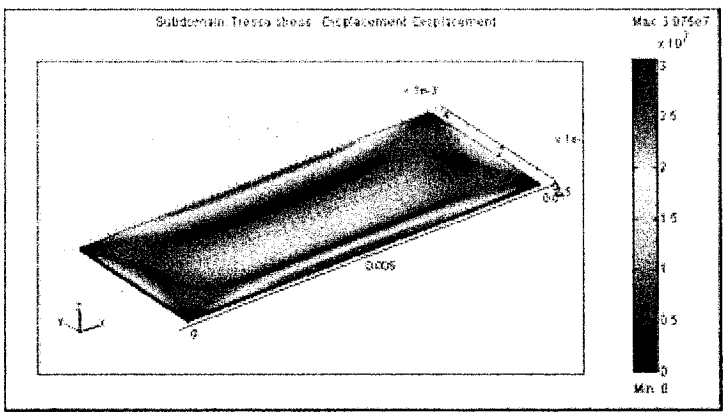

Figure 3.6 The stress in the PVDF film covering a rectangular hole while $P = 40456N/m^2$

Figure 3.7 shows the result simulated by using FEMLAB. The maximum displacement is $z_{\max} = 0.143mm$, and is approximately equal to the result of equation (3.22).

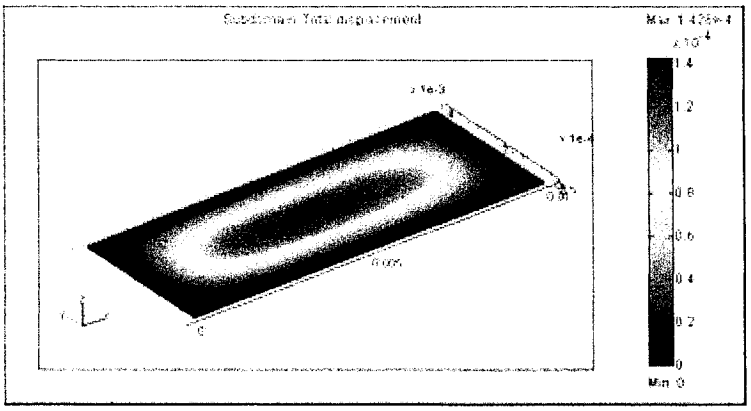

Figure 3.7 The displacement of the PVDF film covering a rectangular hole while $P = 40456N/m^2$

Hence, it is suggested that the rectangular hole has a length of 10mm, a width of 4mm, and a depth of 2mm.

3.2.2.5 The design of an interface circuit

Usually, a PVDF film sensor requires an appropriate interface circuit the parameters of which are determined by the raw signal. Generally, the pulse pressure of the human palm is much less than that of the human wrist because the pulse transmits from the wrist to the palm. Dupuis and Eugène [2000] have measured the cardiac pulse by using a cuff, and have found that the amplitude of the cardiac pulse is 0.05mmHg (i.e. $7N/m^2$) at the human wrist. Thus, the pulse pressure of a driver's palm is very weak. Assume that the pulse pressure of a driver's palm is 0.05mmHg. The PVDF film sensor outputs

$$V = (800 \times P) \times g_{31} \times t = 800 \times 7 \times 216 \times 10^{-3} \times 100 \times 10^{-6} = 0.121(V) \qquad (3.23)$$

Thus, while it is being measured, the output of the PVDF film sensor is small and requires an amplifier. In addition, the typical range of the adult pulse rate and the

breathing frequency are 50~100/minute and 12~20/minute, respectively. Their minimum frequency is 0.2Hz, which indicates the operation frequency of the PVDF film sensor. The present research specifies the cut-off frequency of the sensor as 0.1Hz. Hence, the interface circuit requires a large resistance to achieve the low cut-off frequency and requires an operational amplifier of low leakage and high impedance to obtain a large magnification. Using an operational amplifier, two kinds of interface circuits are available: (1) charge-model amplifier and (2) voltage-model amplifier (Figure 3.8). Theoretically, a charge amplifier can eliminate the effect from the capacitance of a long cable connecting the PVDF film sensor and can minimize the charge leakage through the external capacitance around the sensor. Compared to the charge amplifier, a voltage amplifier with a PVDF film sensor has better stability when the ambient temperature changes. In the case of the smart wheel, the ambient temperature of the PVDF film sensor usually follows the temperature of the inner vehicle or follows the skin temperature of a driver's palms. There is no long cable connecting the PVDF film sensor to the interface circuit.

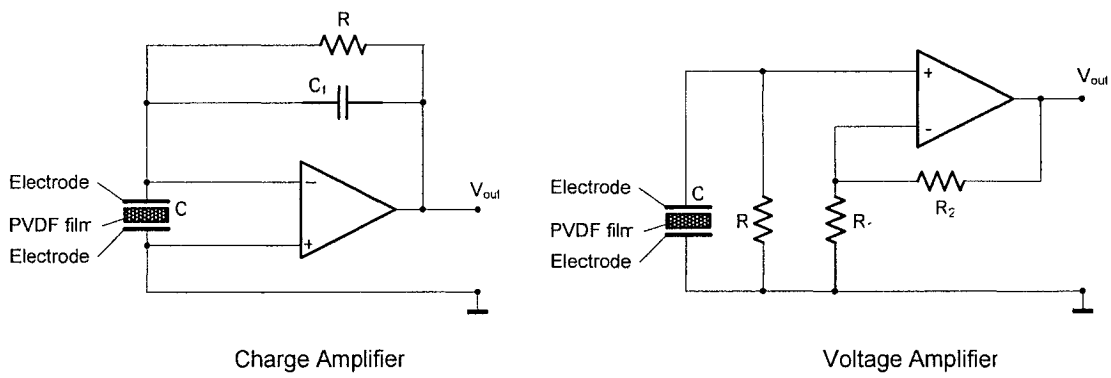

Figure 3.8 A charge amplifier and a voltage amplifier

In addition, the experiments conducted in the present research indicate that the PVDF film sensor with a charge amplifier is highly sensitive to the approach of the human body and is difficult to measure the pulse pressure. However, a sensor with a voltage amplifier eliminates this problem. Hence, the present research designs a voltage amplifier by using a TL082CN. TL082CN is a wide bandwidth dual JFET (Junction field effect transistor) input operational amplifier, which has a quick response and uses internally trimmed input offset voltage [National Semiconductor Corporation, 2000] (Figure 3.9). When the supply voltage is 5V, the output voltage changes in a range of -5V~+5V. If the PVDF film sensor has a length of 10mm, a width of 4mm, and a thickness of 100μm, its capacitance

$$C = \frac{\varepsilon A}{t} = \frac{106\times10^{-12}\times(0.01\times0.004)}{100\times10^{-6}} = 4.24\times10^{-11}(F) \text{ [MSI, 1998]} \quad (3.24)$$

$$R = \frac{1}{2\pi C f_{cut\_off}} = \frac{1}{2\times3.14159\times4.24\times10^{-11}\times0.1} = 3.754\times10^{10}(\Omega) \approx 4(G\Omega) \text{ [MSI, 1998]} \quad (3.25)$$

The voltage gain

$$\frac{V_{out}}{V_{in}} = 1+\frac{R_1}{R_2} \text{ [MSI,1998]} \quad (3.26)$$

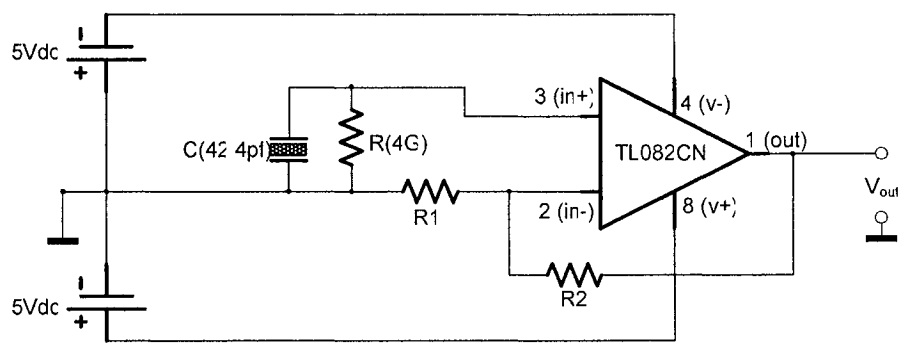

Figure 3.9 The amplifier circuit of the PVDF film sensors of a smart wheel

3.2.2.6 Disturbances of the PVDF film sensor

(1)Gripping force

In the case of the smart wheel, the output of a PVDF film sensor is influenced by the driver's gripping force because it is variable during driving (Figure 3.10). If the gripping force $P = 1000(N/m^2)$, the output voltage of a PVDF film sensor is as follows:

$$V = (800 \times P) \times g_{31} \times t = 800 \times 1000 \times 216 \times 10^{-3} \times 100 \times 10^{-6} = 17.28(V) \qquad (3.27)$$

Hence, the influence of the gripping force on the PVDF film sensor is remarkable. To eliminate the disturbance, a pressure sensor is required to measure the gripping force applied to the PVDF film sensor. Then, the output voltage of the PVDF film sensor from the gripping force can be calculated and can then be removed from the total output voltage.

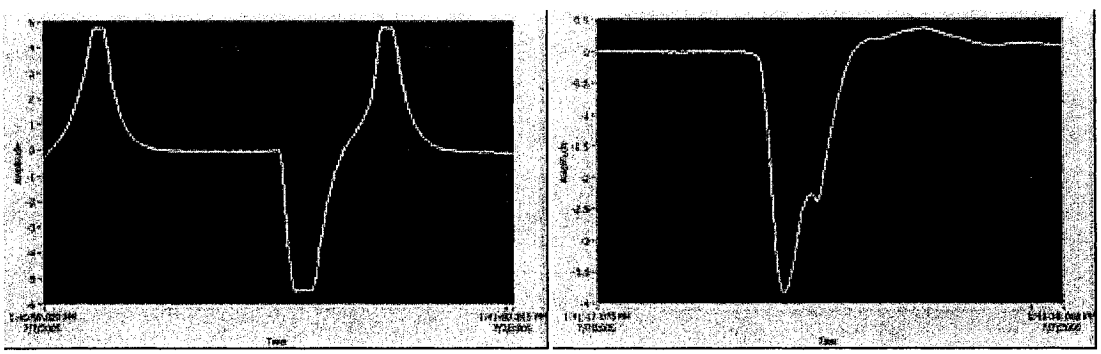

Input: pulse force Input: constant force

Figure 3.10 The output of a PVDF film sensor for pulse force and for constant force

(2)Vibration

A vehicle is a multi-body system the vibration of which is complicated. The vibration source includes the engine, the transmission system, the suspension mechanism, the road,

etc. Being a part of a vehicle, the smart wheel is exposed to all the vibration. The vibration continuously changes the force between a diver's palm and the PVDF film sensor while he grips the smart wheel. The PVDF film sensor produces a noticeable output from the force produced by the vibration (Figure 3.11). Hence, an appropriate method, such as compensating or filtering, is required to eliminate the disturbance.

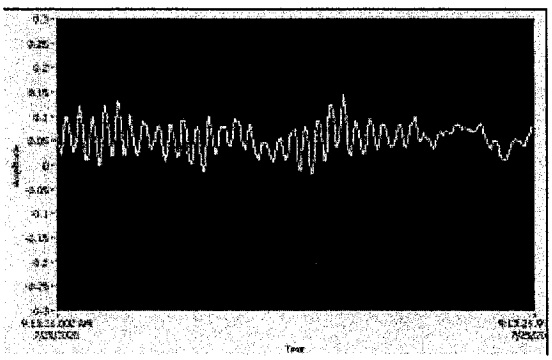

Figure 3.11 The output of a PVDF film sensor for vibration

(3) The pyroelectric effect

Besides the piezoelectric effect, PVDF also has a pyroelectric effect according to which a PVDF film sensor generates a charge in response to the change in the ambient temperature. A pyroelectric effect can be defined by using two kinds of pyroelectric coefficients: a pyroelectric charge coefficient P_Q and a pyroelectric voltage coefficient P_V. The charge ΔQ and voltage ΔV due to the pyroelecteic effect can be calculated by using equation (3.28) and (3.29), respectively.

$$\Delta Q = P_Q \times A \times \Delta T \quad \text{[Fraden, 1997]} \tag{3.28}$$

$$\Delta V = P_V \times t \times \Delta T \quad \text{[Fraden, 1997]} \tag{3.29}$$

Where ΔT is the change in temperature, A and t are the area and thickness of a PVDF film sensor, respectively. If $t = 100\mu m$ and $\Delta T = 1^{\circ}K$,

$$\Delta V = P_Q \times \frac{t}{\varepsilon} \times \Delta T = 30 \times 10^{-6} \times \frac{100 \times 10^{-6}}{106 \times 10^{-12}} \times 1 = 28.302(V) \qquad (3.30)$$

Hence, the influence of the pyroelectric effect on the output of a PVDF film sensor is remarkable. To eliminate the disturbance of the pyroelectric effect, one method is to use a temperature sensor to take continuous measurements of the ambient temperature of the PVDF film sensor. Then, the output voltage of the PVDF film sensor caused by the pyroelectric effect can be calculated and can then be subtracted from the total output voltage. Finally, the residual output voltage does not include any of the influence of the pyroelectric effect.

3.2.3 Measurement of a driver's skin temperature

3.2.3.1 Introduction to a driver's skin temperature

The evaluation of the body temperature is one of the basic and important diagnostic methods because body temperature is an important indicator of health and disease. Normal body temperature has a range of 33.2°C~38.2°C and has a mean of 37.0°C or above. A high body temperature usually follows fever, inflammation, infectious disease, etc. For example, a fever is indicated by a body temperature of 38.0°C. Commonly, there is a thermal gradient from the skin to the internal tissue, increasing 1°C per 4 mm of depth [Hasday, 1997]. Theoretically, the temperature of thoracic and abdominal tissue or of the brain is named the core temperature. The temperature of skin is named the peripheral temperature. Physicians usually utilize the reading of rectal, oral, ear or

axillary measurement to evaluate the core temperature [Blatties, 1998]. In addition, people usually use a hand to feel the skin temperature of the human forehead and to estimate the core temperature in daily life. Hence, to evaluate a driver's condition, the present research measures the skin temperature of a driver's palm by using temperature sensors.

3.2.3.2 The principles of a temperature sensor

A temperature sensor is one of the widespread sensors in the field of engineering. Commonly, its sensing methods include a thermoresistive effect, a thermoelectric effect, a semiconductive transducer, an optical transducer, and the piezoelectric effect.

Firstly, the thermoresistive effect refers to the resistivity of a material ρ which changes with the temperature T as

$$\rho = \rho_0[1+\alpha(T-T_0)] \quad \text{[Fraden, 1997]} \tag{3.31}$$

where ρ_0 is the resistivity at the reference temperature T_0, α is the temperature coefficient of resistance (TCR). Thermoresistive sensors are usually divided into three categories: (1) a resistance temperature detector (RTD), which is usually produced by using a metal or an alloy. The most widespread material is platinum and its alloy because it has an expectable output and good stability. It is usually used to produce a thin film RTD and a wire-wound RTD. The temperature coefficient of resistance of all RTDs are positive; (2) a silicon resistive sensor of which the material is bulk silicon. Pure silicon initially has a negative temperature coefficient of resistance. After depositing an n type impurity on it, the silicon has a positive temperature coefficient of resistance in a certain

temperature range. Some silicon resistive sensors have good linearity and good stability; (3) a thermistor, which is made from metal-oxide. If a thermistor has a negative temperature coefficient, it is called a NTC thermistor. If it has a positive temperature coefficient, it is called a PTC thermistor. A thermistor usually has a highly nonlinear output and good stability.

Secondly, the thermoelectric effect refers to the physical phenomenon according to which two different coupling wires can generate an open-circuit voltage. The voltage changes according to the temperature of their junction. A thermocouple is a common thermoelectric temperature sensor. The Instrument Society of America (ISA) lists many types of thermocouples such as type T, J, E. Different types of thermocouples use different metallic material. A thermoelectric sensor has a linear output and requires a "cold" junction the temperature of which is precisely given.

Thirdly, the PN-junction of a semiconductor has a remarkable thermal dependence. Supplying a constant current to the junction, its voltage is a function of its temperature. A semiconductor PN-junction sensor has a good linearity, a quick response and good stability. However, it can measure only a low temperature in a limited range (the typical range is -55°C~+150°C).

Fourth, some optical sensors can be employed to measure temperature. These optical sensors consist of (1) a thermal infrared detector of which the sensing element is responsive to electromagnetic radiation in the infrared wavelength range. A passive

infrared (PIR) detector can convert the incoming radiation to heat. An active infrared (AFIR) detector emits thermal radiation to the measured object and measures the heat loss in the form of thermal radiation. (2) a fluoroptic sensor, which utilizes a special phosphor compound. It can emit a fluorescent signal due to light excitation. The shape of the response pulse can be used to calculate the temperature; (3) an interferometric sensor, which employs two light beams. Compared to the reference beam, the other beam travels through a temperature sensitive medium and is somewhat delayed depending on the temperature of the medium; (4) a thermochromic solution sensor, which has a certain effect of spectral absorption for certain temperatures.

Finally, the piezoelectric effect of some material is temperature dependent. Besides the pyroelectric effect mentioned in section 3.2.5, the variability of the oscillating frequency of a quartz crystal Δf has

$$\frac{\Delta f}{f_0} = a_0 + a_1 \Delta T + + a_2 \Delta T^2 + a_3 \Delta T^3 \quad \text{[Fraden, 1997]} \tag{3.32}$$

where ΔT is the temperature change, f_0 is the calibrating frequency, a_0, a_1, a_2, a_3 are the coefficients. However, the nonlinear relationship increases the difficulty of processing the signal.

In the case of the smart wheel, the temperature sensor measures a driver's skin temperature the typical range of which is 20°C~+40°C. However, the sensor also requires the ability to withstand the possible extreme temperatures in the inner space of a vehicle. For example, the temperature may attain +60°C or over when the vehicle is exposed to strong sunlight for a long time, or it may be as low as 0°C or less when the vehicle is

parked in a cold environment for a night. Hence, it is better if the sensor has an input range of -5°C~+70°C so that it has good linearity in measuring a driver's skin temperature and can adapt to extreme temperatures. In addition, the temperature sensor must have a quick response time and a compact size as explained in section 1.3. Hence, the present research selects a semiconductor PN-junction sensor to measure the skin temperature of a driver's palm.

3.2.3.3 Selecting a semiconductor temperature sensor

In fact, a semiconductor temperature sensor is an integrated circuit (IC) temperature sensor a typical input range of which is -55°C~150°C. It usually integrates some signal processing circuitries, such as a linearization circuit, into the same package as the sensor. Common semiconductor temperature sensors can be divided into two categories: (1) an analog semiconductor temperature sensor, which outputs voltage or current proportional to Celsius or Kelvin temperature with an almost constant coefficient and (2) a digital semiconductor temperature sensor, which integrates with an analog-to-digital (A/D) circuit and produces a digital output.

The semiconductor temperature sensor selected should satisfy the requirements of a smart wheel: (1) the supply voltage is 5V DC; (2) the accuracy can achieve 1°C in the range of 10°C~40°C; (3) it outputs a voltage signal or digital signal. A digital semiconductor temperature sensor does not require an external circuit for a signal condition but requires a long temperature conversion time at the level of a millisecond. However, an analog semiconductor temperature sensor requires an analog-to digital (A/D) circuit to convert

the analog signal to digital data. If several analog sensors share one A/D circuit, the A/D requires a multiplexer to select and connect one of them. The A/D circuit and the multiplexer have a conversion time at the level of microsecond or nanosecond, respectively. Thus, the speed of an analog semiconductor temperature sensor with A/D is much quicker than that of a digital semiconductor temperature sensor. Finally, the present research recommends an analog semiconductor temperature sensor such as LM35CAH, TMP36 (Table 3.2) and selects LM35CAH as an example.

Table 3.2 Specifications of three temperature sensors

Parameters ↓	LM92	LM35CAH	TMP36
Supply Voltage	2.7V~5.5V	4V~30V	2.7 V~5.5 V
Input	−25°C to 150°C	−55° to +150°C	−40°C~+125°C
output	Digital: 12-bit + sign	Analog: −1.0V~ +6V	Analog:100~2000 mV
Accuracy	±0.50°C(10°C to 50°C)	0.5°C(+25°C)	±1°C(+25°C)
Linearity	±0.5°C (max)	± 1/4°C	0.5°C
Resolution	0.0625°C	+ 10.0 mV/°C	10 mV/°C
Conversion Time	500ms	---	---
Interface Type	2-Wire Serial	---	---
Dimension(mm)	6.2×5×1.8	Ø5.6×2.7	2.9×2.8×1.45
Application	*(a), (c), etc.	*(b), etc.	*(d), etc.
	* (a) Medical equipment (b) Centigrade temperature sensor (c) Electronic Test Equipment (d) Environmental control		

3.2.4 The measurement of a driver's gripping force

3.2.4.1 Introduction of the gripping force

While a driver grips the smart wheel, the coupling between the hand and the wheel is power grasp. The term power grasp means that a handle is grasped by using the inner hand surface. The handle extends in the direction of the knuckles and exceeds both sides of the hand [Kroemer, 2001]. Edgren *et al.* [2000] have reported that the handle diameter and the subject's condition influence his gripping force. In addition, according to

common experience, the gripping force is generally decreased while a driver feels sick or pays little attention to driving. Hence, the gripping force is an important indicator of a driver's condition. The present research assigns the function of measuring the gripping force to the smart wheel.

3.2.4.2 The principles of a force sensor

There are two kinds of force sensors currently available on the market: (1) a quantitative sensor such as a strain gauge, which can actually measure the force, and (2) a qualitative sensor such as a computer mouse, which decides only whether the measured force is larger than a specified threshold. The smart wheel requires a quantitative sensor for measuring the actual value of the gripping force.

Widespread force sensors include the strain gauge, the piezo-resistive sensor, the piezoelectric force sensor, the tactile sensor, etc. The strain gauge and the piezo-resistive sensor, which have been explained in section 3.2.2.2, are also available to measure force. Next, the piezoelectric sensor uses another method to measure a force besides the method mentioned in section 3.2.2.2. The natural mechanical frequency of a piezoelectric crystal

$$f_n = \frac{n}{2l}\sqrt{\frac{c}{\rho}} \quad \text{[Fraden, 1997]} \tag{3.33}$$

Where n is the harmonic number, l is the dimension of determining the resonance, c is the effective elastic stiffness constant, ρ is the density of the crystal material. When a force is applied to the crystal, its parameter c produces an efficient change that can induce a shift of f_n. Then, the force can be measured by using the frequency variation.

Finally, a tactile sensor utilizes an exceedingly thin layer to respond to a stress or force in the direction of the thickness. The thin layer can be made of foil, a conductive ink, PVDF, a conductive elastomer, etc.

3.2.4.3 Selecting a force sensor

In the present research, the range of the gripping force is $0 \sim 40456 N/m^2$ (section 3.2.2.3). During driving, a driver's gripping force may be constant, may slowly change, or may rapidly change. Thus, a piezoelectric sensor is not suitable in this case because it can not produce a constant output from a constant force. The strain gauge requires an elastic diaphragm in order to achieve high sensitivity. However, it is not easy to produce an elastic diaphragm on a smart wheel. The piezo-resistive sensor has good sensitivity for small stress and does not require a special structure. A tactile sensor has a high sensitivity to small stress, good flexibility and reasonable cost. However, its input range is limited because of technological limitations. Finally, the present research selects the FlexiForce® standard sensor A201-1, which is a tactile sensor using a kind of patent piezo-resistive material (Figure 3.12). The sensor has two layers of substrate (polyester/polyimide) film each of which is deposited a layer of silver followed by a layer of pressure-sensitive ink. The sensor has an effective sense area of $71mm^2$. The resistance of A201-1 proportionally decreases while the applied force increases. A force of 0~4.44N (i.e. $0 \sim \frac{4.44N}{71mm^2} = 62245 N/m^2$) can be measured by using A201-1. Figure 3.13 describes the interface circuit of A201-1, which employs a monolithic operational amplifier, MC34071 from ON Semiconductor [TEKSCAN cooperation, 2004]. The output voltage is as follows:

$$V_{out} = -V_D \times \frac{R_1 + R_F}{R_s}$$ [TEKSCAN cooperation, 2004] (3.34)

Where V_D is the excitation voltage of the sensor, R_s is the resistance of the sensor, R_1 is a protecting resistor, R_F is an adjustable reference resistor. The sensitivity of the sensor is determined by R_F the smaller resistance of which induces less sensitivity but a larger input force range. If the supply voltage is 5Vdc, the output voltage changes in a range of 0.1V~4V.

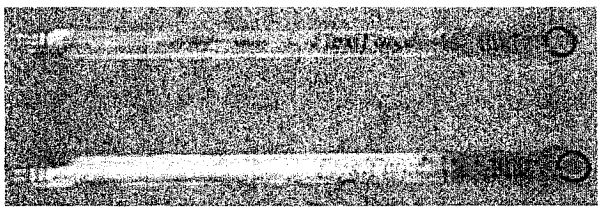

Figure 3.12 FlexiForce® standard sensors A201-1

3.2.4.4 The disturbance of a piezo-resistive sensor

(1) Ambient temperature

Generally, the output of a piezo-resistive sensor is influenced by the change of the ambient temperature. In the case of the smart wheel, FlexiForce sensors can work at a temperature range of -9°C~74°C since the load of the sensor is half that of the standard maximum load, 4.44N. However, the output of the FlexiForce sensor possibly changes as much as 0.36% per Celsius degree for the same input. Hence, the A201-1 requires a temperature sensor for the correction of the output and to ensure accuracy. If the ambient temperature of A201-1 is measured, the effect of the temperature on the output of A201-1 can be calculated and removed from the total output.

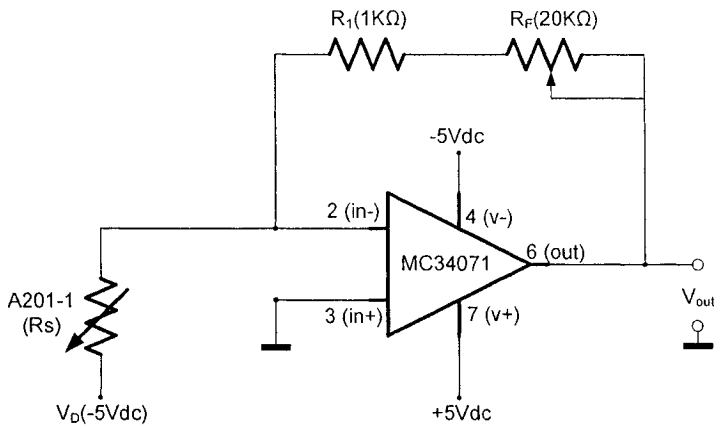

Figure 3.13 The interface circuit of a FlexiForce® standard sensor A201-1

(2) Vibration

During the measurement of the gripping force, the vibration of the vehicle can change the output of the piezo-resistive sensor of a smart wheel. However, the magnitude of the gripping force is much larger than that of the vibration. The piezo-resistive sensor produces much less output from the vibration than that from the gripping force. Hence, the effect of vibration on a piezo-resistive sensor can be ignored.

3.3 The design of a data acquisition (DAQ) system

3.3.1 Functional design

From the point of view of engineering, the smart wheel consists of three parts: (1) sensors; (2) a data acquisition (DAQ) system the function of which is described in Figure 3.14 and (3) a mechanical structure that can install the sensors and can withstand the force applied by the driver. The sensors and their interface circuits are installed on a specially designed wheel. A data acquisition (DAQ) system executes analog-to-digital

(A/D) converting, data buffering and data processing. The sensors, the DAQ system and the wheel constitute a smart wheel. A driver's condition can be evaluated by using the data from the smart wheel.

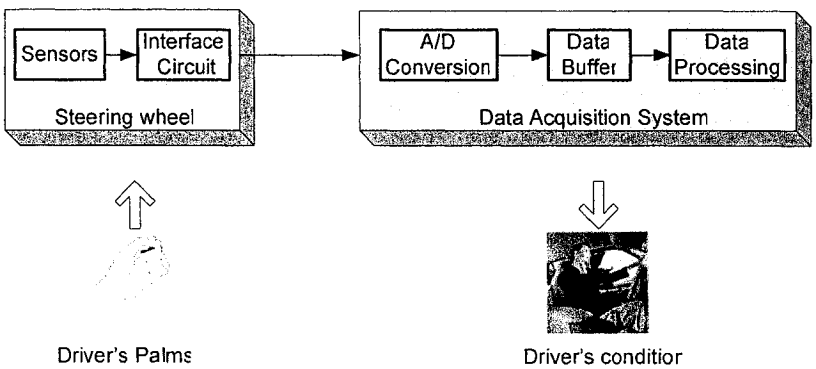

Figure 3.14 The functional design of a smart wheel

A Data Acquisition (DAQ) system is an electronic instrument or system that can measure and quantify analog signals. With it, an analog signal is converted into a digital signal that can be collected, stored, and analyzed by employing a computer. The computer can automate and speed the process of data acquisition. A DAQ system usually has a hardware configuration as shown in Figure 3.15. The analog multiplexer can select one of the signal sources to be measured by using the same data acquisition hardware. Depending on the type of package, it may have two to several hundred channels. The function of the signal conditioning is to optimize the electrical signals from the sensors into the input range of the DAQ hardware and includes amplification, filtering, peak detection, or sample-and-hold, etc. The analog-to-digital (A/D) converter can transform an analog signal into a digital format by using one of the technologies of dual-slope integration, successive approximation, etc. The digital clock is the master timer of a DAQ

system. The module for manual data entry is utilized to label the experimental data or to add some useful information by the experimenter. The digital buffer is employed to store digital signals temporarily at moments when the speed of processing data can not follow that of inputting data. The output buffer collects the data from many sources such as an A/D converter, manual data entry, digital buffer, etc., and transforms the data into the appropriate format that can be processed by a computer system such as a desktop computer, a portable digital assistant (PDA), an embedded microprocessor system

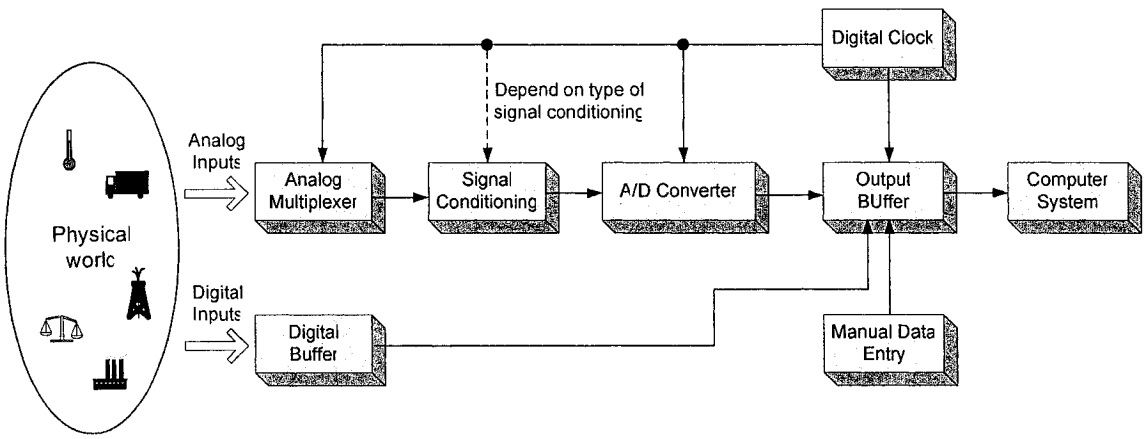

Figure 3.15 A basic DAQ system

In addition, software integrates the DAQ hardware and the computer into a complete DAQ system. It is important for a DAQ system to execute the specified function and to achieve good performance. Commonly, the important application of a DAQ system includes (1) a data logger that can measure the analog input and store the corresponding digital data for later analysis, (2) a signal analysis that can extract useful data from time-varying signals, (3) an automatic factory test system that usually involves a computer and can repeatedly and rapidly execute a specified test process, (4) a process control system

that can monitor, control and optimize certain industrial processes, etc. Thus, measuring a driver's condition requires a signal analysis system for daily driving or requires a data logger for research.

3.3.2 Overall design

Designing the DAQ system of the smart wheel should take into consideration that (1) the smart wheel has $17 \times 3 = 51$ sensors (more details are given in chapter 4), which operate at 5Vdc and have the output ranges described in Table 3.3; (2) the sensors produce voltage signals by using respective interface circuits. These analog signals require A/D converting; (3) the maximum frequency of the adult pulse rate and breathing frequency is 1.67Hz. The sampling theorem suggests that the sampling frequency must be twice the maximum frequency component of the input signal at least in order to describe it completely [Vandoren, 1982]. To increase the reliability of sampling, people usually select a sampling frequency which is tens of times greater than the frequency of the original signal. Thus, the present research specifies a sampling frequency of 200Hz. Then the total sample frequency is $51 \times 200 = 10200 Hz$; (4) the three kinds of sensors have different output ranges. While using the same A/D converter (e.g. 16bits), the accuracies of A/D converting are different (Table 3.3); (5) if the DAQ system produces 2 bytes of data per sample per channel, the speed of producing data can achieve $51 channel \times 200 Hz \times 2 Byte \approx 20 Kb/s$. However, the speed of processing the data depends on the computer system and software. It may be slower than the speed of producing the data. While the data can not be processed immediately, it can be temporarily stored in a data buffer. Thus, an appropriate data buffer is necessary for a

reliable DAQ system. These characteristics must be taken into consideration when selecting the electronic devices for the DAQ system.

Table 3.3 The output ranges and A/D parameters of three sensors

Sensor	Measurand	Output voltage range	Resolution (bit)	Accuracy of A/D (mV)
PVDF film sensor	Pulse wave, breathing wave	-5V~+5V	16	0.15
A201-1	Gripping force	0.1V~4V	16	0.06
LM35CAH	Skin temperature	−1.0V~ +6V	16	0.11

3.4 The hardware configuration

3.4.1 Overall architecture

For the scanning of the output voltage of the 51 sensors of a smart wheel, the present research selects three ADG732, which are the monolithic CMOS 32-channel analog multiplexers from Analog Devices Company (Figure 3.16). It can operate on a single +5V supply and with a transition time of 23 nanoseconds. In addition, an ADC16061 is utilized to execute analog-to-digital converting. ADC16061 is a self-calibrating 16-bit analog-to-digital converter. It operates on a single +5V supply and with a speed of 2.5 mega samples per second (MSPS). Next, the DAQ system requires a computer or an embedded system to execute logical control, data storage and data processing. An embedding system is better in the case of the smart wheel since it has compact sizes, low energy consumption and little weight. Finally, Figure 3.17 describes the hardware configuration of the electronic system of a smart wheel. ADG732 #1 accepts the command of the embedded microprocessor system and then connects one of the seventeen PVDF film sensors to a TL082CN, which can amplify the output of the connected sensor. Similarly, ADG732 #2 can connect one of the seventeen piezo-

resistive sensors to a MC34071, which can condition the output of A201-1. The 17 temperature sensors, LM35CAH, do not require an external interface circuit. The TL082CN, MC34071 and all LM35CAH are connected to ADG732 #3, which can switch on one of the 19 inputs to the ADC16061. The embedded microprocessor system can read, store and process the digital data from the ADC16061.

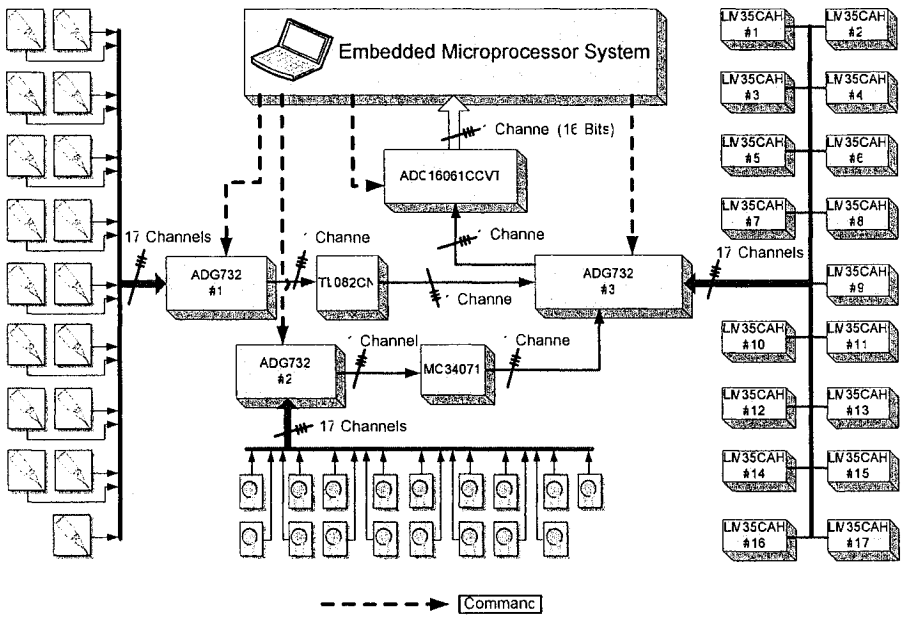

Figure 3.16 The hardware configuration of the electronic system of a smart wheel

3.4.2 An embedded microprocessor system

An embedded microprocessor system is a simplified and diminished computer that is integrated with products such as engines, printers, etc. Basically, it consists of a microprocessor, a random access memory (RAM), a nonvolatile memory, an input or output interface (I/O), etc (Figure 3.17). However, some single-chip microprocessors can also provide RAM, nonvolatile memory and I/O. An embedded microprocessor system is widespread because it has good flexibility, programmability and adaptability. In the

present research, the DAQ system is a real-time measurement system. The embedded microprocessor system has the following characteristics: (1) it operates on a +5V supply; (2) the microprocessor has high speed and can directly process data of 16 bits from ADC16061; (3) it requires a 16 bit data bus at least; (4) a large nonvolatile memory is required since the software is complicated; (5) a large RAM is important since a large volume of data is processed. Finally, the embedded microprocessor system can transmit the processed data to the central computer of a vehicle and/or display it by using liquid crystal display (LCD), head up display (HUD), etc.

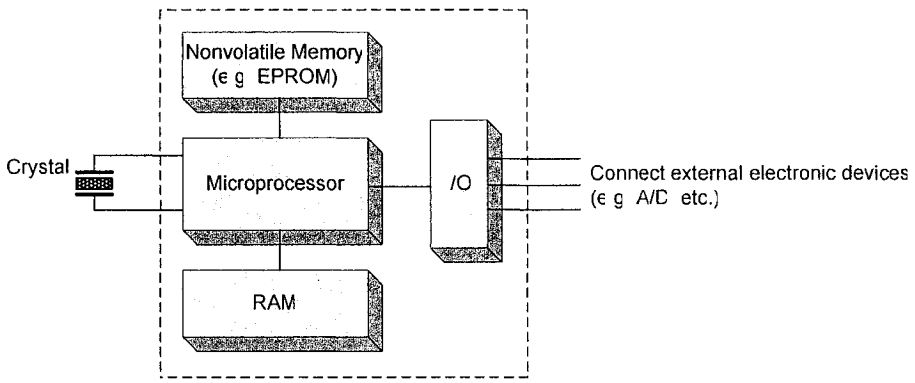

Figure 3.17 The architecture of an embedded microprocessor system

3.5 Software design

3.5.1 Overall design of software

The software of the DAQ system of a smart wheel is different from that of a personal computer. The former requires better real-time ability. To decrease the cost of the hardware and to increase the flexibility, the software of the DAQ system is assigned four important functions: comparing, compensating, filtering and calculation. Its workflow is

shown in Figure 3.18. The output of the temperature sensors of a smart wheel is directly employed to evaluate a driver's condition. The output of the piezo-resistive sensors is corrected by using compensation for temperature. Then, the curve of the gripping force is obtained. The output of the PVDF film sensors are corrected by compensating and filtering. The processed signal consists of the driver's pulse wave and breathing wave. Then, both waves are separated by using another filter and are then used to calculate the driver's pulse rate and respiratory frequency, respectively. Finally, a driver's condition can be evaluated based on his skin temperature, gripping force, pulse rate and respiratory frequency.

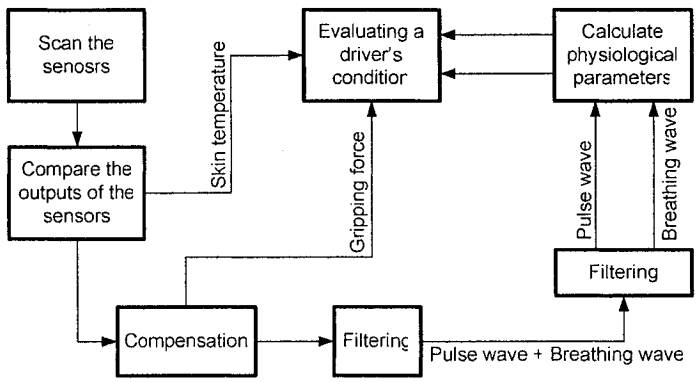

Figure 3.18 The workflow of the software of the DAQ system

3.5.2 Comparing the output of the sensors

The smart wheel has 17 groups of sensors. Each sensor group includes one PVDF film sensor, one piezo-resistive sensor and one temperature sensor. Which group of sensors is being gripping at any one time by the driver? The answer depends on the result of comparing the output of all sensor groups. While the smart wheel is being gripped, the temperature sensor outputs a voltage representing the driver's skin temperature. The

output voltage may be higher than, equal to, or lower than that of the other temperature sensors because the driver's skin temperature may be higher than, equal to, or lower than the ambient temperature. The piezo-resistive sensor outputs a larger voltage than the other piezo-resistive sensors. The PVDF film sensor outputs a voltage pulse when the gripping force is beginning to be applied and then outputs a voltage wave based on the pulse wave and the breathing wave. The other PVDF film sensors output a constant voltage. Hence, the instantaneous reading of the gripping force, skin temperature and pulse pressure can be obtained in two steps: (1) find the gripped piezo-resistive sensor of which the output voltage is the maximum in all piezo-resistive sensors; (2) read the output voltages of the temperature sensor and PVDF film sensor in the same group of the gripped piezo-resistive sensor. The piezo-resistive sensor can be the indicator of the sensor group that is being gripped because it has a quick, remarkable and reliable output.

3.5.3 Compensation

In the world of sensors, a widespread characteristic is cross-sensitivity because of which a sensor simultaneously produces output from several physical variables, not only from one. For example, a PVDF film sensor has a pyroelectric effect as well as a piezoelectric effect. The phenomenon also influences the performance of the sensors of a smart wheel (Figure 3.19). Firstly, the change of ambient temperature influences the output of the piezo-resistive sensor and the PVDF film sensor. If the skin temperature is measured versus time, the effect of temperature change on the piezo-resistive sensor $V_{temperature}$ can be calculated by using certain equations. Assume that the outputs before and after the temperature compensation are V_{total} and V_{true}, respectively,

$$V_{true} = \begin{cases} V_{total} - V_{temperature} & if\ V_{temperature} > 0 \\ V_{total} & if\ V_{temperature} = 0 \\ V_{total} + V_{temperature} & if\ V_{temperature} < 0 \end{cases} \tag{3.35}$$

Similarly, the same temperature compensation can be applied to the PVDF film sensor. Then, the effect of the temperature on the piezo-resistive sensor and PVDF film sensor is eliminated.

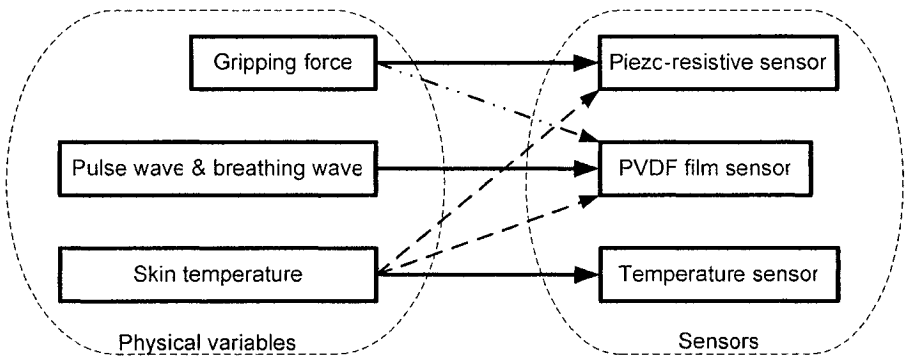

Figure 3.19 The cross-sensitivity of the sensors of a smart wheel

In addition, the output from the PVDF film sensor includes the disturbance of the gripping force. If the true gripping force is known after the temperature compensation, the effect of the gripping force on the PVDF film sensor $V_{Gripping\ force}$ can be calculated. Then

$$V_{true} = \begin{cases} V_{total} - V_{Gripping\ force} & if\ V_{Gripping\ force} > 0 \\ V_{total} & if\ V_{Gripping\ force} = 0 \\ V_{total} + V_{Gripping\ force} & if\ V_{Gripping\ force} < 0 \end{cases} \tag{3.36}$$

where V_{total} and V_{true} are the output from the PVDF film sensor before and after the gripping force compensation, respectively. So the effect of the gripping force on the PVDF film sensor is eliminated. Finally, the compensation above removes the influence

of the temperature on the piezo-resistive sensor and on the PVDF sensor and corrects the influence of the gripping force on the PVDF film sensor. More accurate data about the pulse wave, the breathing wave, and the gripping force are obtained.

3.5.4 Removing vibration noise

From the point of view of physics, vibration is a rapid linear motion of a particle or an elastic solid about an equilibrium position. A vehicle is exposed to different kinds and sources of vibration such as the engine, the road, and the suspension mechanism. All these vibrations have an influence on the smart wheel since it a part of the vehicle. Pottinger *et al.* [1986] have found that the vibration of the steering wheel and column produces large resonant peaks in the power spectrum at frequencies from 20 to 50 Hz. The vibration can influence the output of the piezo-resistive sensor and the PVDF film sensor of a smart wheel. The effect of vibration on the piezo-resistive sensor can be ignored. However, the vibration is an important disturbance on the PVDF film sensor. Basically, there are two methods that can be used to eliminate the influence of vibration: (1) employ a sensor to measure the vibration transmitted from the vehicle to the smart wheel, and then execute the compensation for the vibration; (2) filter the noise signal of the vibration from the output of the PVDF film by using a filter because the frequency of vibration is much larger than the maximum frequency of a driver's pulse wave and the breathing wave, 1.67Hz. The present research utilizes the second method because (1) the first method requires extra sensors and introduces new error; (2) the second method decreases the cost since the filter can be implemented by software. Moreover, the

software filter has better flexibility because testing or modifying the design of the filter is easy.

3.5.5 Separating the pulse wave and the breathing wave

It is mentioned above that the output of a PVDF film sensor includes the driver's pulse wave and the breathing wave the frequencies of which are 0.83~1.67Hz and 0.2~0.33Hz, respectively. There is an important difference between the two ranges of frequency. Hence, the pulse wave and breathing wave can be separated by using a filter when the output signal of the PVDF film sensor has been corrected. The filter can select a band-pass filter, or a band-stop filter, or an assembled filter of a low-pass filter and a high-pass filter. The band-pass filter transmits the signal the frequency of which belongs to a specified range. The band-stop filter blocks the signal of which the frequency belongs to a specified range. The low-pass filter transmits the signal of which the frequency is lower than a specified value. The high-pass filter transmits the signal of which the frequency is larger than a specified value (Figure 3.20). The present research selects a band-pass filter.

3.5.6 The calculation of physiological parameters

After compensating and filtering, the outputs of the PVDF film sensor and piezo-resistive sensors are corrected. A driver's pulse wave, breathing wave, skin temperature and gripping force are obtained. However, more calculation is required to obtain the parameters of the cardiovascular system and respiration system from the pulse wave and breathing wave, respectively. For example, Figure 3.21 shows a pulse wave measured by

using a smart wheel. In the pulse wave, t_1 is the contracting time of the heart. t_2 is the relaxing time of the heart. The sum of t_1 and t_2 can be used to calculate the heart rate. From the breathing wave, similarly, the breathing frequency can be calculated.

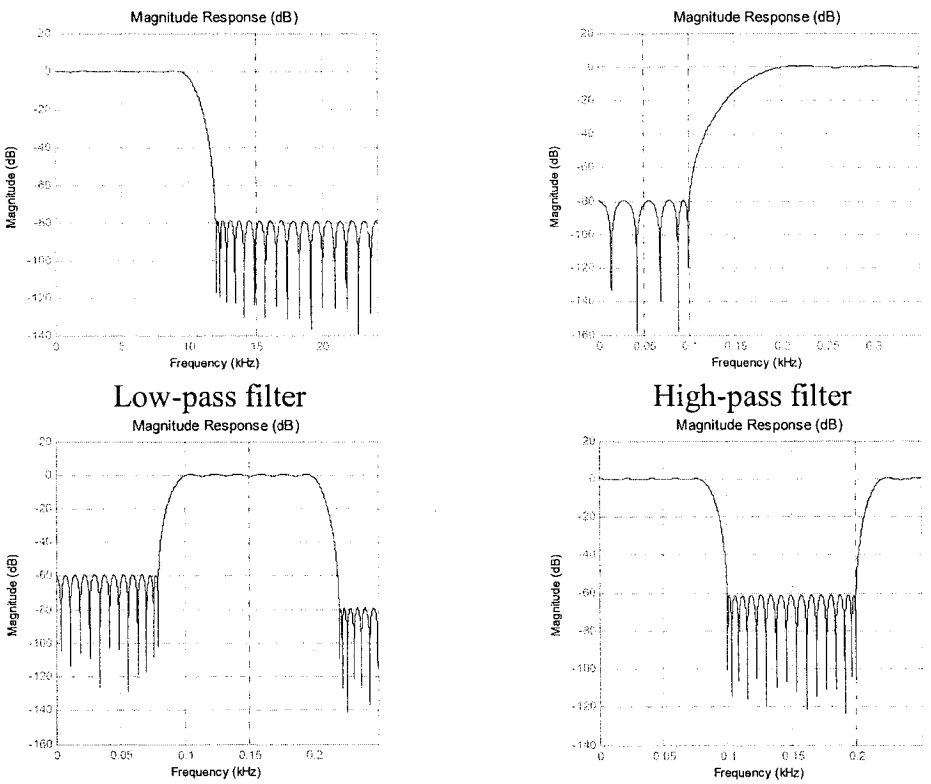

Figure 3.20 Four kinds of filters

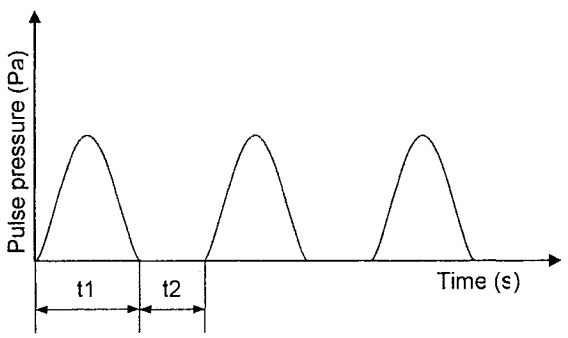

Figure 3.21 A pulse wave

While calculating a driver's pulse rate, there is a special method that should be discussed as follows: a pulse wave from the sensors consists of many frequency components one of which can be utilized to calculate the pulse rate. However, the frequency components in a pulse wave can not be distinguished merely by observing the pulse wave. The common method is to calculate the power spectrum of a pulse wave. All important frequency components produce peaks in the power spectrum. The calculation of the power spectrum requires using a Fourier transform a simple deduction of which is described as follows: Assume $f(x)$ is a function of independent variable x. Saying

$$F(\omega) = \int_{-\infty}^{\infty} f(x)e^{-i\omega x}\,dx \quad \text{[Gray and Goodman, 1995]} \tag{3.37}$$

and

$$f(x) = \frac{1}{2\pi}\int_{-\infty}^{\infty} F(\omega)e^{ix\omega}d\omega \quad \text{[Gray and Goodman, 1995]} \tag{3.38}$$

where $i = \sqrt{-1}$ and $e = 2.71828183$. (3.37) and (3.38) is so-called Fourier Transform pair. Hence, the Fourier transform of $f(x)$ is defined as:

$$\Gamma[f(x)] = F(\omega) = \int_{-\infty}^{\infty} f(x)e^{-i\omega x}\,dx \quad \text{[Gray and Goodman, 1995]} \tag{3.39}$$

Its inverse transform is:

$$\Gamma^{-1}[F(\omega)] = f(x) = \frac{1}{2\pi}\int_{-\infty}^{\infty} F(\omega)e^{ix\omega}\,d\omega \quad \text{[Gray and Goodman, 1995]} \tag{3.40}$$

(3.39) and (3.40) are utilized to analyze continuous single which is produces by a continuous function. While the signal is discrete,

$$f(x) \to f(x_k) \quad k = 0,1,...,(N-1)$$

Then

$$F_n = \sum_{k=0}^{N-1} f(x_k) e^{-i\times 2\pi n\times \frac{k}{N}},\ f(x_k) = \sum_{k=0}^{N-1} F_n e^{i\times 2\pi n\times \frac{k}{N}} \quad \text{[Gray and Goodman, 1995]} \quad (3.41)$$

where n is a variable. In the case of a smart wheel, the pulse wave is not a continuous curve and is described by a set of discrete values of voltage. Analyzing it requires the discrete Fourier transform (DFT). The calculation of a discrete Fourier transform (DFT) can be speeded up by using the fast Fourier transform (FFT) algorithm. After obtaining the power spectrum of a driver's pulse wave, his pulse beats per minute can be calculated by using

$$R_{pulse} = f_{\max\_power} \times 60\ (times/\min) \quad (3.42)$$

Where $f_{\max\_power}$ is the frequency of which the power is the maximum in the power spectrum. The R_{pulse} is the average pulse rate over the whole duration of measuring the pulse wave. If the instantaneous pulse rate in the duration is calculated, an algorithm named the short-time Fourier transform (STFT) is required. The algorithm applies a moving window to the signal and then applies the Fourier transform to the signal in the window. STFT has many kinds of windows from which the Hanning window function is selected in the present research. Hence, after improving the software, a driver's average pulse rate and instantaneous pulse rate can be obtained by using a smart wheel.

3.6 Power consumption and cost analysis

Electrical power is an important limitation in designing the instruments for monitoring a driver's condition. The electronic system of a smart wheel consists of many sensors and electronic devices. The PVDF film sensor generates a charge when a stress is applied and does not consume external electrical power. Its interface circuit requires a stream of

direct-current electricity of 5V and 3.6mA and consumes little energy. The piezo-resistive sensor and its interface circuit operate on direct-current electricity of +5V and -5V. Their maximum current can not exceed 2.1mA. Thus, they consume limited electrical power. The temperature sensor LM35CAH is manufactured by using the technology of an integrated circuit (IC) and can operate on a direct-current electricity of +5V. Its current drain is less than 60μA. In addition, most of the electronic devices of the DAQ system are in an integrated circuit (IC). They operate on a direct-current electricity of +5V and consume a little power at the level of a milliwatt. For example, the power consumed by the ADC16061 is 390mW. Hence, the electronic system of a smart wheel can satisfy the requirement of electrical power mentioned in section 1.3.

In the design of a smart wheel, the present research utilizes commercial sensors and common electronic devices. Most of them have low costs. In addition, some modules and functions are implemented by using software. This method decreases the hardware cost and simplifies the process of optimizing the systemic performance. Hence, the design of the electronic system effectively controls the cost while achieving the proposed functions.

3.7 Summary

The electronic system is the most important part of a smart wheel because it executes the function of measuring a driver's physiological parameters. Its performance determines (1) whether a driver's condition can be measured by using a smart wheel and (2) the accuracy in the measurement of a driver's physiological parameters. After comparing the available methods of sensing, the PVDF film sensor, analog semiconductor temperature

and tactile piezo-resistive sensor are selected to design the smart wheel because their features are more suitable than the other sensing methods. Next, the DAQ system requires a sampling frequency of 200 Hz per sensor and a resolution of 16 bits. In addition, the hardware can be established by using an embedded microprocessor system, an A/D converter, 3 multiplexers and operational amplifiers. The software can execute the comparison of the output of the sensors, the compensation for the temperature and the gripping force, filtering of the noise signal, the separation of the pulse wave and breathing wave, and the calculation of the driver's physiological parameters. Finally, the electronic system consumes limited electrical power and has low cost. Hence, the electronic system of the smart wheel can reliably measure and evaluate a driver's condition during daily driving and achieves a good cost/performance ratio.

Chapter 4 Mechanical design of the smart wheel

4.1 Introduction

Generally, the mechanical structure of a common steering wheel includes a rigid circular ring, a hub and 2, 3 or 4 spokes. The circular ring is manufactured by bending a tube. The hub is fixed on the steering shaft or the steering column and provides the position for installing an airbag. The spokes connect the circular ring and the hub. The cross-sections of the circular ring and spokes may be solid, tubular or have a u-channel. While driving, a driver grips the circular ring and rotates it about the hub. The moment of the couple is transmitted to the steering mechanism by the steering shaft or steering column. Then, the driver can control the motion direction of the vehicle. In the case of the smart wheel, many sensors are installed. They require a special mechanical structure that is different from that of the common steering wheel.

This chapter first analyzes a driver's steering behavior during driving and then presents the design of the mechanical structure of a smart wheel. Finally, it discusses the application of engineering aesthetics and ergonomics in designing a smart wheel.

4.2 A driver's steering behavior during driving

While driving, a driver may use simultaneously either one palm or both palms to grip and control the steering wheel, or he may use alternately one palm and then the other to grip and control the steering wheel. Figure 4.1 shows four of the possible behaviors. Generally, there is little likelihood that a driver will simultaneously remove both palms

from the steering wheel. This suggests that, during driving, a driver utilizes at least one palm to grip the steering wheel. Thus, it is possible to measure a driver's physiological parameters by employing a smart wheel. However, the location of a palm on the steering wheel is uncertain. The gripping force applied to the steering wheel is variable. Thus, the contact also is dynamic and variable. In addition, a vehicle is subject to complicated vibration due to the engine, suspension system, transmission system, road, tire, etc. The contact between a smart wheel and the driver's palms is also influenced by this vibration. Hence, the process is dynamic while a driver's physiological parameters are being measured by the smart wheel.

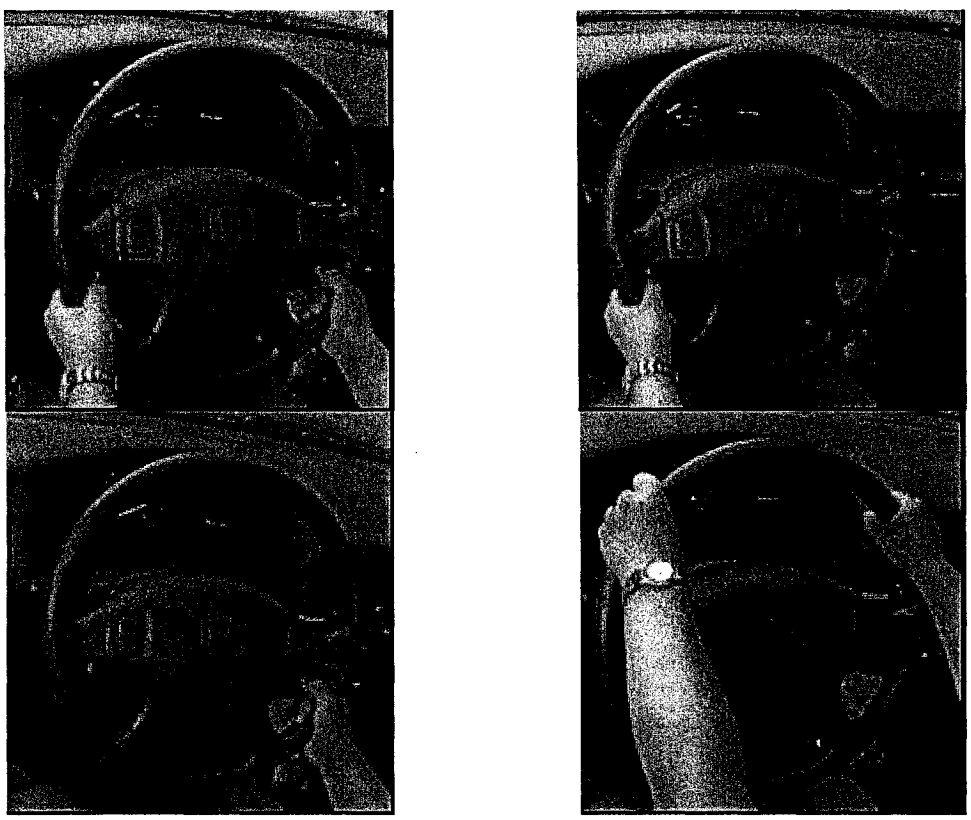

Figure 4.1 A driver's steering behavior during driving

4.3 Mechanical design

The smart wheel can measure a driver's condition while at the same time fulfilling the functions of a common steering wheel. The primary particularity in the mechanical design of the smart wheel derives from the sensors. The research presented in this thesis first addresses the design of this feature of the mechanical structure of a smart wheel (Figure 4.2).

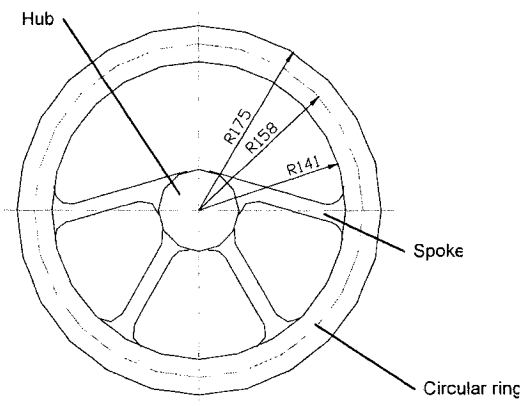

Figure 4.2 The mechanical structure of a smart wheel

The smart wheel is in most important regards similar to a common steering wheel. Its main mechanical structure is designed to withstand any and all stress that a driver may apply to it. Still, so far as the installation of the sensors is concerned, the smart wheel does require some special structures (Figure 4.3). The surface of the circular ring is bisected into an inner part and an external part by a median circle 158mm in radius. The section A-A of the circular ring is a disk a small part of which is exscinded by a chord BC, which belongs to the inner surface. Chord BC is the resting position of the fingers while a driver's palm is gripping the circular ring. In order to install the PVDF film sensor, some rectangular grooves, e.g. groove #1 of Figure 4.3, are produced on the plane

part of the inner surface due to chord BC. The groove has a width of 4mm, a depth of 2mm and a circumferential length of 32mm. The circumferential distance between the two adjacent grooves is 9.4mm. Thus, the whole circumference, excepting the positions of the spokes, can arrange 17 grooves in series. In addition, the other circular grooves, e.g. groove #2 of Figure 4.3, are produced on the external face. Groove #2 has a diameter of 6 mm and a depth of 3 mm so that a temperature sensor, LM35CAH, can be installed in it. The circumferential position of each groove #2 is determined by its corresponding groove #1. Both of them can be bisected by utilizing a vertical section involving the central point O such as A-A of Figure 4.3.

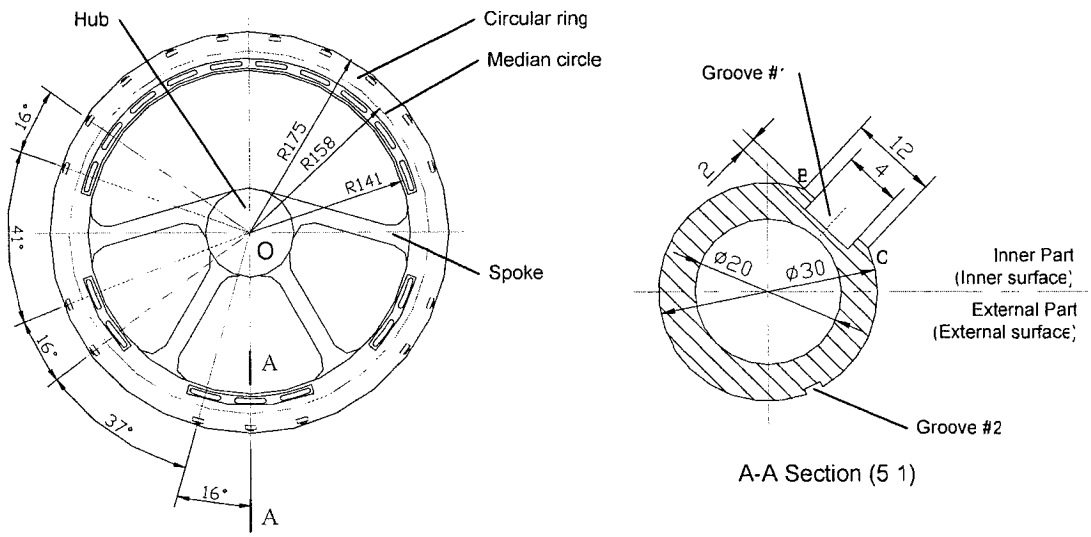

Figure 4.3 The detailed design of a smart wheel before installing sensors

Then, each groove #1 is covered with a PVDF film sensor by using special adhesives such as acrylic adhesives and synthetic rubber resins. As explained in section 3.2.2.3, groove #1 can greatly increase the output of a PVDF film sensor. Next, each groove #2 is installed with a LM35CAH. Moreover, a gripping force sensor is stuck to the external

surface between groove #1 and #2 with a professional glue (Figure 4.4). Then, the three sensors make up a sensor group and can be bisected by employing the same vertical section involving the central point O. Since the sensors in the same sensor group are very close, they can simultaneously contact the palm when anyone of them is gripped by a driver. Thus, the temperature sensor can provide an effective signal for the temperature compensation for the piezo-resistive sensors and PVDF film sensor while it measures the driver's skin temperature. The piezo-resistive sensor can output a reliable signal for the gripping force compensation for PVDF film sensor while it measures the driver's gripping force.

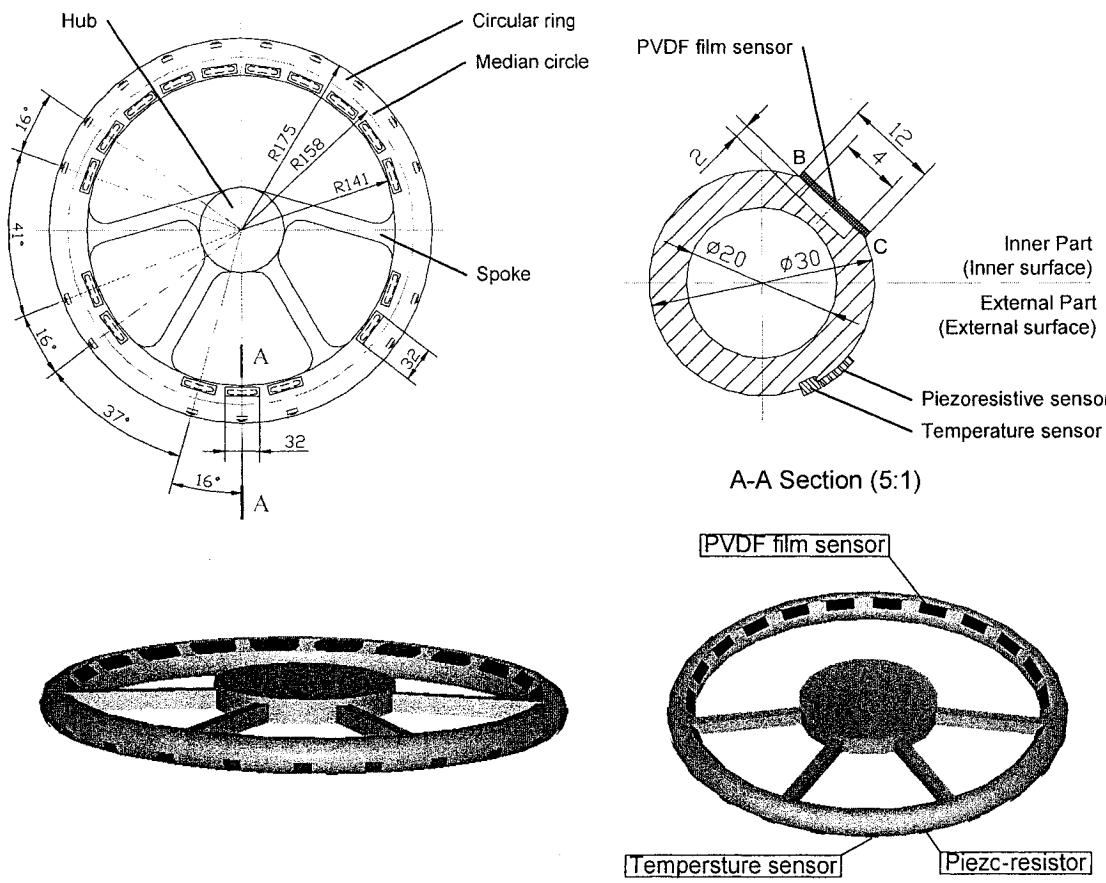

Figure 4.4 The detailed design of a smart wheel after installing sensors

Finally, Kroemer [2001] has ascertained that the hand breadth is 73.4mm for 5% of women, 83.6mm for 5% of men, 85.6mm for 95% of women, and 97.6mm for 95% of men. To guarantee that a palm contacts a group of sensors at all times, the maximum circumferential distance between two sensor groups can not exceed $(73.4-2\times L_{Max})$ in which L_{Max} is the maximum circumferential length of the three sensors of a sensor group (Figure 4.5). The design above satisfies this requirement.

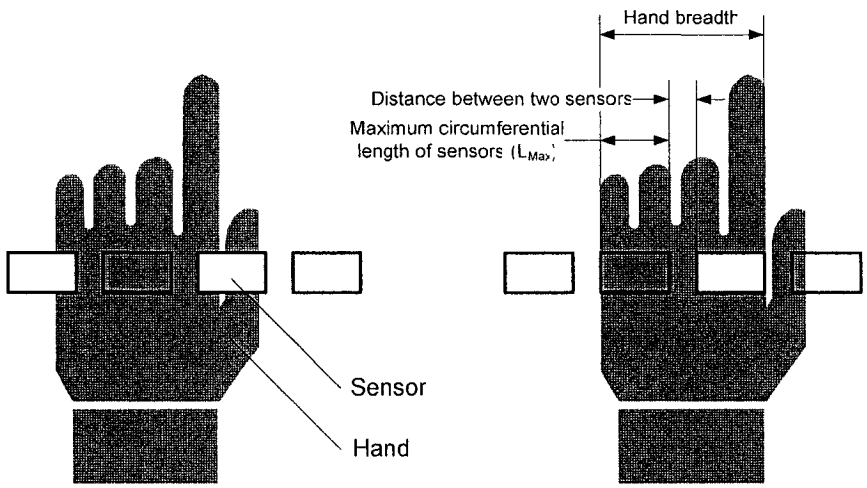

Figure 4.5 Determine the length and distance of sensors

4.4 Engineering aesthetics and ergonomics of the smart wheel

Up to the present day, aesthetics has played an important role in industrial design. Engineering aesthetics studies how to use scientific methods to study aesthetic concepts in engineering design and how to apply the principles of aesthetics in the area of engineering [Liu, 2003]. The theoretical foundation deals mainly with philosophy, psychophysiology, cognitive and social theories, ecology, etc.

The smart wheel has a symmetrical and proportional structure and works in good harmony with the driver's palms. The driver can easily and comfortably grip and rotate it as if using a common steering wheel. The PVDF film sensor of the smart wheel has a rectangular shape and can take on diverse colors if the protecting film selects different colors. The piezo-resistive sensor is circular in shape and an extra layer of different colors can be deposited on it. The temperature sensor of the smart wheel selects the type of metal can package since the package has a strong mechanical structure and a smooth surface. To eliminate visual distractions, it is better to assign the color of the circular ring to all the sensors. Then, the driver can ignore the colors and shapes of the sensors. In addition, the depth at which the temperature sensor is embedded is determined by two necessities. The first is to ensure a reliable approach to the skin of palm. The second is to decrease the uncomfortable stimulus to the driver. As solutions to these problems, the surface of the circular ring can be changed from uniform to wavy. With such a change, the surface would be better fitted to a driver's hand parts such as the thenar pad and the fingers. The waviness along the circular ring produces a "form-fit" that can strengthen the contact between the sensors and the driver's palm and can increase the resistance of the sliding palm. Hence, the smart wheel can achieve good engineering aesthetics and ergonomics by improving the external design.

4.5 Summary

In this chapter are presented the designs of the mechanical structure of a smart wheel based on the analysis of a driver's steering behavior. The design takes into account the appropriate installation of the sensors and guarantees the contact between a driver's palm

and at least one sensor group. Thus, the contact is reliable even though the driver may continuously engage in changing the gripping position during driving. In addition, the engineering aesthetics and ergonomics of the smart wheel are discussed and are applied to improve the mechanical design. The special mechanical structure must be taken into account if the smart wheel is to measure a driver's physiological parameters continuously during driving. By improving the exterior design, a smart wheel can achieve good engineering aesthetics and ergonomics.

Chapter 5 Application of the smart wheel to the monitoring of a driver's condition

5.1 Introduction

Common sense suggests that a driver's heart rate changes as the driving scenario alters. In addition, the heart rate is usually utilized to indicate whether the driver is strained, nervous, or sleepy, etc. However, most previous studies employ an electrocardiograph (ECG) to record and measure a driver's heart rate. An ECG, which requires that some electrodes be attached to a driver's skin, is not convenient and may influence the subject's natural behavior and condition. To eliminate the influence of instruments, the present research employs a smart wheel to monitor a driver's pulse rate, which represents the heart rate. The objective is to investigate how a driver's pulse rate changes in a typical driving scenario.

This chapter first describes the methodology of the research and then explains how to establish a virtual reality system to simulate a vehicle and driving scenarios. Finally, this chapter explains the process of analyzing data in this research.

5.2 Methodology

The present research monitors a driver's pulse wave while he drives in a certain driving scenario and then utilizes the appropriate method to calculate his pulse rate against time. Based on the curve of his pulse rate, the changes in the driver's pulse rate in different

driving scenarios can be compared. To increase the experimental efficiency and economize on resources, the present research establishes a virtual reality system to simulate a vehicle and three typical driving scenarios: the single line, the double line and the sinusoidal line. By using this virtual reality system, which provides a reasonable and low-cost approach to reality, a driver can approximately perform the actual driving in a laboratory. Simultaneously, a smart wheel is utilized to measure his pulse wave while he drives the virtual vehicle. However, the skin temperature and the gripping force are not required. The data of the driver's pulse wave is recorded in a certain Excel file for later analysis instead of being processed immediately. In order to speed up the software of the smart wheel and save more computer resources for the virtual reality system, optimizing the software of the smart wheel is worthwhile.

5.3 Typical driving scenarios

A driver may experience a large number of driving scenarios in daily traffic. It is difficult to simulate and analyze all of them. In research dealing with driving, several typical scenarios have usually been investigated in accordance with certain objectives. A single line, a double line and a sinusoidal line are frequently utilized in the research of drivers since most driving scenarios can be decomposed into these three lines the results of which are representative. The present research also utilizes these three scenarios.

(1) Single line

A single line refers to a single-lane change maneuver, which is a common operation during driving (Figure 5.1). For example, a driver changes his/her lane from a slow lane

to a fast lane. Generally, a single line consists of three segments: (1) a longitudinal segment before the lane change (AB). The driver collects the information about the ambient traffic and determines whether and when a single-lane change can be executed; (2) a diagonal segment during the lane change proper (BC). During this segment, the driver carefully controls the forward direction of the vehicle since the vehicle speed is possibly high; (3) a longitudinal segment after the lane change (CD). The driver controls the vehicle speed and follows the anterior vehicle.

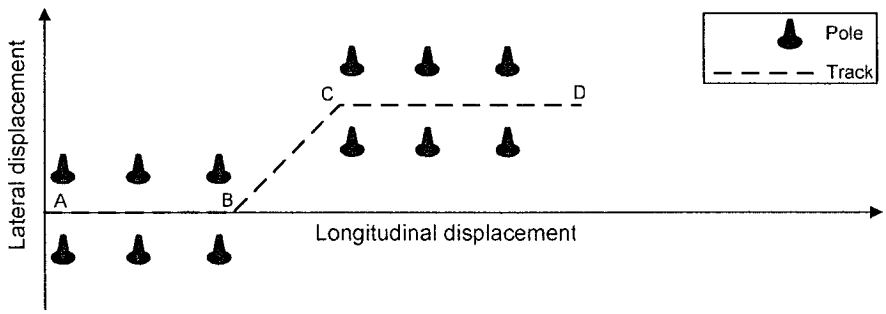

Figure 5.1 A single line

(2) Double line

A double line refers to a double-lane change maneuver, which is a frequent operation while driving (Figure 5.2). For example, a driver overtakes an anterior vehicle or avoids an anterior roadblock. A double-line includes five segments: a longitudinal segment before the first lane change (AB), a diagonal section during the first lane change (BC), a longitudinal segment after the first lane change (CD), a diagonal section during the second lane change (DE), and a longitudinal segment after the second lane change (EF). In AB and CD, the driver observes the ambient traffic and decides whether and when he/she changes lanes. In BC and DE, the driver must carefully control the forward

direction. In EF, the driver keeps the direction and follows the anterior vehicle. Theoretically, a double line can not be described as a combination of two single lines because the former consists of two consecutive lane changes.

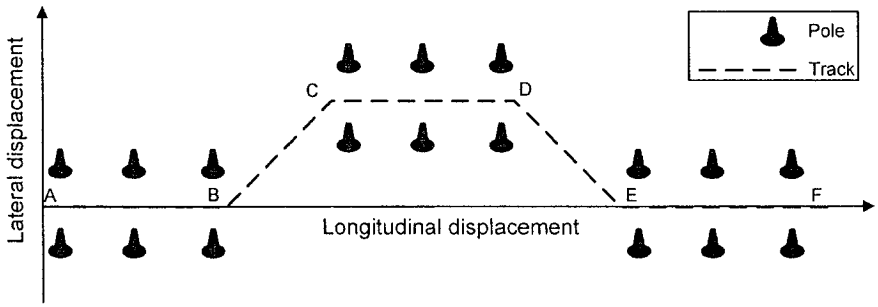

Figure 5.2 A double line

(3) Sinusoidal line

A sinusoidal line refers to a movement along a continuous sinusoidal track (Figure 5.3). It includes many turning maneuvers. A sinusoidal line is useful in evading obstacles or evaluating the dynamic characteristics of a vehicle, etc. During the whole track, the driver quickly collects information about the ambient environment and then controls the forward direction and the speed of the vehicle. Thus, the challenge for the driver is greater than that in single-line and double-line changes.

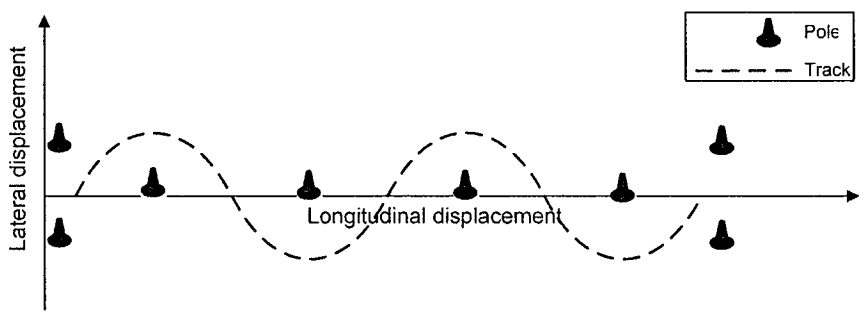

Figure 5.3 A sinusoidal line

The present research attempts to investigate the influence of the scenarios above on the variance of the driver's pulse rate. To decrease the number of contributing factors, in the experimental scenarios there are no traffic signs and no other vehicles, except one virtual vehicle. Then, a driver's pulse rate is influenced only by the track of the driving scenarios.

5.4 The virtual system of simulating vehicle and driving scenarios

5.4.1 Introduction of the virtual system

A virtual system is a reasonable approximation of an actual system. Commonly, it consists of a computer that runs the simulation software and communicates with the external devices. The external devices can interact with the external world in a realistic manner. A virtual system has enough accuracy in simulating reality since it follows the physical theory of the actual system. Its advantages consist of the following: (1) modifying the design of the system is easier and more convenient in a virtual system; (2) a virtual system can effectively decrease the cost and period of design; (3) it eliminates the difficulty of optimizing a complicated system; (4) it can expose the mistakes earlier and save costs incurred by mistakes; (5) It can simulate the extreme operations or status with little cost and enough safety; (6) It can be used in training and testing. Thus, the use of virtual systems is widespread in the field of engineering and research. Generally, virtual systems can be classified into three categories: (1) a virtual prototype, which does not engage in real-time interaction with the external environment; (2) a virtual reality (or virtual environment), which engages in real-time interaction with one or more people; (3) a hardware-in-the-loop (HIL) simulation, which engages in real-time interaction with

hardware and updates much faster than the system of virtual reality. Consequently, the present research utilizes a virtual reality system to simulate driving a vehicle in typical scenarios.

5.4.2 The design of a virtual reality system

5.4.2.1 Overall design

In the present research, the virtual reality system combines multi disciplines such as computer engineering, the dynamics of vehicles, electronic engineering, etc. It can simulate real-time and dynamic scenarios of three dimensions (3D). While the driver rotates the smart wheel to follow the track of a virtual scenario and adjust the accelerator and brake to control the speed, the virtual vehicle performs according to the dynamics of a real vehicle. The virtual 3D scene before the virtual vehicle has depth perception and shading and continuously changes with the direction and the location of the virtual vehicle. Generally, while a driver executes an operation, the virtual system requires time to calculate and regenerate the new 3D scene and so causes some delay. The time delay should be as small as possible. In addition, it is not easy to obtain smooth 3D animation by using a computer system since the calculation is complicated. Hence, the difficulty of the virtual system includes the appropriate dynamic model of the vehicle, conformation of typical scenarios and vivid 3D animation.

5.4.2.2 The hardware configuration

To provide interacting tools and to simulate the typical scenarios, hardware is required. The hardware of the virtual reality system consists of a smart wheel, an accelerator (i.e.

gas pedal), a brake (i.e. brake pedal) and a desktop computer (Figure 5.4). The smart wheel is used to control the motion direction of the virtual vehicle and measure the driver's pulse wave. The accelerator and the brake are used to adjust the speed of the virtual vehicle. The desktop computer is the platform that runs the simulation software. The accelerator and the brake are integrated into one device and employ one 9-pin serial connector to connect with the smart wheel. The smart wheel can communicate with the desktop computer by using a universal serial bus (USB) connector (Figure 5.4). The desktop computer requires a strong hardware configuration and has a high performance in calculation and 3D graphics since the simulation requires a good deal of 3D real-time animation.

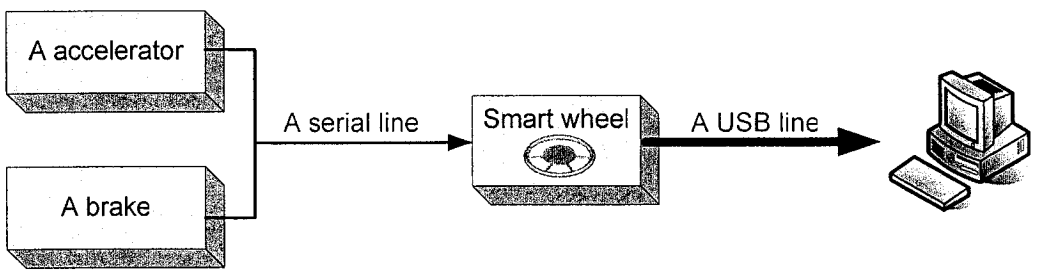

Figure 5.4 The hardware configuration of a virtual reality system

5.4.2.3 Software design

Generally, the software of the virtual reality system includes four important functions: (1) the communication with the smart wheel; (2) a dynamic model of an actual vehicle; (3) the generation of 3D scenes and animation; (4) the output of simulating data. At the beginning of a driving scenario, the software initializes the position, speed and forward direction of the virtual vehicle and generates a 3D scene. A driver utilizes the smart

wheel and pedals to input a new forward direction and the speed of the virtual vehicle to the vehicle model, respectively. The vehicle model calculates the successive position and the visual angle. Based on these calculations, a new 3D scene is generated. Simultaneously, the longitudinal displacement, the lateral displacement of the virtual vehicle, and the time are recorded in an Excel file for later analysis (Figure 5.5).

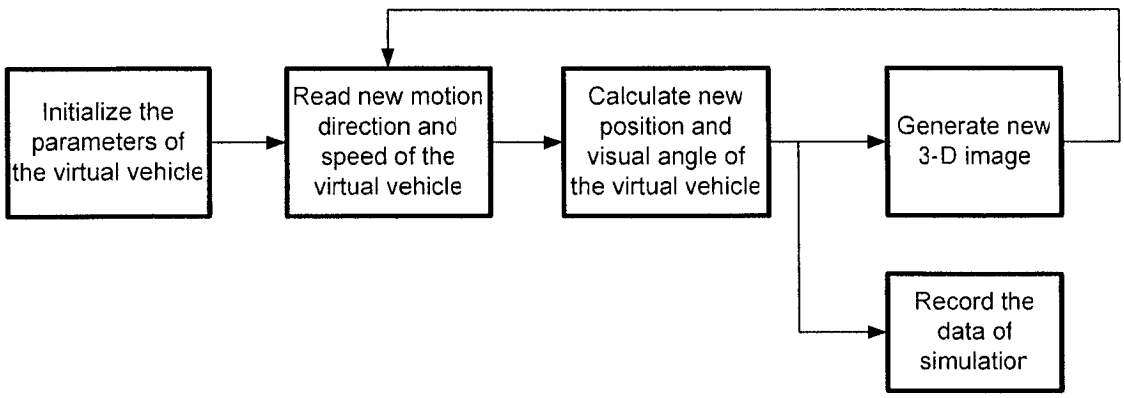

Figure 5.5 The flow chart of the simulation software

In the field of virtual reality, Microsoft DirectX is an important tool for developing applications. It provides a series of standard multimedia application programming interfaces (APIs) for a Windows platform. By using it, software developers can access specialized hardware features and do not require hardware-specific code. The present research utilizes DirectX and C++ to develop the software of the virtual reality system.

(1) Module for communicating with the smart wheel

In the present research, the smart wheel is an input device of the virtual reality system. It transfers a driver's operation into digital data, which includes the steering angle, the position of the accelerator, and the position of the brake. Then, the computer can process

the driver's operations and produce a response. In addition, for better simulation, the smart wheel can output force or vibration according to the software. The communication between the smart wheel and the computer requires Microsoft DirectInput, which is an API for input devices such as mouse, etc, as well as for force-feedback (input/output) devices.

(2) The dynamic model of the vehicle

An object in virtual reality responds to external stimuli according to certain dynamic models of the physical world and is not independent. It is a part of the main difference between virtual reality and pure animation. For instance, while braking, a vehicle in virtual reality continues moving for some time and shows a certain displacement before coming to a complete stop. The inertia of moving objects induces this phenomenon in the actual world. However, a vehicle in pure animation can completely stop at once. Hence, the virtual reality system of the present research requires an appropriate dynamic model of a vehicle that is a mathematical model identifying the behavior and performance of the vehicle under certain road conditions and operations.

To simplify the deduction, it is assumed that the virtual vehicle is moving on flat ground. The present position of a vehicle is defined by (x_0, y_0). The new position after time Δt is (x_t, y_t). Assume the components of the displacement of the virtual vehicle are D_x in the direction of x and D_y in the direction of y. Then, $x_t = x_0 + D_x$, $y_t = y_0 + D_y$. If the displacement of the virtual vehicle can be calculated, the new position is determined. The input parameters of the vehicle model consist of speed, steering angle and time. The

vertical displacement, roll angle, and pitch angle of the virtual vehicle are constant and zero. Thus, the present research selects the bicycle-model, the simplest dynamic model of a vehicle. The model employs one tire to represent the pair of tires on an axle. The center of mass of the vehicle is located between the front axle and the rear axle (Figure 5.6). When a steering angle δ_F is input, the motion direction of the vehicle is changed. However, the yaw angle is different from the steering wheel because of the dynamic characteristics of the vehicle. The present research utilizes the forth-order Runge-Kutta method to solve the mathematical model of the bicycle-model and calculate the displacement of the virtual vehicle. Finally, the module of the vehicle is developed by using C++.

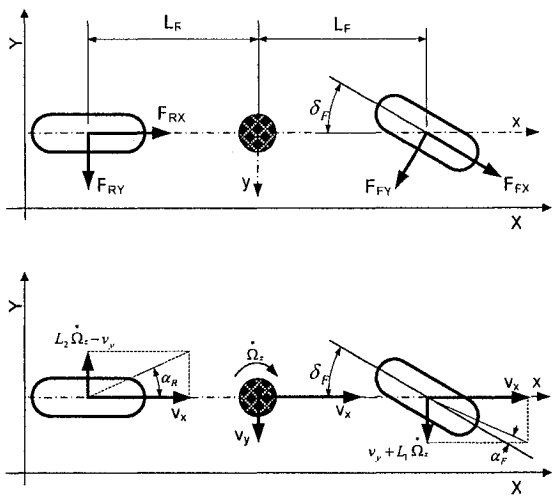

Figure 5.6 The bicycle model

(3) The module for generating the 3D image

After calculating the new position and view angle of the virtual vehicle, the module for generating the 3D scene updates the present scene. The main structure of this module

employs the technology of Microsoft Direct3D, which consists of Component Object Model (COM) objects and interfaces. In the present research, a 3D scene includes ground, road, numerous trees, sky and a virtual vehicle. The ground is planar and is produced by overspreading numerous textured triangles of which the texture is meadow. The road consists of overspread textured triangles with the texture of concrete and has two lanes, which are emphasized by using a white left boundary, a white right boundary and a yellow lane line (Figure 5.7).

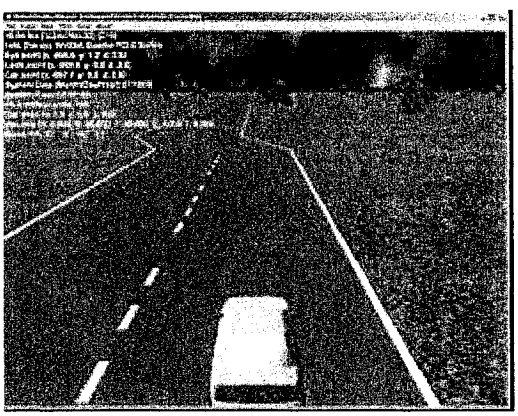

Single line

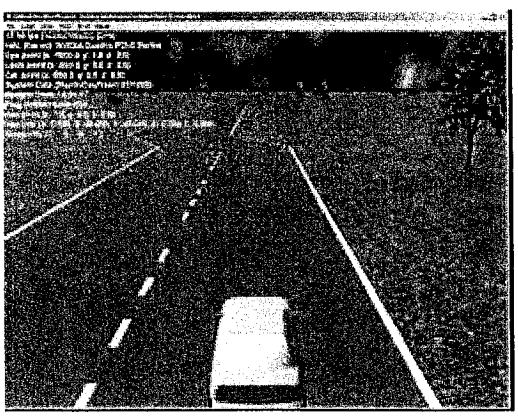

Double line

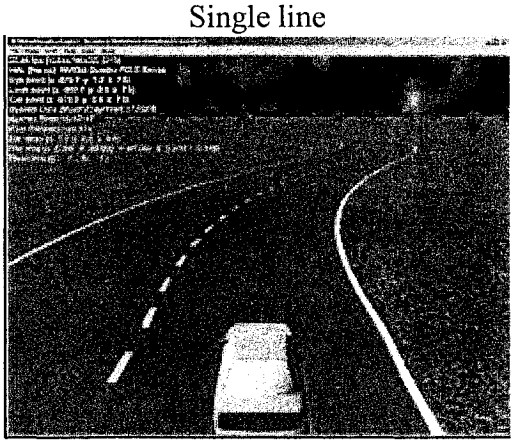

Sinusoidal line

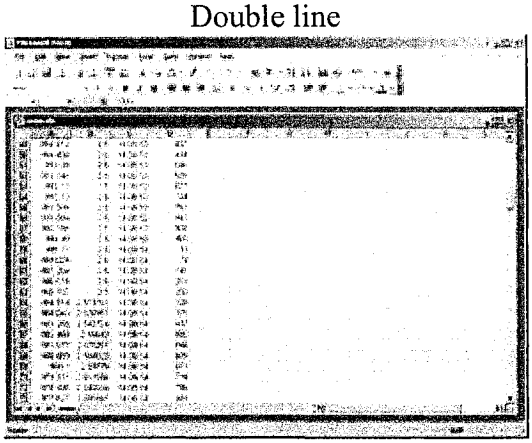

A data File

Figure 5.7 The driving scenarios and a data file of the virtual reality system

To simulate the three typical scenarios, the software design includes three kinds of roads: a single line, a double line and a sinusoidal line. While one of the scenarios is being simulated, the corresponding road is generated. The trees, which have random colors and sizes, are 2-D pictures and are randomly placed along the road. The sky consists of a blue background and randomly moving clouds. The virtual vehicle has the approximate shape of a sedan. The location and the angle of viewing can be adjusted by using the menu. The default setting is the rear upper position of the virtual vehicle. In addition, light is an important factor of a virtual scene since appropriate light and shading can effectively enhance the 3D scene and the animation. If objects in a scenario are illuminated by certain types of light, Direct3D can calculate the color of each object vertex based on (1) the current material color and the texels; (2) the diffuse and specular colors at the vertex; (3) the color and intensity of light due to light sources in the scene; (4) the scene's ambient light level. The result remarkably influences the appearance of the rendered scene.

(4) The module for outputting the data

The software utilizes this module to record time, longitudinal displacement and lateral displacement and then to store the data into an Excel file for later analysis (Figure 5.7). Then, the actual track of the virtual vehicle can be described by using the curves of the lateral displacement versus the longitudinal displacement or versus the time. The software of the smart wheel runs independently and has no relationship with that of the virtual reality system. The driver's pulse wave is stored in another Excel file. Thus, time is required to relate the position of the virtual vehicle to the driver's pulse rate. If the

position of the vehicle and the driver's pulse rate at a certain time are (x_t, y_t) and $P_{ulse\_beat\_t}$, it means that the driver's pulse beat is $P_{ulse\_beat\_t}$ while he is driving the virtual vehicle and passing the position (x_t, y_t).

5.5 Data analysis

After obtaining a driver's curve of the pulse rate and the track of the virtual vehicle, the next step is to analyze the relationship between both of them.

(1) Analysis tool

The present research chooses MATLAB to analyze the data. MATLAB is a widespread software in the field of technical computing and can enable engineers or researchers to execute intensive computing tasks faster than with traditional programming languages. It provides (1) numerous mathematical functions for linear algebra, statistics, Fourier analysis, filtering, optimization, and numerical integration; (2) 2-D and 3-D graphics functions for visualizing data; (3) tools for developing personnel interface and functions for communicating with external applications and languages, such as Microsoft Excel, C++. Hence, the present research develops a special MATLAB program to read and process the data stored in Excel files and to plot the result in graphics.

(2) Format of data file

Large capacity, good compatibility and easy usage are the important factors in determining the format of the data file of the present research. The software of the smart wheel outputs Excel files. The C++ provides special functions for the easy processing of

an Excel file. MATLAB can conveniently read an Excel file by using certain functions. Moreover, Excel is also a convenient software with the function of computing. This function is useful in converting the data from one type to another or in preprocessing the data. Hence, all data files in the present research are Excel files.

(3) The index of evaluating the variance of a driver's pulse rate

To evaluate the acute level at which a driver's pulse rate changes, there are two candidates for the index. Candidate No.1 is the difference between the maximum and the minimum of a driver's pulse rate. Candidate No.2 is the standard deviation of a driver's pulse rate. Candidate No.1 ignores the frequency with which a driver's pulse rate changes and possibly induces the wrong conclusion. For example, there are two cases: (1) a driver's pulse rate changes one time from 60 bpm to 80 bpm in 3 minutes and (2) a driver's pulse rate changes three times from 60 bpm to 75 bpm in 3 minutes (Figure 5.8).

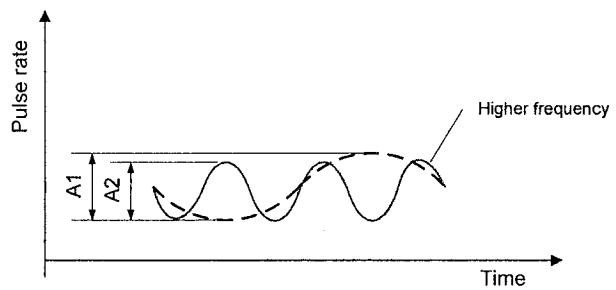

Figure 5.8 Indexes for evaluating the variance of a driver's pulse rate

According to candidate No.1, case #1 is more acute than case #2 because the changing amplitude of case #1, A_1, is larger. The result is contrary to the fact. In addition, according to common sense, the frequent change of the pulse rate enables human to feel

tired more easily than occasional changes of the pulse rate because the cardiovascular system must continually adjust the work rhythm. Hence, candidate No.2 is more reasonable and can eliminate the potential mistake of candidate No.1. The present research utilizes candidate No.2 to evaluate the acute level of the variance of the driver's pulse beat.

5.6 Summary

This chapter discusses how to utilize a smart wheel to monitor a driver's pulse rate and to investigate the relationship between the standard deviation of a driver's pulse rate and the driving scenarios. It indicates that the results of a single line, a double line and a sinusoidal line are applicable to numerous driving scenarios. In addition, the investigation can be performed in the laboratory by employing a smart wheel and a virtual reality system. The software of the virtual reality system employs the technologies of DirectX and a bicycle model of a vehicle. The simulation data can be analyzed by using MATLAB.

Chapter 6 The experimental evaluation of the smart wheel

6.1 Introduction

An experiment is a test in which the input variables of a process or system are purposely changed so that the reasons for the changes in the output response are observed and identified. Before an experiment is performed efficiently, the experiment should be designed according to a scientific approach: the statistical design for experiments. Then, the data that is collected in the experiments can be analyzed by statistical methods, and can result in valid and objective conclusions.

A smart wheel is a new instrument for monitoring a driver's condition. It requires experiments to verify the principle and performance. Firstly, this chapter states the experimental purpose and the experimental questions. Next, it designs the experiments by using statistical methods. Then, it explains the detailed experimental hardware and software. After describing the analysis tools, the chapter explains the experimental results and conclusions.

6.2 Experimental purposes

According to previous studies, it is suitable to use the semiconductor temperature sensor to measure a driver's skin temperature. The piezo-resistive sensors selected in the present research are frequently utilized in studies and applications to measure a human's gripping force. Some professional DAQ system has been developed to measure and analyze the force applied to the piezo-resistive sensor. Thus, there is no experiment designed to

investigate their principles and performance in the present research. Moreover, the frequency of the driver's breathing wave is about 20% that of the pulse wave. Measuring the breathing wave requires a stronger hardware configuration, which is not available in the present research because of the limitation of resources. However, the principle is the same as that used in measuring the pulse wave. Hence, the following experiments are focused on verifying one of the functions of the smart wheel: measuring a driver's pulse wave.

In addition, the pulse beat is an important parameter of the pulse wave and can be manually measured in a wrist artery. The manual method of measuring the pulse rate is usually used in primary medical examinations. Its output can be a reasonable reference for verifying the output of the smart wheel. Thus, the experimenter can simultaneously use a hand and the smart wheel to measure a subject's pulse beat and can then evaluate the performance of the smart wheel by comparing the data from both methods. However, a subject's pulse rate is influenced by many factors such as strong exercise and excitement. It may change with time under some situations. The change of a subject's pulse rate may increase the experimental error. Thus, a subject requires a period of rest before the experiments.

According to section 3.2.2.6, the gripping force, vibration and ambient temperature are the main disturbances in the measurement of a pulse wave. Since all experiments are performed in the laboratory the temperature of which is stable, the disturbance of the

temperature can be ignored.. Hence, the experimenter mainly investigates how the gripping force and the vibration disturb the measurement of the pulse wave.

Finally, the experiments are designed to achieve three purposes: (1) verify that the smart wheel has the same output as in the manual method while the pulse rate is being measured; (2) investigate the effect of the gripping force and the vibration on the difference between the observations of both methods; (3) investigate the effect of an experimental scenario on the standard deviation of a driver's pulse rate by using a smart wheel.

6.3 The design of the experiments

One of the important benefits of experimental design is the systematic control of the disturbance arising from known sources. It commonly consists of seven steps: (1) Understand and clarify the problem; (2) Define the factors and levels; (3) Determine the response variable; (4) Select the appropriate experimental design; (5) Perform the designed experiments; (6) Analyze the experimental data; (7) Induce reasonable conclusions. The basic principles are replication, randomization and blocking. Replication, which means replicating the basic experiment, is different from repeated measurements. For example, factor A has three levels. While the same subject's height is measured twice in each level of factor A, the two measurements are repeated measurements; while the same subject's height is measured once in each of the three levels of factor A, respectively, the three measurements are one replication. Replication is useful in estimating experimental error and factorial effect. Randomization is the

fundament of statistical methods in experimental design and suggests that the order of experiments is randomly selected. Blocking means that a certain group of experiments uses a batch of homogeneous samples so that the experimental error due to inhomogeneous samples is decreased. Some basic concepts of the statistical hypothesis test are explained in Appendix A. In addition, the experimental unit of the present research is the people who are called "subject". Under the same treatment or measurement, the observations made of different people may be highly different due to their race, region, experience, etc. The differences between people will produce experimental error if not controlled. Thus, it is better to design the experiments by using repeated measures design in which each of the treatments or measurements is applied to each subject. The method is widely used in the experiments of physical, social and behavioral sciences, etc.

(1) Experimental group 1

Experimental group 1 serves two purposes: (1) verifying the output accuracy of a smart wheel and (2) investigating the effect of the gripping force and the vibration on the accuracy. However, these purposes require different statistical methods. This section firstly describes their theoretical deductions and then explains the experimental scenario, procedure, subjects, and data recording.

To verify the output accuracy of the smart wheel, a good solution is to compare its output with that of the manual method while a subject's pulse rate is being measured by simultaneously utilizing both methods. Cugini *et al.* [2000] have stated that a clinically

healthy subject's pulse rate has a standard deviation of 5 beats per minute (bpm). This means that the subjects differ in their pulse rate. The difference between subjects is a contributing factor to the variance of the experimental data in addition to the random error. In order to decrease the experimental error by as much as possible, the experimenter utilizes the repeated measures design of a single factor to design the experiments. The experimental factor is the method of measuring the pulse rate and consists of two levels: the smart wheel and the manual method. Theoretically, the order of applying each method to the same subject is random. However, in this case, there is no necessity of randomizing the order of applying methods to the same subject because the experimenter measures each subject by simultaneously using both methods. Then, the observations of the repeated measures design can be described by using Table 6.1.

Table 6.1 Observations of experiments designed by using repeated measures design of single factor

Factorial level ↓		Subject No.				Factorial totals
		1	2	···	n	
1	Manual method	y_{11}	y_{12}	···	y_{1n}	$y_{1\bullet}$
2	Smart wheel	y_{21}	y_{22}	···	y_{2n}	$y_{2\bullet}$
Subject Totals		$y_{\bullet 1}$	$y_{\bullet 2}$	···	$y_{\bullet n}$	$y_{\bullet\bullet}$

The theoretical model of this design is

$$y_{ij} = \mu + \tau_i + \beta_j + \gamma_{ij} \quad \begin{cases} i = 1,2 \\ j = 1,2,\ldots,n \end{cases} \quad \text{[Montgomery, 2001]} \qquad (6.1)$$

Where y_{ij} is the observation, μ is the overall mean, τ_i is the effect of i th factorial level, β_j is the effect of j th subject, and γ_{ij} is the random error. It is noted that the factorial levels are fixed factors. The subjects are randomly selected from a large number of

potential subjects. A common assumption is that the effects of the factorial level and the subject have

$$\sum_{i=1}^{2}\tau_i = 0,\ \sum_{j=1}^{n}\beta_j = 0 \quad \text{[Montgomery, 2001]} \tag{6.2}$$

It is noted that the covariance between y_{1j} and y_{2j} is generally unequal to zero because β_j is common while all factorial levels are applied to the same subject. The covariance between y_j and y_j is usually assumed to be constant among all factorial levels and subjects. The experimental hypotheses are

$$H_0 : \mu_1 = \mu_2$$

$$H_1 : \mu_1 \neq \mu_2$$

or

$$H_0 : \tau_1 = \tau_2 = 0$$

$$H_1 : \tau_1 \neq 0 \ or \ \tau_2 \neq 0 \tag{6.3}$$

Say

$$y_{i\bullet} = \sum_{j=1}^{n} y_{ij} \quad i = 1,2 \tag{6.4}$$

$$y_{\bullet j} = \sum_{i=1}^{2} y_{ij} \quad j = 1,2,...,n \tag{6.5}$$

$$y_{\bullet\bullet} = \sum_{i=1}^{2}\sum_{j=1}^{n} y_{ij} = \sum_{i=1}^{2} y_{i\bullet} = \sum_{j=1}^{n} y_{\bullet j} \tag{6.6}$$

The average of the observations of ith factorial level $\bar{y}_{i\bullet}$, of the observations of jth block $\bar{y}_{\bullet j}$, of all observations $\bar{y}_{\bullet\bullet}$

$$\bar{y}_{i\bullet} = \frac{y_{i\bullet}}{n},\ \bar{y}_{\bullet j} = \frac{y_{\bullet j}}{2},\ \bar{y}_{\bullet\bullet} = \frac{y_{\bullet\bullet}}{2n} \tag{6.7}$$

The total sum of squares

$$\sum_{i=1}^{2}\sum_{j=1}^{n}(y_{ij} - \bar{y}_{\bullet\bullet})^2 = 2\times\sum_{j=1}^{n}(\bar{y}_{\bullet j} - \bar{y}_{\bullet\bullet})^2 + \sum_{i=1}^{2}\sum_{j=1}^{n}(y_{ij} - \bar{y}_{\bullet j})^2 \quad \text{[Montgomery, 2001]} \tag{6.8}$$

The sum of squares (SS) is defined

$$SS_T = \sum_{i=1}^{2}\sum_{j=1}^{n}(y_{ij} - \bar{y}_{\bullet\bullet})^2,\ SS_{Between\_subjects} = 2\sum_{j=1}^{n}(\bar{y}_{\bullet j} - \bar{y}_{\bullet\bullet})^2 \tag{6.9}$$

$$SS_{Within\_subjects} = \sum_{i=1}^{2}\sum_{j=1}^{n}(y_{ij} - \bar{y}_{\bullet j})^2 \tag{6.10}$$

Then

$$SS_T = SS_{Between\_subjects} + SS_{Within\_sunjects} \tag{6.11}$$

$SS_{Between\_subjects}$ and $SS_{Within\_sunjects}$ have a degree of freedom $(2n-1)$ and have statistical independence between them. And

$$SS_{Within\_subjects} = \sum_{i=1}^{2}\sum_{j=1}^{n}(y_{ij} - \bar{y}_{\bullet j})^2 = n\sum_{i=1}^{2}(\bar{y}_{i\bullet} - \bar{y}_{\bullet\bullet})^2 + \sum_{i=1}^{2}\sum_{j=1}^{n}(y_{ij} - \bar{y}_{i\bullet} - \bar{y}_{\bullet j} + \bar{y}_{\bullet\bullet})^2$$

[Montgomery, 2001] (6.12)

The sum of squares (SS) is defined

$$SS_{factorial\_level} = n\sum_{i=1}^{2}(\bar{y}_{i\bullet} - \bar{y}_{\bullet\bullet})^2 \tag{6.13}$$

$$SS_E = \sum_{i=1}^{2}\sum_{j=1}^{n}(y_{ij} - \bar{y}_{i\bullet} - \bar{y}_{\bullet j} + \bar{y}_{\bullet\bullet})^2 \tag{6.14}$$

Then

$$SS_{Within\_subjects} = SS_{factorial\_level} + SS_E \text{ or } SS_E = SS_{Within\_subjects} - SS_{factorial\_level} \tag{6.15}$$

where $SS_{factorial\ level}$ is statistically independent from SS_E.The degree of freedom of $SS_{Within\_subjects}$ is $n(2-1)=n$. Define

$$MS_{factoria\_level}=\frac{SS_{factorial\_level}}{2-1}=SS_{factorial\_level} \quad \text{[Montgomery, 2001]} \qquad (6.16)$$

$$MS_E=\frac{SS_E}{(2-1)(n-1)}=\frac{SS_E}{n-1} \quad \text{[Montgomery, 2001]} \qquad (6.17)$$

For testing the null hypothesis, the test statistic

$$F_0=\frac{MS_{factorial\_level}}{MS_E} \quad \text{[Montgomery, 2001]} \qquad (6.18)$$

If the null hypothesis is true, the probability distribution of F_0 is $F_{1,(n-1)}$. For a specified α, H_0 is rejected while $F_0 > F_{\alpha,1,(n-1)}$. Table 6.2 shows the important statistics of the analysis of variance for this case.

Table 6.2 The analysis of variance under repeated measures design of single factor

Source of variation	Sum of squares	Degrees of freedom	Mean square	F_0
Between subjects	$SS_{Between\_subjects}$	$n-1$		
Within subjects	$SS_{Within\_sunjects}$	n		
Methods of measuring pulse rate	$SS_{factorial\ level}$	1	$SS_{factorial\ level}$	$\frac{MS_{factorial\ level}}{MS_E}$
Error	SS_E	$n-1$	$\frac{SS_E}{n-1}$	
Total	SS_T	$2n-1$		

The next important issue is to choose the number of subjects. Verifying small effects generally requires more subjects than verifying large effects. In repeated measures design, the choice of the number of subjects depends on a parameter Φ and on operating characteristic curves for the fixed-effect-model analysis of variance. The curves draw the

β of a statistical test for a certain number of subjects versus Φ. Φ describes the degree at which the null hypothesis is false and

$$\Phi^2 = \frac{nD^2}{2\times 1\times \sigma^2} = \frac{nD^2}{2\sigma^2} \quad \text{[Montgomery, 2001]} \tag{6.19}$$

Where D is the possibly maximum difference between the means of observations of a smart wheel and the manual method, σ^2 is the variance of the random error. An unbiased estimator of σ^2 is a sample variance which is 25 beats per minute (bpm) [Cugini *et al.*, 2000]. The experimenter specifies $D = 3.8$beats/minute, $\alpha = 0.05$. Assume $n = 20$, $\Phi = 1.70$, the degree of freedom of error $(n-1) = 19$. The degree of freedom of factorial levels is $(2-1) = 1$. According to the operating characteristic curve for the fixed effects model analysis of variance, $\beta = 0.4$. The results of similar calculations are recorded in Table 6.3. Thus, the experiments require 30 subjects in order to achieve the power of 0.80.

Table 6.3 Choices of the number of subjects

n	Φ^2	Φ	$(n-1)$	β	Power=$(1-\beta)$
20	2.89	1.70	19	0.4	0.6
25	3.61	1.90	24	0.25	0.75
30	4.33	2.08	29	0.20	0.80

Verifying the effect of the gripping force and the vibration on the output accuracy of a smart wheel requires the method of factorial design, which is usually utilized to design experiments involving several factors. The purpose of factorial design is to evaluate the joint effects of the factors on a response. It investigates all possible combinations of the levels of all factors. The levels can be quantitative or qualitative such as 10°C and 20°C,

"high" and "low", etc. A change in the level of a factor produces a change in response, which is named the effect of the factor or a main effect. Possibly, the interaction among the factors results in that one factor has a different effect while the levels of the other factors change. For instance, the effect of factor A is 5 while the level of factor B is "low" and is 20 while the level of factor B is "high". This implies that there is interaction between the two factors. Generally, factorial designs are more efficient than experiments, which investigate the factors individually and in succession. The experiments for purpose (2) consist of two factors: gripping force and vibration. The gripping force has two levels: "high" and "low". To obtain a stable measurement of the pulse wave, the critical gripping force is required to keep the contact between a subject's palm and the PVDF film sensors although the force is small. The critical force is named "low" gripping force. "High" gripping force is a force the amplitude of which is larger than that of the critical force. The vibration also consists of two levels: "yes" and "no". These terms mean that a vibration is applied or is not applied, respectively. The vibration is produced by utilizing the experimental smart wheel and has a frequency of 35Hz. Then, the two factors have $2\times 2 = 4$ kinds of combinations. The number of subjects is specified as n. Each subject runs through four experiments each of which is executed under one of the four factorial combinations, respectively. This method is the repeated measures design of two factors. Table 6.4 describes the experimental observations. The design is a randomized complete block design because the order of the four observations of the same subject is randomly selected. The linear statistical model of this design is

$$y_{ijk} = \mu + \tau_i + \beta_j + (\tau\beta)_{ij} + \delta_k + \gamma_{ijk} \quad \begin{cases} i = 1,2 \\ j = 1,2 \\ k = 1,2,...,n \end{cases} \quad \text{[Montgomery, 2001]} \quad (6.20)$$

Where y_{ijk} is the observation, μ is the overall mean effect, τ_i is the effect of i th level of gripping force, β_j is the effect of j th level of vibration, $(\tau\beta)_{ij}$ is the effect of the interaction between τ_i and β_j, δ_k is the effect of n th subject, γ_{ijk} is the random error. The model ignores the interaction between the subject and the factorial combination. It is initially assumed that both factors are fixed and

$$\sum_{i=1}^{2}\tau_i = 0\,,\ \sum_{j=1}^{2}\beta_j = 0 \qquad \text{[Montgomery, 2001]} \tag{6.21}$$

$$\sum_{i=1}^{2}(\tau\beta)_{ij} = \sum_{j=1}^{2}(\tau\beta)_{ij} = 0\,,\ \sum_{i=1}^{n}\delta_k = 0 \quad \text{[Montgomery, 2001]} \tag{6.22}$$

Table 6.4 The observations of experiments designed by using repeated measures design of two factors

Gripping force ↓	Vibration							
	Yes				No			
	Subject No.				Subject No.			
	1	2	···	n	1	2	···	n
Low	y_{111}	y_{112}	···	y_{11n}	y_{121}	y_{122}	···	y_{12n}
High	y_{211}	y_{212}	···	y_{21n}	y_{221}	y_{222}	···	y_{22n}

The hypotheses about the effects of the gripping force at different levels are

$$(H_0)_A : \tau_1 = \tau_2 = 0$$

$$(H_1)_A : \text{at least one } \tau_i \neq 0 \tag{6.23}$$

The hypotheses about the effects of vibration at the different levels are

$$(H_0)_B : \beta_1 = \beta_2 = 0$$

$$(H_1)_B : \text{at least one } \beta_j \neq 0 \tag{6.24}$$

The hypotheses about the effects of the interaction between the gripping force and the vibration are

$$(H_0)_{AB} : (\tau\beta)_{ij} = 0 \quad \text{for all i,j}$$

$$(H_1)_{AB} : \text{at least one } (\tau\beta)_{ij} \neq 0 \tag{6.25}$$

Say

$$y_{i\bullet\bullet} = \sum_{j=1}^{2}\sum_{k=1}^{n} y_{ijk}\,,\ \bar{y}_{i\bullet\bullet} = \frac{y_{i\bullet\bullet}}{2n},\ i = 1,2 \tag{6.26}$$

$$y_{\bullet j\bullet} = \sum_{i=1}^{2}\sum_{k=1}^{n} y_{ijk}\,,\ \bar{y}_{\bullet j\bullet} = \frac{y_{\bullet j\bullet}}{2n},\ \ j = i = 1,2 \tag{6.27}$$

$$y_{ij\bullet} = \sum_{k=1}^{n} y_{ijk}\,,\ \bar{y}_{ij\bullet} = \frac{y_{ij\bullet}}{n},\ \ i = 1,2\,,\ j = 1,2 \tag{6.28}$$

$$y_{\bullet\bullet\bullet} = \sum_{i=1}^{2}\sum_{j=1}^{2}\sum_{k=1}^{n} y_{ijk}\,,\ \bar{y}_{\bullet\bullet\bullet} = \frac{y_{\bullet\bullet\bullet}}{2\times 2\times n} = \frac{y_{\bullet\bullet\bullet}}{4n} \tag{6.29}$$

where $y_{i\bullet\bullet}$ and $\bar{y}_{i\bullet\bullet}$ are the sum and mean of all observations at the i th level of gripping force, $y_{\bullet j\bullet}$ and $\bar{y}_{\bullet j\bullet}$ are the sum and mean of all observations at the j th level of vibration, $y_{ij\bullet}$ and $\bar{y}_{ij\bullet}$ are the sum and mean of all observations in the ij th combination, $y_{\bullet\bullet\bullet}$ and $\bar{y}_{\bullet\bullet\bullet}$ are the sum and mean of all the observations, respectively. Table 6.5 describes the statistics of the analysis of variance. The sum of squares (SS) is defined

$$SS_{Subject} = \frac{1}{4}\sum_{k=1}^{n} y_{\bullet\bullet k}^2 - \frac{y_{\bullet\bullet\bullet}^2}{4n} \quad \text{[Montgomery, 2001]} \tag{6.30}$$

$$SS_A = \sum_{i=1}^{2} \frac{y_{i\bullet\bullet}^2}{2n} - \frac{y_{\bullet\bullet\bullet}^2}{4n} \quad \text{[Montgomery, 2001]} \tag{6.31}$$

$$SS_B = \sum_{j=1}^{2} \frac{y_{\bullet j\bullet}^2}{2n} - \frac{y_{\bullet\bullet\bullet}^2}{4n} \quad \text{[Montgomery, 2001]} \tag{6.32}$$

$$SS_{AB} = \frac{1}{n}\sum_{i=1}^{2}\sum_{j=1}^{2} y_{ij\bullet}^2 - \frac{y_{\cdots}^2}{4n} - SS_A - SS_B \quad \text{[Montgomery, 2001]} \qquad (6.33)$$

$$SS_T = \sum_{i=1}^{2}\sum_{j=1}^{2}\sum_{k=1}^{n} y_{ijk}{}^2 - \frac{y_{\cdots}^2}{4n} \quad \text{[Montgomery, 2001]} \qquad (6.34)$$

$$SS_E = SS_T - SS_{Subject} - SS_A - SS_B - SS_{AB} \quad \text{[Montgomery, 2001]} \qquad (6.35)$$

Table 6.5 The analysis of variance under repeated measures design of two factors

Source of variation	Sum of squares	Degrees of freedom	Expected Mean square	F_0
Subjects	$SS_{Subject}$	$(n-1)$	$\sigma^2 + \sigma_\delta^2$	
Levels of gripping force	SS_A	1	$\sigma^2 + 2n\sum_{i=1}^{2}\tau_i^2$	$\frac{MS_A}{MS_E}$
Levels of vibration	SS_B	1	$\sigma^2 + 2n\sum_{j=1}^{2}\beta_j^2$	$\frac{MS_B}{MS_E}$
Interaction	SS_{AB}	1	$\sigma^2 + n\sum_{i=1}^{2}\sum_{j=1}^{2}(\tau\beta)_{ij}^2$	$\frac{MS_{AB}}{MS_E}$
Error	SS_E	$4(n-1)$	σ^2	
Total	SS_T	$(4n-1)$		

And

$$MS_A = \frac{SS_A}{1} = SS_A \quad \text{[Montgomery, 2001]} \qquad (6.36)$$

$$MS_B = \frac{SS_B}{1} = SS_B \quad \text{[Montgomery, 2001]} \qquad (6.37)$$

$$MS_{AB} = \frac{SS_{AB}}{1} = SS_{AB} \quad \text{[Montgomery, 2001]} \qquad (6.38)$$

$$MS_E = \frac{SS_E}{4(n-1)} \quad \text{[Montgomery, 2001]} \qquad (6.39)$$

If $(H_0)_A, (H_0)_B, (H_0)_{AB}$ are false (i.e. $(H_1)_A, (H_1)_B, (H_1)_{AB}$ are true),

$$MS_A > MS_E,\ MS_B > MS_E,\ MS_{AB} > MS_E \quad \text{[Montgomery, 2001].} \qquad (6.40)$$

Thus, testing the signification of both main effects and their interaction depends on the corresponding mean square over the error mean square, $\frac{MS_A}{MS_E}$, $\frac{MS_B}{MS_E}$ and $\frac{MS_{AB}}{MS_E}$.

Moreover, the distributions of $\frac{MS_A}{MS_E}$, $\frac{MS_B}{MS_E}$ and $\frac{MS_{AB}}{MS_E}$ are F distribution of which the degrees of freedom of the numerators are 1, 1, 1, respectively. The degree of freedom of the denominator is $(4-1)(n-1) = 3(n-1)$. The critical region is the upper tail of the F distribution. If the ratio is large, the null hypothesis is rejected.

In addition, an important step is to choose an appropriate number of subjects. While designing experiments by using randomized complete block design of two factors, the experimenter requires a parameter Φ and operating characteristic curves for the fixed-effect-model analysis of the variance to determine how many subjects is enough. Table 6.6 describes the expression of Φ, the degree of freedom of numerator and the degree of freedom of denominator. However, people usually calculate Φ based on a specified difference between two factorial level means. For the gripping force,

$$\Phi^2 = \frac{n \times 2 \times D^2}{2 \times 2 \times \sigma^2} = \frac{nD^2}{2\sigma^2} \quad \text{[Montgomery, 2001]} \qquad (6.41)$$

Where n is the number of subjects, D is the maximum difference among all row means of Table 6.4, σ^2 is the variance of the random error. Similarly, for the vibration,

$$\Phi^2 = \frac{n \times 2 \times D^2}{2 \times 2 \times \sigma^2} = \frac{nD^2}{2\sigma^2} \quad \text{[Montgomery, 2001]} \qquad (6.42)$$

Where D is the maximum difference among all column means of Table 6.4. For the interaction of the gripping force and the vibration,

$$\Phi^2 = \frac{nD^2}{2\sigma^2[(2-1)(2-1)+1]} = \frac{nD^2}{4\sigma^2} \quad \text{[Montgomery, 2001]} \qquad (6.43)$$

where D is the maximum difference in two means of any two interaction effects. Equations (6.41), (6.42), and (6.43) can calculate three values of Φ^2. The appropriate sample size is determined by the minimum value. While specifying $D = 3.8$, $\sigma = 5$ and $n = 20$, the minimum Φ

$$\Phi = \sqrt{\frac{nD^2}{4\sigma^2}} = \sqrt{\frac{20\times 3.8^2}{4\times 5^2}} = 1.70 \qquad (6.44)$$

Table 6.6 The parameters of the operating characteristics curve for the two-factor factorial, fixed effects model

Factor	Φ^2	Numerator degrees of freedom	Denominator degrees of freedom
Gripping force	$\frac{n\sum_{i=1}^{2}\tau_i^2}{\sigma^2}$	1	$4(n-1)$
Vibration	$\frac{n\sum_{j=1}^{2}\beta_j^2}{\sigma^2}$	1	$4(n-1)$
Gripping force and vibration	$\frac{n\sum_{i=1}^{2}\sum_{j=1}^{2}(\tau\beta)_{ij}^2}{2\sigma^2}$	1	$4(n-1)$

The numerator degree of freedom is 1. The denominator degree of freedom is $4(n-1) = 76$. $\alpha = 0.05$. According to the operating characteristics curve for the fixed effects model analysis of variance, it is determined that $\beta = 0.35$. The results of similar

calculations are recorded in Table 6.7. Thus, the experiments require 30 subjects in order to achieve the power of 0.81.

The deduction above suggests that the experiments designed for purpose (2) are also useful for verifying purpose (1) because the experiments of both purposes are designed by using repeated measures design and require the same number of subjects and a random order of experiments performed by the same subject. Moreover, purpose (1) can be more fully verified by using the experiments for purpose (2) since four typical experimental conditions are specified. Then, the total number of experiments run by experimental group 1 is decreased. The experimental combination can effectively decrease the time and resources required in the experiments.

Table 6.7 Choices of the number of subjects

n	Φ^2	Φ	Numerator degrees of freedom	Denominator degrees of freedom	β	Power=$(1-\beta)$
20	2.89	1.70	1	76	0.35	0.65
25	3.61	1.90	1	96	0.21	0.79
30	4.33	2.08	1	116	0.19	0.81

Finally, the experimenter establishes the experimental scenario for experimental group 1. The experiments are performed in a laboratory the environment of which is clean and clear. The temperature is controlled by employing an air conditioning system and is stable. A prototype of the smart wheel is fixed on a table and connected to a computer on which the software of the smart wheel runs. A subject sits in a chair in front of the smart wheel and can adjust the chair to achieve a suitable position and pose. The order in which the subjects perform the experiment depends on their available time and is random. Every

subject receives four experiments each of which is performed under one of the four factorial combinations: (1) low gripping force and no vibration, (2) high gripping force and no vibration, (3) low gripping force and vibration, (4) high gripping force and vibration. Under certain factorial combinations, the gripping force is randomly changed by the subject. The vibration is produced by the experimenter. The order of the four experiments of the same subject is selected randomly by using a MATLAB program and is listed in Table 6.8.

Table 6.8 The order of the four experiments of each subject

Gripping force	Vibration	Subject									
		No.1	No.2	No.3	No.4	No.5	No.6	No.7	No.8	No.9	No.10
Low	No	4	1	2	1	3	3	1	2	4	2
High	No	2	4	4	3	4	4	3	4	3	1
Low	Yes	1	3	1	2	1	1	2	1	1	3
High	Yes	3	2	3	4	2	2	4	3	2	4
		Subject No.									
		No.11	No.12	No.13	No.14	No.15	No.16	No.17	No.18	No.19	No.20
Low	No	3	4	3	1	1	3	1	3	3	4
High	No	2	2	1	2	4	2	4	1	4	1
Low	Yes	1	1	4	3	2	1	3	4	2	3
High	Yes	4	3	2	4	3	4	2	2	1	2
		Subject No.									
		No.21	No.22	No.23	No.24	No.25	No.26	No.27	No.28	No.29	No.30
Low	No	3	2	1	1	1	2	3	1	4	1
High	No	4	3	4	2	4	1	2	3	3	4
Low	Yes	2	4	3	3	2	4	1	4	2	2
High	Yes	1	1	2	4	3	3	4	2	1	3
		Numbers 1~4 means the experimental order for the same subject									

When a subject arrives at the laboratory, he rests one hour until his pulse rate achieves a stable state. During the rest, the experimenter presents to the subject the experimental purposes, methods and process, and verifies whether the subject's pulse rate can be

measured by using the smart wheel and hand. Then, the first experiment is performed. Each of the three other experiments is executed five minutes after the last experiment. In every experiment, a subject utilizes one palm to grip the smart wheel at the position of the PVDF film sensor. The experimenter simultaneously utilizes the smart wheel and the manual method to measure the subject's pulse rate. Every experiment lasts one minute and produces two observations. One observation is the number of pulse beats measured by the manual method in one minute. The other observation is the pulse rate calculated by using the pulse wave from the smart wheel. To satisfy the requirements of the experimental design, thirty subjects should be randomly selected from drivers. However, the experimenter invites thirty available persons to perform the $30 \times 4 = 120$ experiments because of the limitation of experimental resources. They consist of 4 female adults and 26 male adults and belong to the age group of 20~50. Their ages have a mean of 32.5 and a standard deviation of 8.

(2) Experimental group 2

Experimental group 2 is designed to verify the relationship between the standard deviations of a driver's pulse rate and the driving scenarios. This section firstly describes the theoretical deduction and then explains the experimental scenario, procedure, subjects and data recording.

A dynamic traffic environment induces the variance of a driver's heart rate. The change is determined by the degree of complication of the driving scenario. The similar phenomenon occurs in the driver's pulse rate because his/her pulse beat follows the heart

beat. The relationship between the standard deviation of a driver's pulse rate and the experiment scenario can be investigated by comparing the curves of the pulse rate in different driving scenarios. The experiments require a single fact experimental design, which involves a single factor, driving scenarios, and three factorial levels: a single line, a double line, and a sinusoidal line. Utilizing the repeated measures design of single factor,

$$y_{ij} = \mu + \tau_i + \beta_j + \gamma_{ij} \quad \begin{cases} i = 1,2,3 \\ j = 1,2,\ldots,n \end{cases} \quad \text{[Montgomery, 2001]}$$

where y_{ij} is the observation, μ is the overall mean, τ_i is the effect of i th factorial level, β_j is the effect of j th subject, and γ_{ij} is the random error. The hypotheses

$$H_0 : \tau_1 = \tau_2 = \tau_3 = 0$$

$$H_1 : \text{at least one } \tau_i \neq 0$$

are utilized to test the equality of the three means of the three factorial levels. The appropriate approach is to analyze the standard deviations and calculate the test statistic

$$F_0 = \frac{MS_{factorial\_level}}{MS_E} \quad \text{[Montgomery, 2001]}$$

where

$$MS_{factoria\_level} = \frac{SS_{factorial\_level}}{3-1} = \frac{n\sum_{i=1}^{3}(\bar{y}_{i\bullet} - \bar{y}_{\bullet\bullet})^2}{2} \quad \text{[Montgomery, 2001]} \quad (6.45)$$

$$MS_E = \frac{SS_E}{(3-1)(n-1)} = \frac{\sum_{i=1}^{3}\sum_{j=1}^{n}(y_{ij} - \bar{y}_{i\bullet} - \bar{y}_{\bullet j} + \bar{y}_{\bullet\bullet})^2}{2(n-1)} \quad \text{[Montgomery, 2001]} \quad (6.46)$$

If the null hypothesis is true, the probability distribution of F_0 is $F_{2,2(n-1)}$. For a specified $\alpha = 0.05$, H_0 is rejected while $F_0 > F_{0.05,2,2(n-1)}$. Table 6.9 shows the important statistics of the analysis of variance for this case and

$$SS_{Between\_subjects} = 3\sum_{j=1}^{n}(\bar{y}_{\bullet j} - \bar{y}_{\bullet\bullet})^2 \quad \text{[Montgomery, 2001]} \tag{6.47}$$

$$SS_{Within\_subjects} = \sum_{i=1}^{3}\sum_{j=1}^{n}(y_{ij} - \bar{y}_{\bullet j})^2 \quad \text{[Montgomery, 2001]} \tag{6.48}$$

In addition, an important question is to choose the number of subjects. In single factor experiments, the choice of the number of subjects depends on the parameter Φ and the operating characteristics curves for the fixed effects model analysis of variance. The theoretical equation of Φ

$$\Phi^2 = \frac{n\sum_{i=1}^{3}\tau_i^2}{3\sigma^2} \quad \text{[Montgomery, 2001]} \tag{6.49}$$

Where n is the number of subjects, σ^2 is the variance of random error.

Table 6.9 The analysis of variance under repeated measures design of single factor

Source of variation	Sum of squares	Degrees of freedom	Mean square	F_0
Between subjects	$SS_{Between\_subjects}$	$n-1$		
Within subjects	$SS_{Within\_sunjects}$	$2n$		
Three Experiment scenarios	$SS_{factorial\ level}$	2	$\frac{SS_{factorial\ level}}{2}$	$\frac{MS_{factorial\ level}}{MS_E}$
Error	SS_E	$2(n-1)$	$\frac{SS_E}{2(n-1)}$	
Total	SS_T	$3n-1$		

However, it is difficult to obtain the $\sum_{i=1}^{3}\tau_i^2$ and σ^2 in this case. One acceptable solution is to calculate Φ as follows

$$\Phi^2 = \frac{nD^2}{2\times 3\times \sigma^2} = \frac{nD^2}{6\sigma^2} \quad \text{[Montgomery, 2001]} \tag{6.50}$$

where D is the possible maximum difference between any two factorial level means. σ^2 can be estimated by using experience, previous experiments, etc. Based on the previous experiments (10 replications), it is estimated that $\sigma = 4.766$. The experimenter specifies $D = 7.525$ and $\alpha = 0.05$. If $n = 5$, $\Phi = 1.44$ and $3(n-1) = 12$. The degree of factorial levels is $(3-1) = 2$. According to the operating characteristics curve for the fixed effects model analysis of variance, $\beta = 0.5$. The results of similar calculations are recorded in Table 6.10. Thus, the experiments require 10 subjects in order to achieve the power of 0.82.

Table 6.10 Choices of the number of subjects

n	Φ^2	Φ	$a(n-1)$	β	Power=$(1-\beta)$
5	2.07	1.44	12	0.50	0.50
8	3.32	1.82	21	0.25	0.75
10	4.15	2.04	27	0.18	0.82

Finally, the experimenter establishes the experimental scenario of experimental group 2. The experiments are performed in a laboratory the temperature of which is stable and comfortable. The environment is clean and clear. An accelerator and brake are fixed on the floor. A prototype of the smart wheel is connected to a computer and is located in front of the computer screen and is fixed on the table. The software of the smart wheel and that of the simulation run on the computer. A subject sits in a chair in front of the

smart wheel and can adjust the chair and the pedals to achieve a suitable position and pose. The order in which the subjects perform the experiments depends on their available time and is random. Every subject undergoes three experiments each of which is performed under one of the three driving scenarios: a single line, a double line, and a sinusoidal line. The order of the three experiments of the same subject is randomly selected by using a MATLAB program and is shown in Table 6.11. When a subject arrives at the laboratory, he rests for one hour until his pulse rate achieves the normal state. During the rest, the experimenter presents to the subject the experimental purposes, methods and process and verifies whether the subject's pulse rate can be measured by employing the smart wheel. Then, the first experiment is performed. Each of the other two experiments is executed twenty minutes after the last experiment because the subject requires time to recover from the experimental state. In every experiment, a subject grips the smart wheel at the position of the PVDF film sensor, controls the accelerator and brake, and drives the virtual vehicle along the road shown on the computer screen. Simultaneously, the smart wheel is utilized to take a continuous measurement of the subject's pulse wave. The experimental data of the virtual vehicle is automatically recorded in an Excel file. The subject's pulse wave is automatically recorded in another Excel file. To satisfy the requirements of the experimental design, ten subjects should be randomly selected from drivers. However, ten available persons are invited to perform the experiments because of the limitation of experimental resources. They consist of 2 female adults and 8 male adults and belong to the age group of 25~45. Their ages have a mean of 31.1 and a standard deviation of 6.

Table 6.11 The order of the four experiments of each subject

Driving scenario	Subjects									
	No.1	No.2	No.3	No.4	No.5	No.6	No.7	No.8	No.9	No.10
Single line	3	3	3	3	3	1	1	1	2	3
Double Line	1	2	1	2	2	2	2	2	3	2
sinusoidal line	2	1	2	1	1	3	3	3	1	1
	Numbers 1~4 means the order for one subject									

6.4 The experimental hardware configuration

(1) Experimental group 1

The experimental purpose is to verify the principle and performance of the smart wheel. Thus, a prototype of the smart wheel is designed and manufactured by the experimenter. Table 6.12 shows the experimental hardware. The NASCAR® racing wheel is an interactive device for electronic games and consists of a game wheel, an accelerator pedal, and a brake pedal. One of its attractive features is the function of force feedback. By using it, the experimenter can conveniently produce the vibration that is required in the experiments. The vibration has a frequency of 35Hz and a small amplitude.

Table 6.12 The experimental hardware

No.	Name	Description	Quantity	Company
1	NASCAR® racing wheel	Game wheel with force feedback vibration(≈35Hz)	1	Logitech®
2	DT1-028K/L w/rivets	PVDF film sensors (wires connected)	2	MSI Sensors
3	Voltage amplifier		1	
4	NI-USB-6009	14bit,48kS/s Multifunction data acquisition for USB	1	National Instruments
5	Personal computer	Dell Precision™ Workstation 370	1	DELL

The DT1-028K/Lw/rivets is a kind of PVDF film sensor manufactured by MSI Sensors. It is a rectangular element of piezo film of which the length, width thickness and capacitance are 41mm, 16mm, 40μm and 1.38nF, respectively. The sensor consists of silver ink screen-printed electrodes, which are connected with 12"/28g wires by rivets. The PVDF film sensor requires a voltage amplifier the circuit and prototype of which are shown in Figures 6.1 and 6.2, respectively. An adjustable resistor is selected for R_2 so that the experimenter can adjust the voltage gain. Its cut-off frequency

$$\frac{1}{2\pi RC} = \frac{1}{2\times 3.14159\times 200\times 10^{6}\times 1.38\times 10^{-9}} \approx 0.577(Hz) \quad \text{[MSI, 1998]} \qquad (6.51)$$

Its voltage gain

$$1+\frac{R_1}{R_2} = 1+\frac{20\times 10^{6}}{2.6\times 10^{3}} \approx 7693 \quad \text{[MSI, 1998]} \qquad (6.52)$$

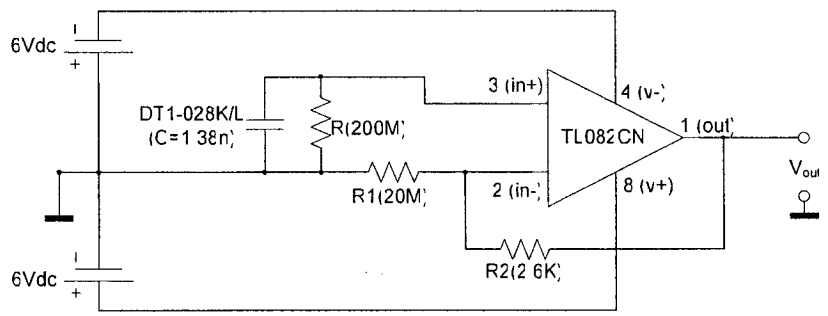

Figure 6.1 The interface circuit for the PVDF film sensors of the experimental smart wheel

The NI-USB-6008 is a portable and multifunctional data acquisition system for USB. It provides eight analog input (AI) channels, two analog output (AO) channels, 12 digital input/output (DIO) channels, and a 32-bit counter. For analog input, it has a resolution of 14 bits for differential input and 13 bits for single-ended input. Its maximum AI sample

rate can achieve 48kS/s. A custom measurement system can be conveniently established by using the NI USB-6009 with the included ready-to-run software, or by programming it with LabVIEW or C. Finally, the experimenter utilizes the same high-performance workstation for experimental group 2 in order to economize on the experimental resources. Firstly, both terminals of a PVDF sensor are stuck to and fixed on the surface of the circular ring of the game wheel by using double-sticky tape. The sensor is set at a distance of 2mm from the surface of the circular ring. The space between them is empty (Figure 6.2). This structure can remarkably enlarge the output of the sensor while it is utilized to measure the pulse wave of a subject's palm. Next, the output of the PVDF sensor is amplified by using the voltage amplifier. Then, the enlarged signal is measured by employing the NI-USB-6009 that is connected to a USB port of the computer. The computer provides a platform for running the software of the DAQ system and for analyzing data. Figure 6.3 shows the overall configuration of the experimental hardware.

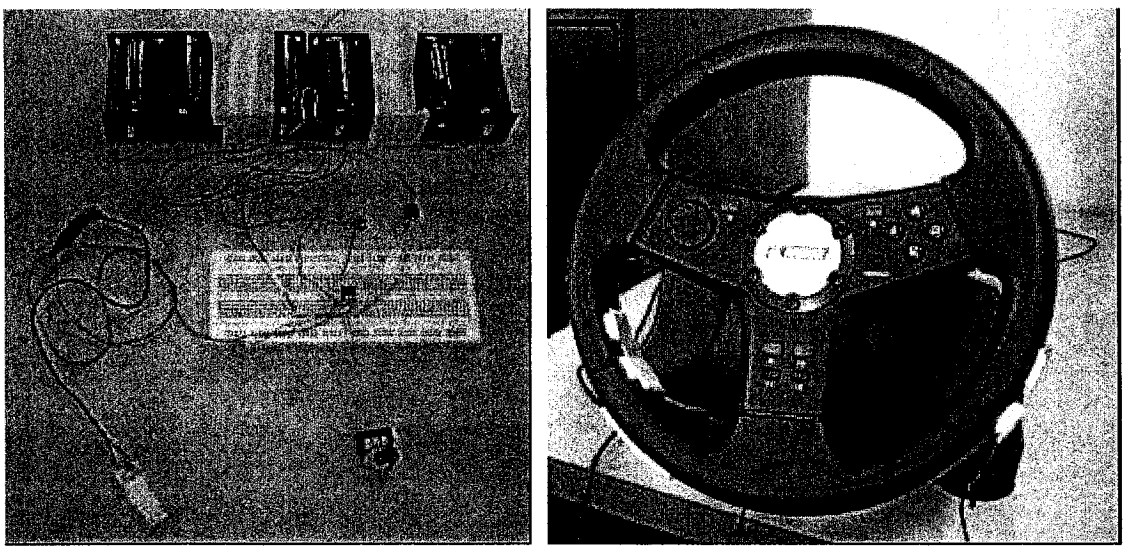

Figure 6.2 The voltage amplifier and the game wheel

(2) Experimental group 2

The experiments utilize the same experimental hardware for experimental group 1. In addition, the experiments require a high-performance workstation because the virtual reality system requires a good deal of calculation and 3D animation. If the computer does not have a strong hardware configuration, the reality of the simulation is decreased. In such a case, the experimenter can not obtain good simulating data that represents the actual situation. The overall configuration of the experimental group 2 is shown in Figure 6.4.

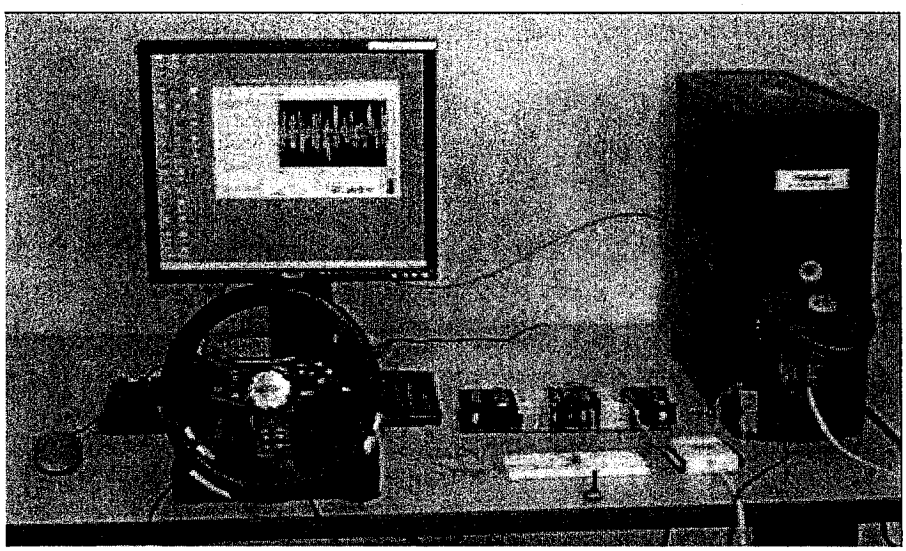

Figure 6.3 The overall hardware configuration of experimental group 1

6.5 Experimental software

(1) Experimental group 1

The experiments require the software named 'NI-DAQmx Base', which works with NI-USB-6009. NI-DAQmx Base can measure all signals connected to NI-USB-6009 and plot the real-time data versus time on the computer screen (Figure 6.5).

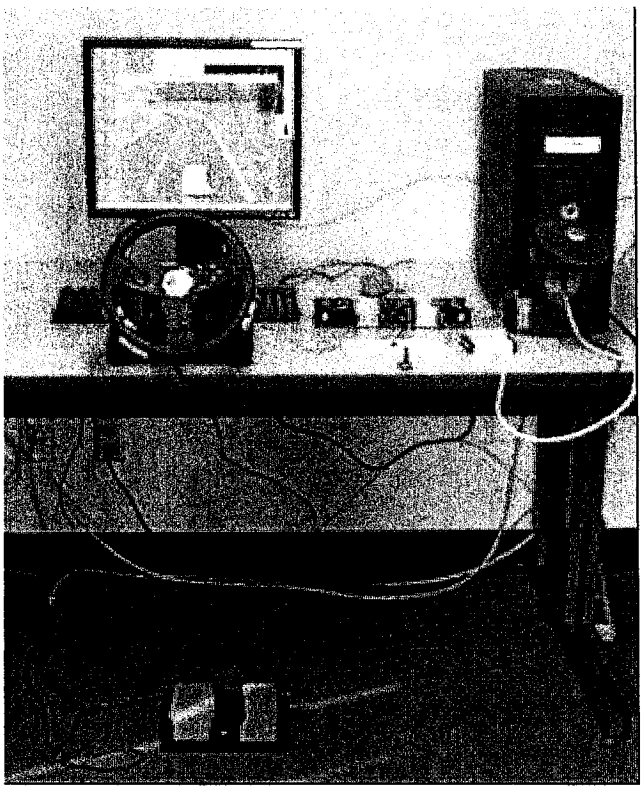

Figure 6.4 The overall hardware configuration of experimental group 2

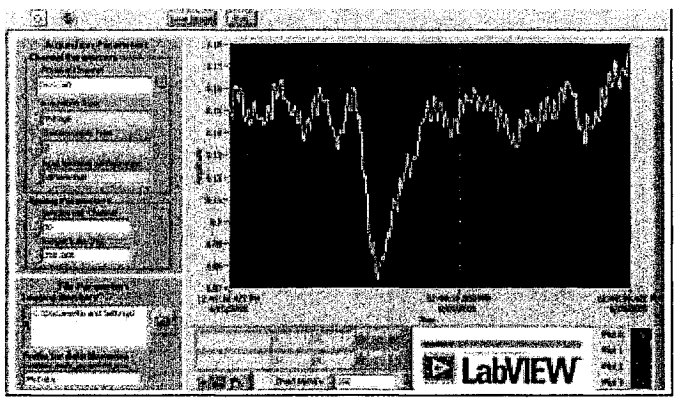

Figure 6.5 The interface of NI-DAQmx Base

When an experiment is finished, NI-DAQmx Base automatically generates an Excel file that includes voltage value and time. Then, the data file can be read and analyzed by a

special MATLAB program that can calculate the subject's pulse rate. In addition, the driver software of the NASCAR® racing wheel is required to produce a vibration when the experimenter presses a certain button. Its interface is shown in Figure 6.6. Hence, NI-DAQmx Base, the driver software of the game wheel, and MATLAB are necessary in the experiments.

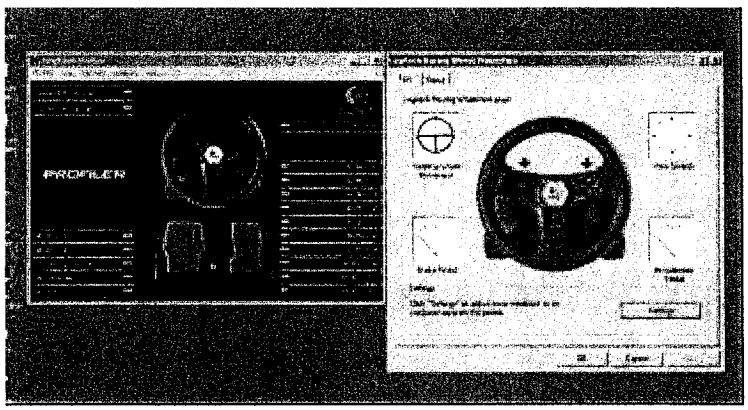

Figure 6.6 The driver software of the NASCAR® racing wheel

(2) Experimental group 2

The experiments require NI-DAQmx Base to measure a subject's pulse wave. The driver software of the NASCAR® racing wheel is utilized to quantify a subject's operation on the wheel and pedals and then send the data to the simulation software. The simulation software simulates the virtual vehicle and the typical experiment scenarios. The three software run simultaneously on the same computer (Figure 6.7) while performing the experiments. When an experiment is finished, NI-DAQmx Base generates a data file that records the subject's pulse wave. The simulating software generates a data file that records the position and the time of the virtual vehicle.

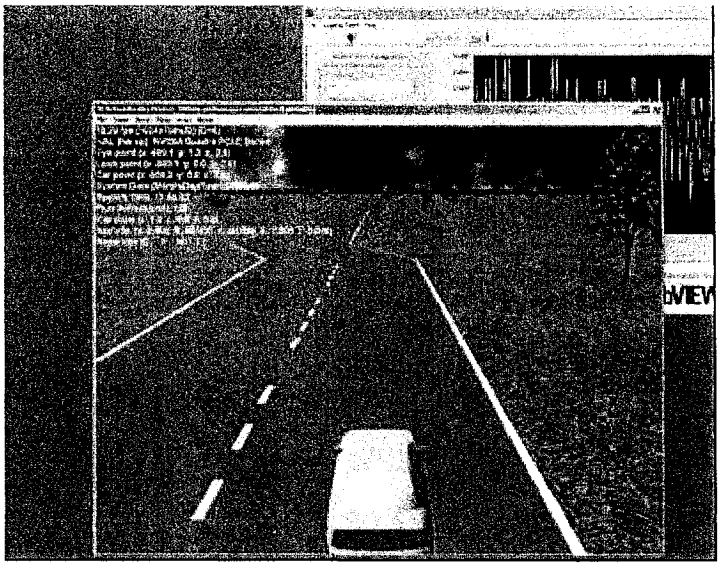

Figure 6.7 The experimental software for experimental group 2

6.6 Analysis tool

(1) Experimental group 1

The experiments require two MATLAB programs. The first program has the workflow shown in Figure 6.8. It utilizes FFT to calculate the power spectrum of the pulse wave recorded in a data file. Then, the subject's pulse rate per minute is calculated based on the frequency the power of which is the largest in the power spectrum. The second program the main function of which is the analysis of the variance (ANOVA) calculates the important statistics based on the experimental observations and plots the result. Based on the result of ANOVA, the experiment purposes can be objectively verified. It is noted that the subject's pulse rate is calculated once before filtering and once after filtering (Figure 6.8). By observing the influence of a filter on the calculated result, the experimenter can compare the performance of filters and optimize their performance. The program utilizes a band-pass filter the pass band of which is specified to have a slightly

larger range than that of the driver's pulse rate so that the signal of other frequencies is filtered. The filter can select a finite impulse response (FIR) filter or an infinite impulse response (IIR) filter. Compared to a IIR filter the output of which is the weighted sum of the current and past inputs and past outputs, the FIR filters of which the output is the weighted sum of the current and past inputs are more widespread for the following reasons: (1) they do not distort the phase of the input signal although they delay it; (2) it is easy to implement them; (3) they exhibit higher computational efficiency; (4) they have inherent numeric properties. Thus, the present research selects a FIR filter to filter the data of the pulse wave measured by using the smart wheel.

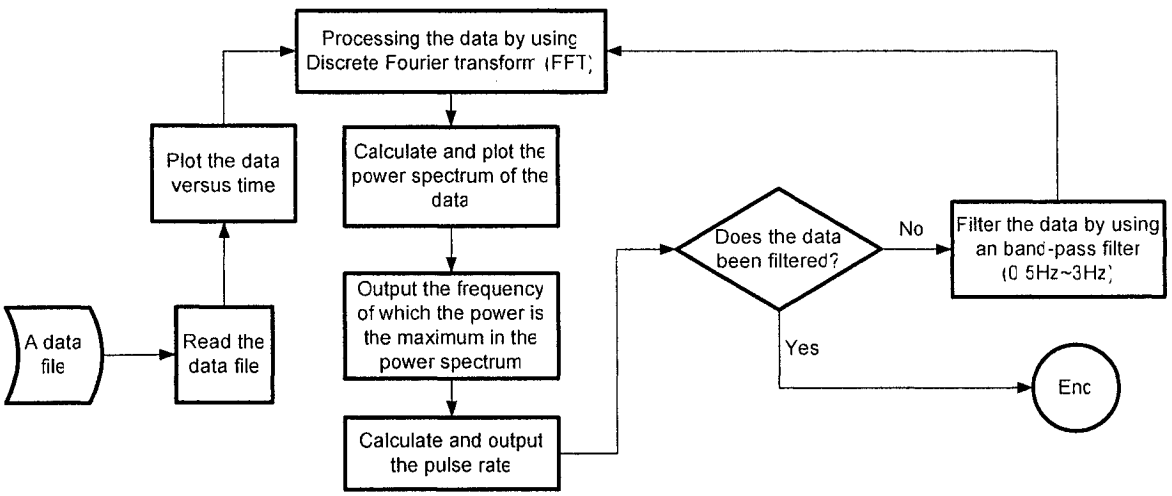

Figure 6.8 The workflow of the software of the experimental system

(2) Experimental group 2

Two tools are employed to analyze the data of experimental group 2. The first tool is a MATLAB program the main functions of which consist of the following: (1) drawing the 3D figure based on the longitudinal displacement, the lateral displacement and the time at

which the virtual vehicle arrives at the location; (2) using STFT to calculate the subject's instantaneous pulse rate; (3) calculating the standard deviation of a subject's pulse rate. The second tool is another MATLAB program that executes the analysis of the variance (ANOVA) of the standard deviations of the subjects' pulse rate in the experiment scenarios. Based on its result, the relationship between the standard deviations of a subject's pulse rate and the typical scenarios can be analyzed.

6.7 Results and discussion

6.7.1 Calculation of the pulse rate

In experimental group 1, the experimenter invites 30 subjects and performs a total of 120 experiments. The experimental order of the subjects is random since their available times are random. The order of the experiments of the same subjects is also random (Table 6.8). When all the experiments are finished, 120 data files are produced by utilizing the smart wheel and NI-DAQmx Base. Every data file involves about 12,000 data which reflects the pressure of a subject's pulse wave because the signal is sampled with a frequency of 200Hz and the experimental period is one minute. Based on the data files, the pulse rates of the subjects can be calculated.

(1) Low gripping force and no vibration

Under this condition, one of the results (Appendix B) is shown in Figure 6.9. The pulse wave is stable during most of the experimental time except at the beginning and the end of the experiment while the subject is adjusting the gripping force or loosening the smart wheel (Figure 6.9(a)). After calculating the power spectrum of the original pulse wave, it

is noticed that (1) there is one peak in the range of 0.5Hz~2Hz and there are three peaks in the range of over 2Hz and (2) the component of 1.26Hz has the maximum power (Figure 6.9(b)). In fact, a normal subject's pulse rate rarely exceeds 1.8Hz. Thus, the experimenter utilizes the filter design and analysis tool of MATLAB to design several band-pass FIR filters to filter the noise signals the frequency of which exceeds the range of 0.4Hz~1.8Hz. While designing the filters, the magnitude of the noise signal is decreased as little as possible. The magnitude of the useful signal is almost zero and constant. The magnitude curve from the useful signal to the noise signal is as vertical as possible. Figure 6.10 shows the important parameters of one of the filters the performance of which is good. Filtered by using the FIR filter, the pulse wave is transformed into a continuous curve with an S-shape (Figure 6.9(c)) and has one peak at 1.26Hz in its power spectrum (Figure 6.9(d)). Thus, the experimenter calculates the subject's pulse rate as follows: $1.26\text{Hz} \times 60\text{second} = 75.6(\text{beats/minute})$.

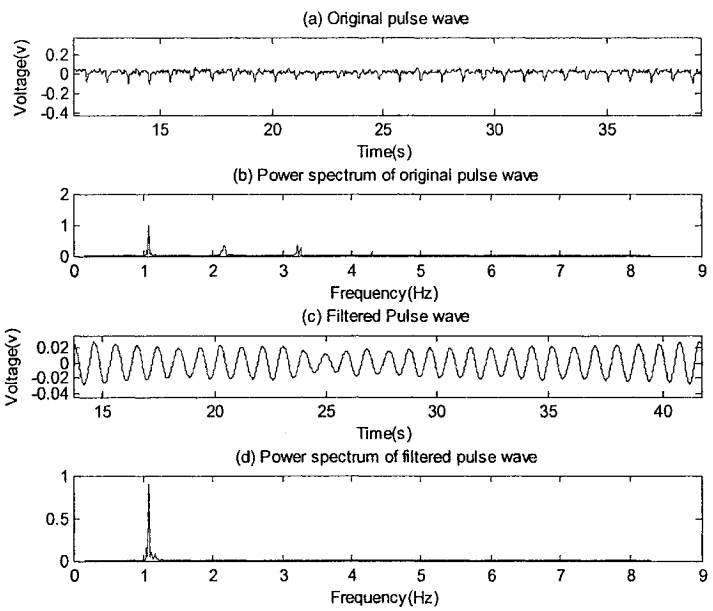

Figure 6.9 A pulse wave and power spectrum under low gripping force and no vibration

Similarly, the thirty subjects' pulse rates under the condition of low gripping force and no vibration can be measured and calculated and are shown in Figure 6.11.

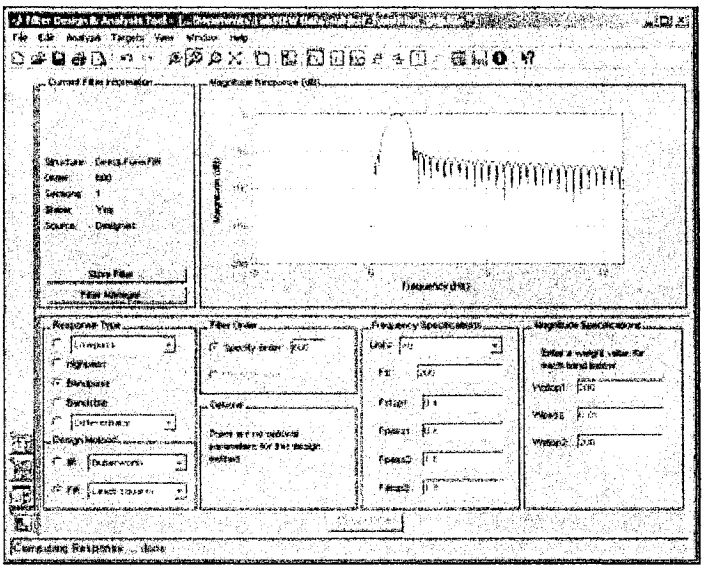

Figure 6.10 Filter design and analysis tool

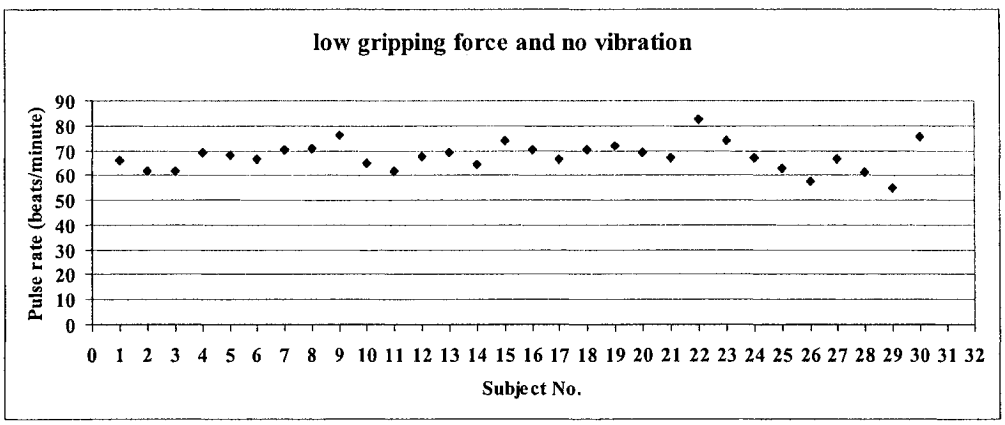

Figure 6.11 Subjects' pulse rates under low gripping force and no vibration

(2) High gripping force and no vibration

Under this condition, one of the results (Appendix B) is shown in Figure 6.12. In the experiment, the subject randomly increases and decreases the gripping force so that 6

positive peaks and 6 negative peaks are produced in the pulse wave. The straight segments reflect the subject's pulse wave of which the voltage is much lower than that of the gripping force (Figure 6.12(a)). The power spectrum of the original signal consists of numerous peaks in which the peak of the subject's pulse rate is difficult to calculate accurately. Thus, an appropriate compensation for the gripping force is required to eliminate its disturbance. One simple method is to limit the amplitude of the output wave of the smart wheel because the experiments indicate that the output voltage of a stable pulse wave does not exceed the range of -0.1v~+0.1v. If the amplitude of the output voltage exceeds this range, the output is not useful and is corrected to a specified constant voltage such as 0.025v. Then, the original curve is modified (Figure 6.12(b)).

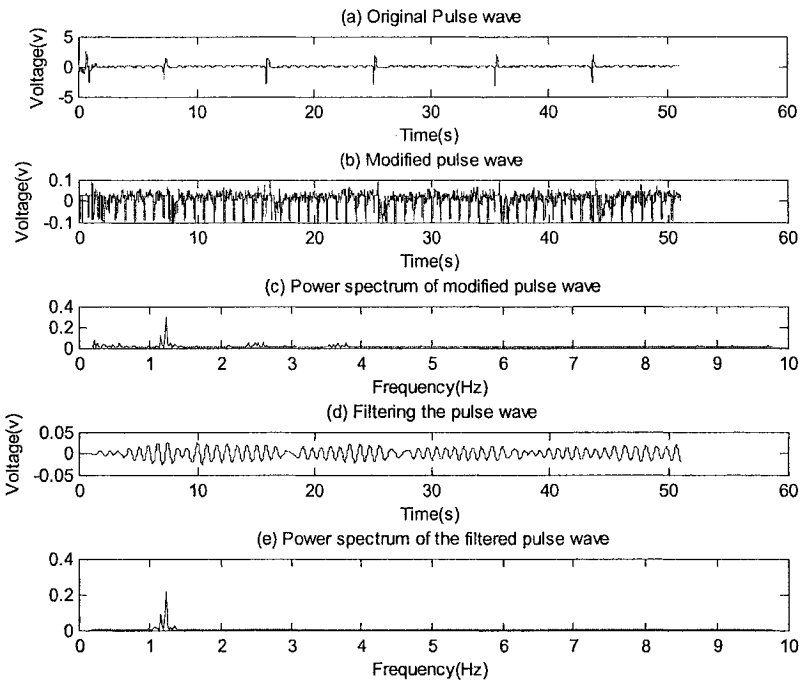

Figure 6.12 A pulse wave and power spectrum under high gripping force and no vibration

After calculating the power spectrum of the modified pulse wave, the experimenter obtains one peak in the range of 1Hz~2Hz and numerous shorter peaks in other frequency ranges (Figure 6.12(c)). Next, the before-mentioned FIR filter is utilized to filter the noise signal of the modified pulse wave. Figures 6.12 (d) and 6.12 (e) show the filtered pulse wave and its power spectrum, respectively. Then, the subject's pulse rate can be calculated based on the frequency the power of which is the maximum. Finally, the thirty subjects' pulse rates under the condition of a high gripping force and no vibration can be measured and calculated and are shown in Figure 6.13.

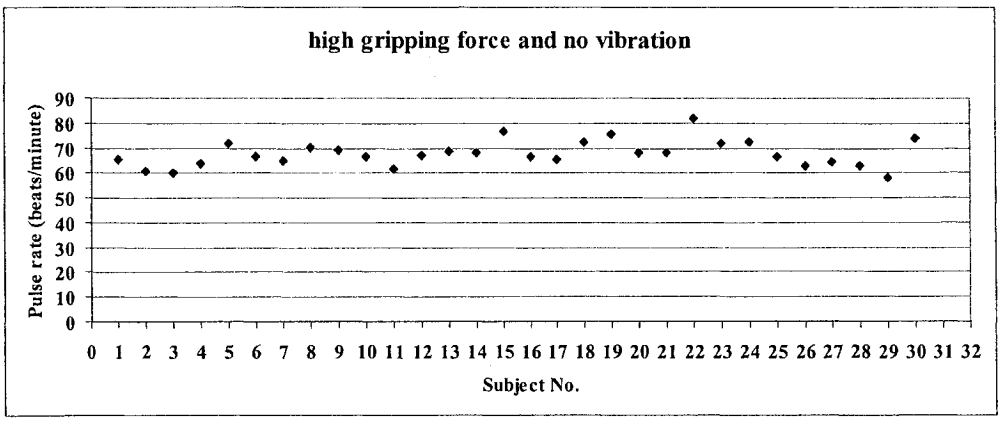

Figure 6.13 Subjects' pulse rates under high gripping force and no vibration

(3) Low gripping force and vibration

Under this condition, one of the results (Appendix B) is shown in Figure 6.14. The original pulse wave consists of several segments that have high frequency and large amplitude. The segments are produced by employing the vibration of the game wheel (Figure 6.14 (a)). The power spectrum mainly includes two parts of peaks: (1) some peaks in the range of 0Hz~10Hz, which is produced by the subject's pulse beat and noise and (2) some peaks in the range of 30Hz~40Hz, which is produced by the vibration. The

experimenter checked and modified the output voltage of the original pulse wave (Figure 6.14 (b)) and then filtered the modified pulse wave (Figure 6.14 (c)). The result indicates that the power spectrum of the filtered pulse wave has one peak between 1Hz and 1.5Hz (Figure 6.14 (d)). The frequency of the peak can be utilized to calculate the subject's pulse rate. Finally, the thirty subjects' pulse rates under low gripping force and vibration can be measured and calculated and are shown in Figure 6.15.

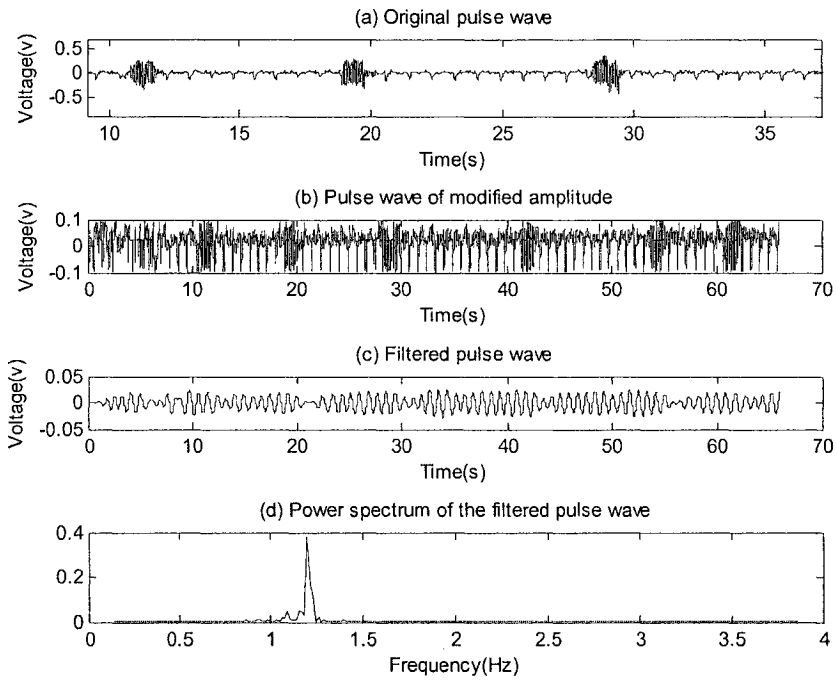

Figure 6.14 A pulse wave and power spectrum under low gripping force and vibration

(4) High gripping force and vibration

Under this condition, one of the results (Appendix B) is shown in Figure 6.16. The peaks of the original pulse wave represent the effect of the gripping force. The thick segments indicate the effect of the vibration of the smart wheel (Figure 6.16 (a)). Both disturbances

simultaneously or alternately appear during the experiment. After the amplitude is corrected, the modified pulse wave (Figure 6.16 (b)) has a power spectrum the frequency components of which distribute in the ranges of 0Hz~5Hz and 30Hz~40Hz. The peaks of 0Hz~5Hz are produced by the subject's pulse beat and noise. The peaks of 30Hz~40Hz occur because of the vibration. Then, the aforementioned FIR filter is utilized to filter the modified pulse wave (Figure 6.16 (c)). The power spectrum of the filtered pulse wave consists of one main peak in 0.3Hz~1.5Hz (Figure 6.16 (d)). Then, the subject's pulse rate is calculated based on the frequency the power of which is the maximum in the power spectrum of the filtered pulse wave. Finally, the thirty subjects' pulse rates under the condition of high gripping force and vibration can be measured and calculated and are shown in Figure 6.17.

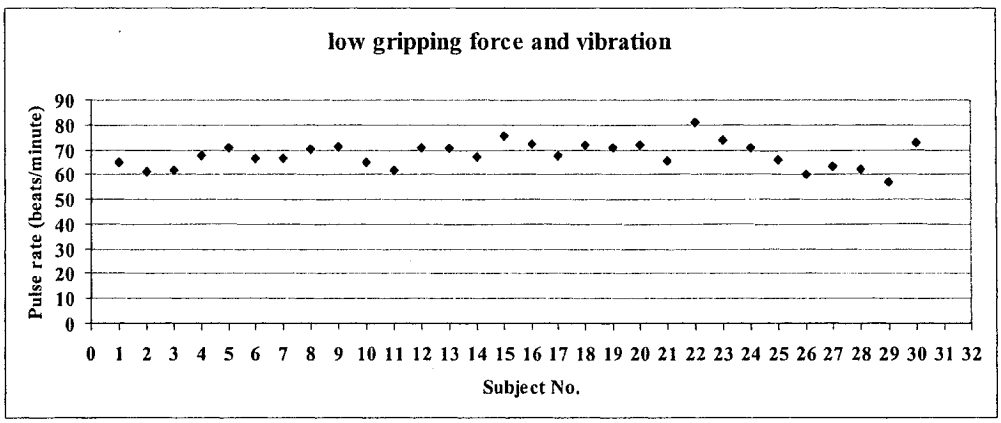

Figure 6.15 Subjects' pulse rates under low gripping force and vibration

Hence, according to Figures 6.12, 6.14, 6.16, when the high gripping force or vibration is applied, the PVDF film sensor produces a large output. However, it produces little output from a subject's pulse wave. Thus, the output from the disturbances influences the calculation of a subject's pulse rate. In order to eliminate their influence, the

experimenter utilizes two methods, limiting the amplitude and filtering, to process the original pulse wave measured by using a smart wheel. Then, a subject's pulse rate can be calculated according to the processed pulse wave.

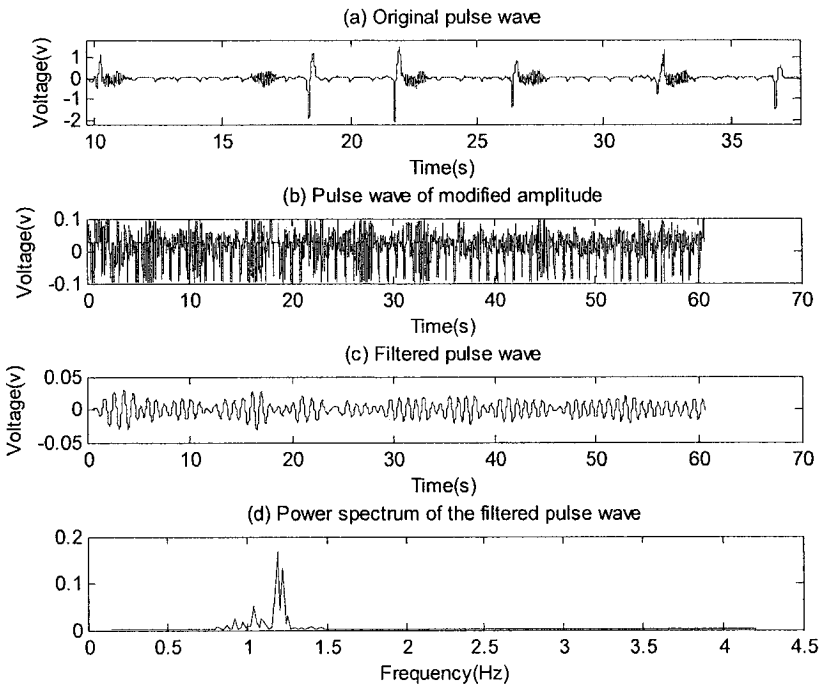

Figure 6.16 A pulse wave and power spectrum under high gripping force and vibration

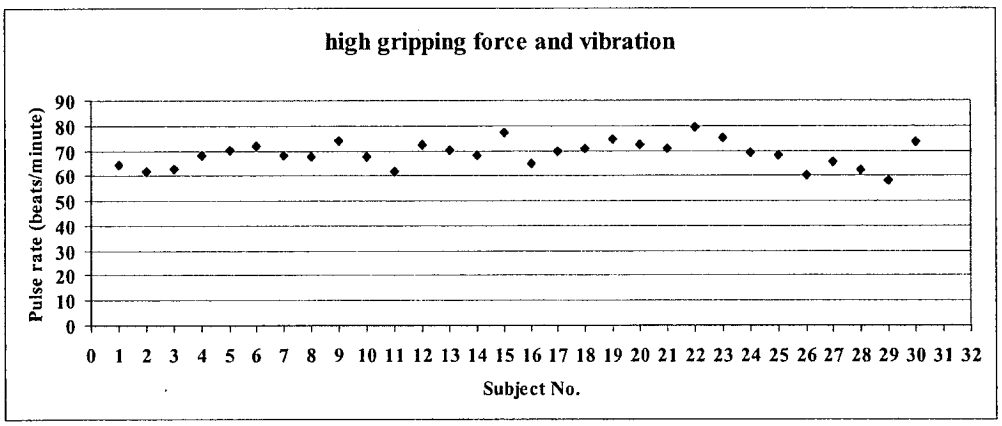

Figure 6.17 Subjects' pulse rates under high gripping force and vibration

6.7.2 Accuracy of the smart wheel

In each experiment, when measuring a subject's pulse rate by using the smart wheel, the experimenter also measures the pulse rate by using a manual method and obtains another observation.

(1) Low gripping force and no vibration

Under this condition, the experimenter obtains the observations shown in Figure 6.18.

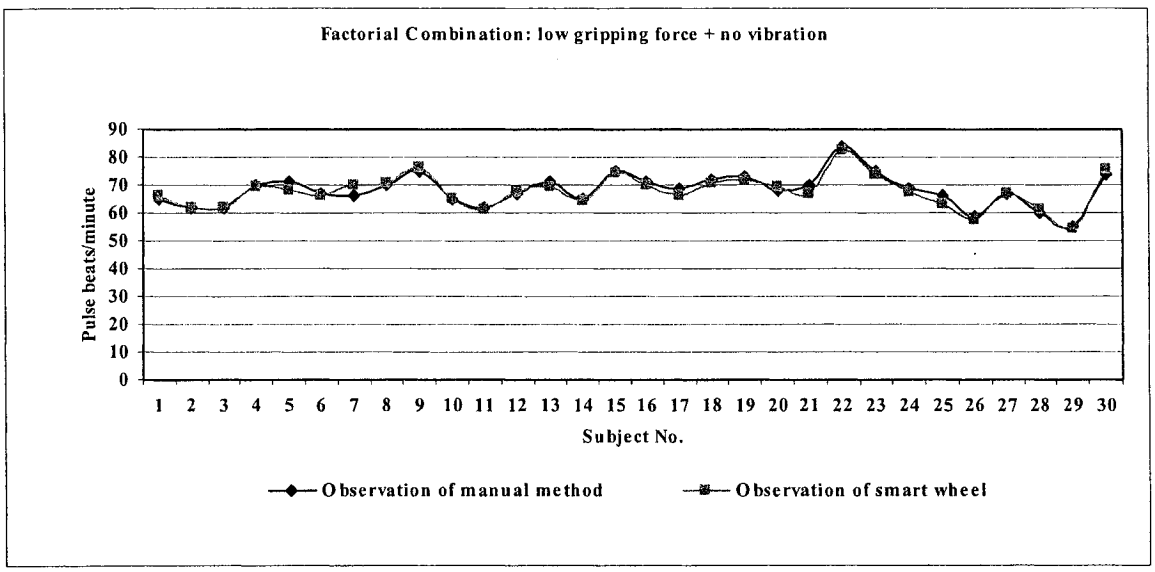

Figure 6.18 Observations under low gripping force and no vibration

Figure 6.19 is the boxplot (see Appendix C) of the observations of both methods. The objective conclusion can be obtained by using the analysis of variance (ANOVA). The important statistics of the observations of both methods are calculated by using a MATLAB program and are recorded in Table 6.13. The source of variation consists of subjects, factorial levels and the error. The F_0 of subjects is much larger than the critical

F, $F_{0.05,29,29}$. This implies that the pulse rates of the subjects are noticeably different. Thus, the repeated measures design is necessary in the design of the experiments of the present research so that the experimental variation due to the differences between the subjects can be distinguished from the experimental error. However, the F_0 of the factorial levels (i.e. both methods of measuring pulse rate, smart wheel and manual method) is less than the critical F, $F_{0.05,1,29}$. Thus, the observations of both methods are statistically equivalent under the condition of low gripping force and no vibration.

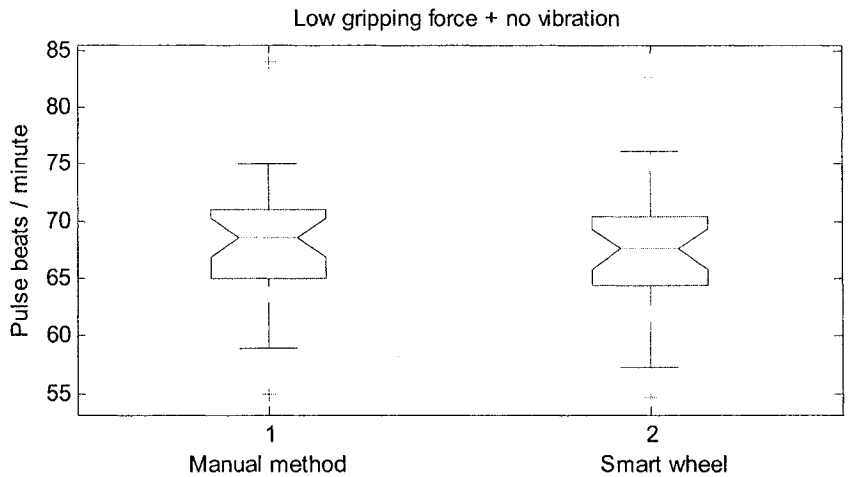

Figure 6.19 The boxplot of observations under low gripping force and no vibration

Table 6.13 The analysis of variance of observations under low gripping force and no vibration

Source of variation	SS	Degrees of freedom	MS	F_0	Critical F
Subjects	1911.301	29	65.907	55.535	$F_{0.05,29,29} = 1.861$
Factorial levels	3.187	1	3.187	2.685	$F_{0.05,1,29} = 4.183$
Error	34.416	29	1.187		
Total	1948.904	59			

(2) High gripping force and no vibration

Under this condition, the observations are plotted in Figure 6.20. There are more differences between the two curves than in the case of Figure 6.18. Figure 6.21 is the boxplot of the observations of both methods.

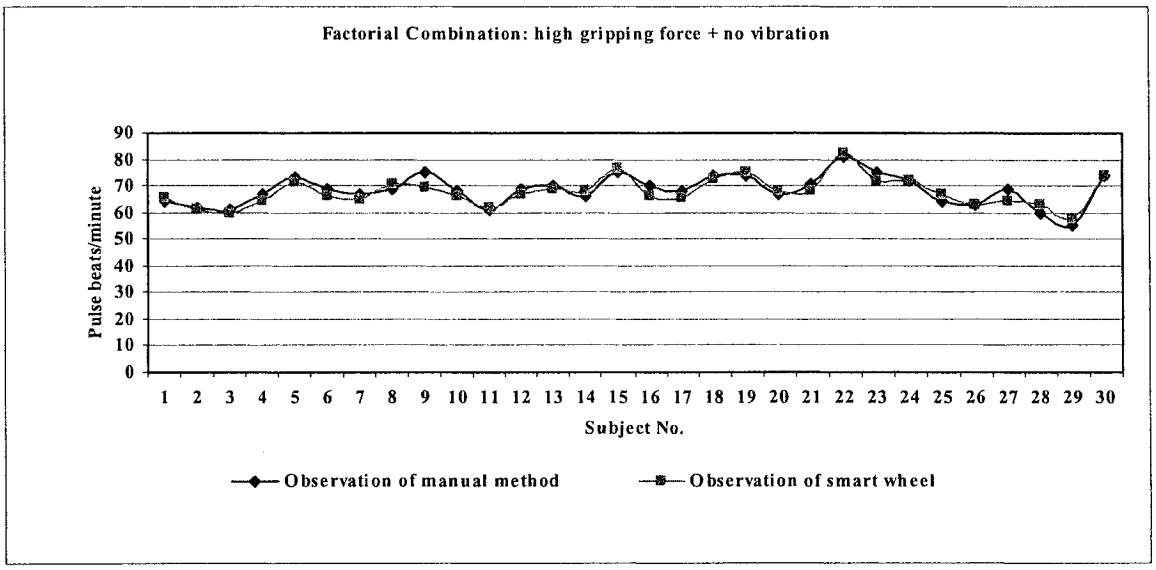

Figure 6.20 Observations under high gripping force and no vibration

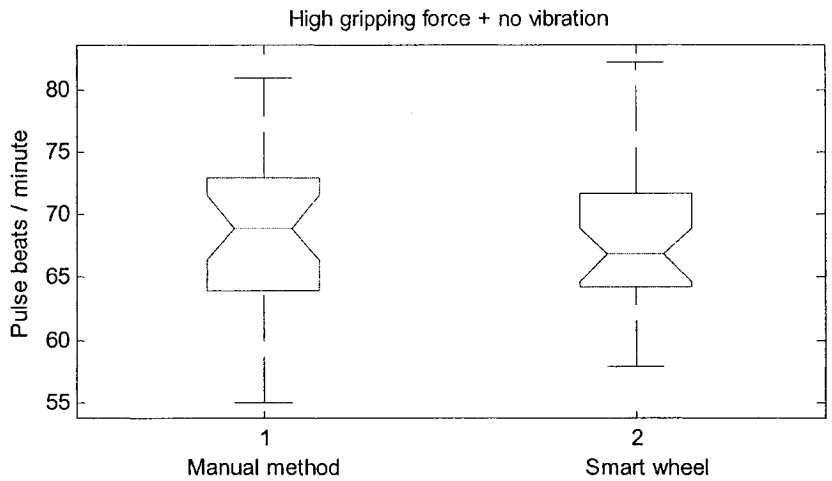

Figure 6.21 The boxplot of observations under high gripping force and no vibration

The important statistics are calculated according to analysis of variance (ANOVA) and are shown in Table 6.14. In the three sources of vibration, the subjects have a much larger F_0 than the critical F, $F_{0.05,29,29}$. Thus, the difference between the subjects produces a noticeable effect on the total experimental error. Nevertheless, the F_0 of the two methods of measuring the pulse rate is less than the critical F, $F_{0.05,1,29}$. Thus, the observations of both methods are statistically equal under the condition of high gripping force and no vibration.

Table 6.14 The analysis of variance of observations under high gripping force and no vibration

Source of variation	SS	Degrees of freedom	MS	F_0	Critical F
Subjects	1642.273	29	56.630	21.462	$F_{0.05,29,29}=1.861$
Factorial levels	7.469	1	7.469	2.830	$F_{0.05,1,29}=4.183$
Error	76.522	29	2.639		
Total	1726.264	59			

(3) Low gripping force and vibration

Under this condition, the observations are plotted in Figure 6.22. There is a similar difference between the two curves as in Figure 6.18. Figure 6.23 is the boxplot of the observations of both methods. Table 6.15 shows the important statistics, which are calculated according to analysis of variance (ANOVA). Comparing the statistics of the three sources of vibration, the experimenter obtains that (1) the difference between the subjects is noticeable because the subjects have a much larger F_0 than the critical F, $F_{0.05,29,29}$, and (2) there is no difference between the observations of both methods because the F_0 of the factorial levels is less than the critical F, $F_{0.05,1,29}$. Hence, both

methods statistically produce the same observations under the condition of low gripping force and vibration.

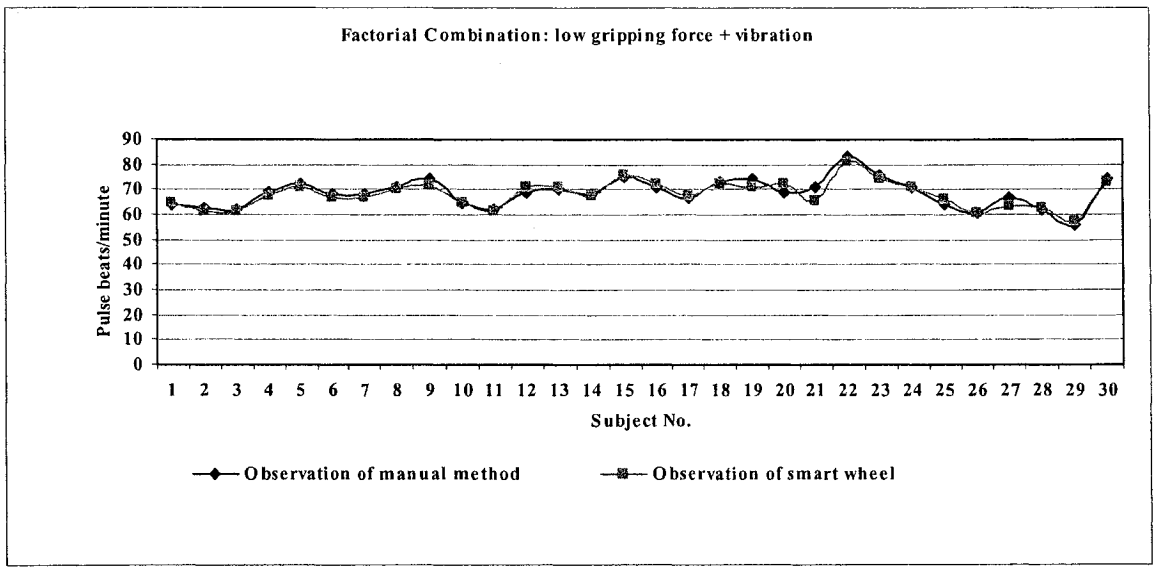

Figure 6.22 Observations under low gripping force and vibration

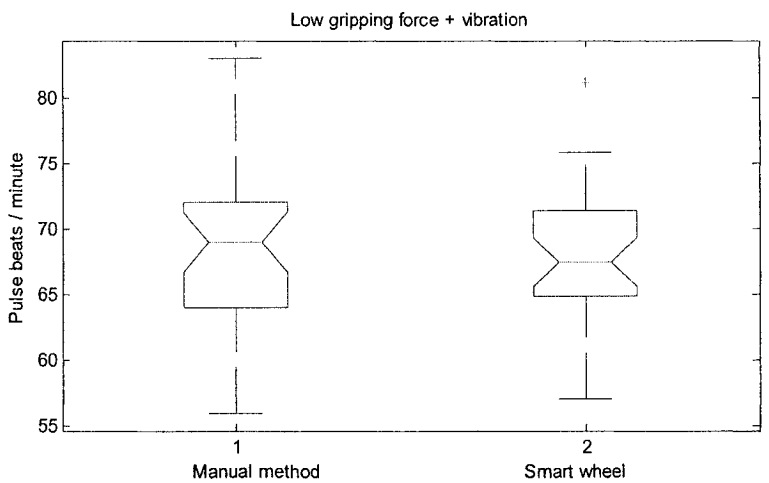

Figure 6.23 The boxplot of observations under low gripping force and vibration

(4) High gripping force and vibration

Under this condition, the observations are plotted in Figure 6.24. Figure 6.25 is the boxplot of the observations of both methods.

Table 6.15 The analysis of variance of observations under low gripping force and vibration

Source of variation	SS	Degrees of freedom	MS	F_0	Critical F
Subjects	1628.607	29	56.159	34.959	$F_{0.05,29,29} = 1.861$
Factorial levels	5.518	1	5.518	3.435	$F_{0.05,1,29} = 4.183$
Error	46.586	29	1.606		
Total	1680.711	59			

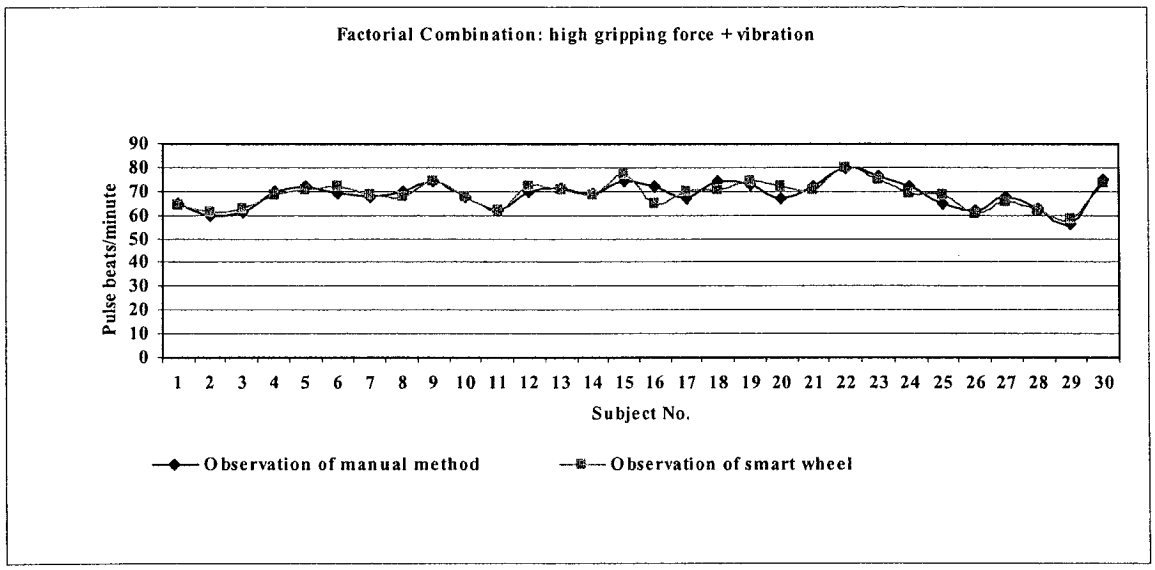

Figure 6.24 Observations under high gripping force and vibration

The method of analysis of variance (ANOVA) is utilized to calculate the important statistics, which are recorded in Table 6.16. The statistics indicate that there is considerable error due to the difference between the subjects because the F_0 is larger than the critical F, $F_{0.05,29,29}$. However, the experimental error from the difference between the two methods is small because its F_0 is less than the critical, $F_{0.05,1,29}$. Hence, the observation based on the smart wheel is statistically equivalent to the observation based on the manual method under the condition of high gripping force and vibration.

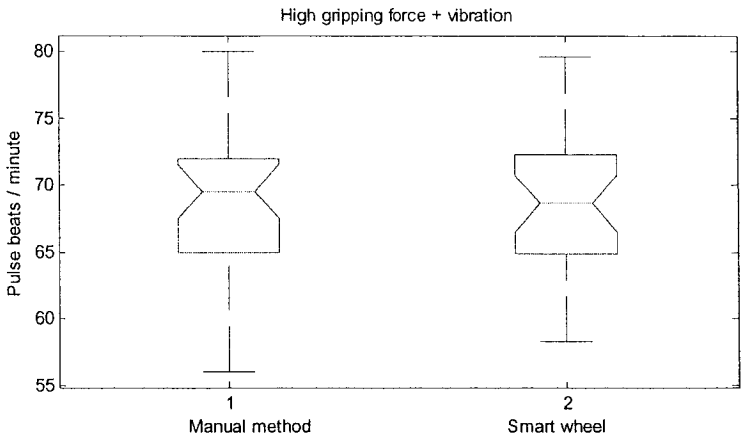

Figure 6.25 The boxplot of observations under high gripping force and vibration

Table 6.16 The analysis of variance of observations under high gripping force and vibration

Source of variation	SS	Degrees of freedom	MS	F_0	Critical F
Subjects	1506.366	29	51.944	16.853	$F_{0.05,29,29} = 1.861$
Factorial levels	0.238	1	0.238	0.077	$F_{0.05,1,29} = 4.183$
Error	89.383	29	3.082		
Total	1595.986	59			

(5) Summary

Finally, under any factorial combination, most of the variation of the experimental data is produced due to the difference of the subjects. Little variation is due to the difference between the two methods of measuring the subject's pulse rate. Hence, the smart wheel is feasible and reliable and shows the same output accuracy as does manual method. In addition, the repeated measures design is necessary because it can calculate and distinguish the variation of the experimental data from the subjects.

6.7.3 Effect of the gripping force and vibration on the accuracy

Under each of the four factorial combinations of gripping force and vibration, a subject's pulse rate is measured by simultaneously using a smart wheel and the manual method. If

the observations of both methods are denoted by R_{Smart_wheel} and R_{manual}, respectively, the difference between the two observations

$$R_{difference} = \left| R_{Smart\_wheel} - R_{manual} \right| .$$

Figures 6.26~6.29 show the $R_{difference}$s of 30 experiments under the four factorial combinations, respectively. Their boxplot is shown in Figure 6.30. Recalling equation (6.20), the effect of the factors on the absolute difference $R_{difference}$ can be analyzed by using ANOVA the important statistics of which are recorded in Table 6.17.

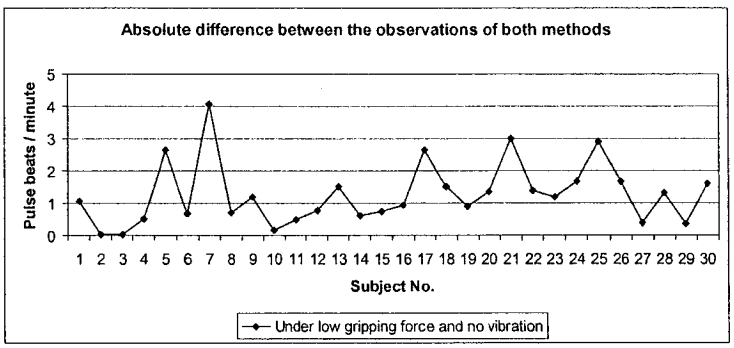

Figure 6.26 The absolute differences between the observations of both methods under low gripping force and no vibration

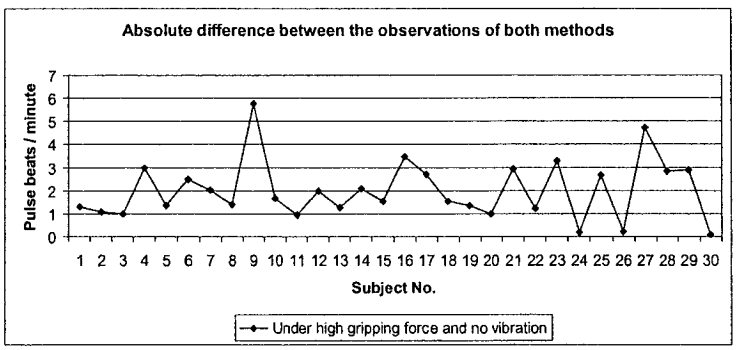

Figure 6.27 The absolute differences between the observations of both methods under high gripping force and no vibration

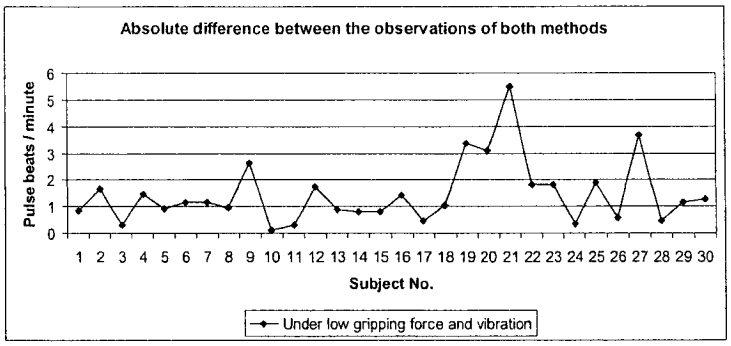

Figure 6.28 The absolute differences between the observations of both methods under low gripping force and vibration

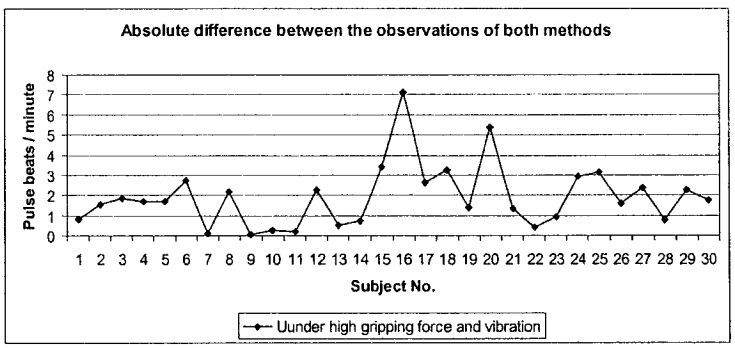

Figure 6.29 The absolute differences between the observations of both methods under high gripping force and vibration

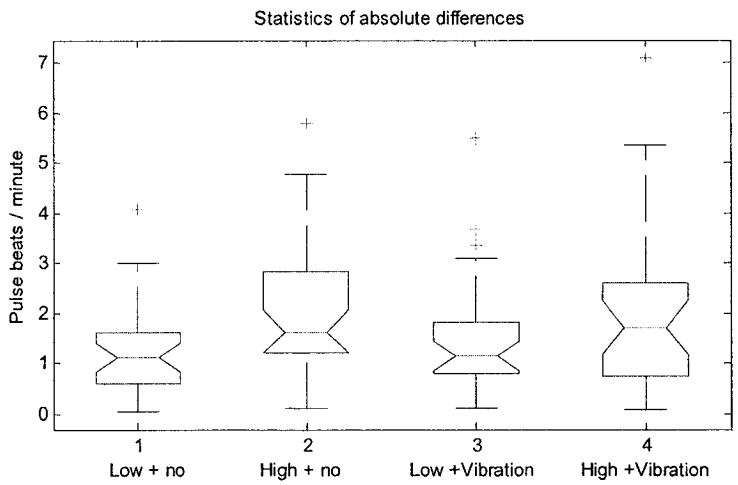

Figure 6.30 The boxplot of the absolute differences under four factorial combinations

Table 6.17 The analysis of variance of the absolute differences between the observations of both methods

Source of variation	SS	Degrees of freedom	MS	F_0	Critical F
Subjects	60.481	29	2.086	1.465	$F_{0.05,29,87} = 1.598$
A (Gripping force)	10.583	1	10.583	7.432	$F_{0.05,1,87} = 3.96$
B (Vibration)	0.078	1	0.078	0.055	$F_{0.05,1,87} = 3.96$
AB	0.572	1	0.572	0.402	$F_{0.05,1,87} = 3.96$
Error	123.826	87	1.424		
Total	195.540	119			

The source of the variation is the subjects, the gripping force, the vibration, the interaction between the gripping force and the vibration, and the other errors. Firstly, the subjects do not make a noticeable contribution to the variation of the $R_{difference}$s because their F_0 is less than the critical F, $F_{0.05,29,87}$. Thus, the variation of the $R_{difference}$s statistically has no relationship with the differences between the subjects. Secondly, the effect of the gripping force on $R_{difference}$ is noticeable because its F_0 is much larger than the critical F, $F_{0.05,1,87}$. This indicates that the levels of the gripping force is one of the main contributing factors to the variation of $R_{difference}$. Appropriate methods are required to eliminate this disturbance. Thirdly, changing the level of vibration produces little effect on the variation of $R_{difference}$ because its F_0 is much less than the critical F, $F_{0.05,1,87}$. This suggests that the filter described in section 6.7.1 is highly useful in eliminating the disturbance of vibration. Thus, a good filter is significant for processing the pulse wave measured by the smart wheel. Fourthly, the interaction between the gripping force and the vibration only slightly influence the variation of $R_{difference}$ because

the F_0 of the interaction is much less than the critical F, $F_{0.05,1,87}$. However, the effect is larger than that of the vibration.

6.7.4 The effect of driving scenarios on the pulse rate

(1) Calculation of standard deviation of pulse rate

In the virtual reality system, the road is established according to the tracks of a single line, a double line, and a sinusoidal line, respectively. Ideally, a subject drives the virtual vehicle strictly along the specified track. However, because of personal condition, habit, driving skill, etc, it is also possible that a subject may drive along the track only approximately. In such a case or cases, the real track along which a subject drives the virtual vehicle differs from the others. Hence, it is useful to record the real track of each subject so that more information can be provided to study the reason for the variance of a subject's pulse rate. Simultaneously, a smart wheel is utilized to monitor the subject's pulse rate against time. The experimental result of one subject is shown in Figure 6.31. More results are shown in Appendix D. The right side of Figure 6.31 is the corresponding curve of the subject's pulse rate. The figure suggests that the subject's pulse rate changes more frequently when the vehicle is driven on a sinusoidal line. There is no noticeable difference between the two curves of a single line and a double line. However, the figure provides only a qualitative deduction. In order to obtain a quantitative result, the experimenter calculates the standard deviations of the three curves that show the subject's pulse rate against time. The calculated results of the ten subjects are plotted in Figure 6.32. Their boxplot is shown in Figure 6.33. According to Figures 6.32 and 6.33, the

subjects have larger standard deviations of pulse rate under the condition of the sinusoidal line than in the cases of the other two driving scenarios.

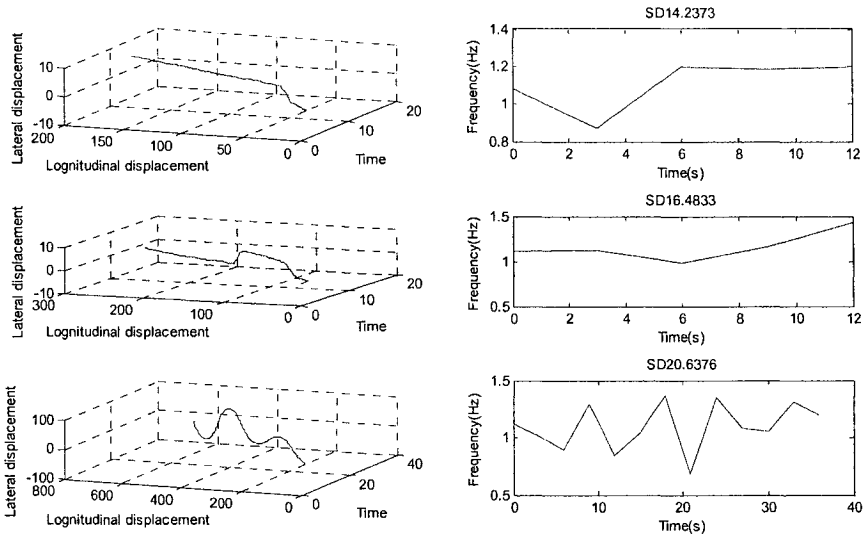

Figure 6.31 Real tracks and curves of pulse rate of the same subject

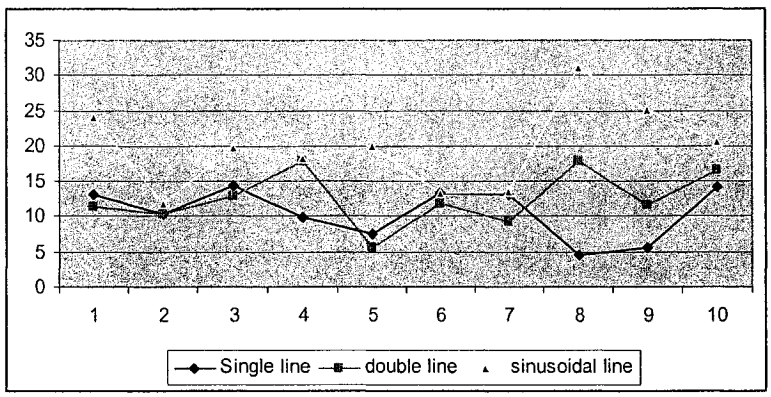

Figure 6.32 Standard deviations of subjects' pulse rates under three driving scenarios

(2) Comparing the data of the three driving scenarios

The effect of the driving scenarios on the standard deviations can be analyzed by using the method of ANOVA. The important statistics are given in Table 6.18. The source of

the variation is the subjects, the driving scenarios and other experimental errors. The effect of the subjects is not noticeable because their F_0 is much less than the critical F, $F_{0.05,9,9}$. In addition, the standard deviation of a subject's pulse rate is noticeably different in the three driving scenarios because the F_0 of the driving scenarios is much larger than the critical F, $F_{0.05,2,18}$. However, the reason for inducing the difference can not be deduced from the ANOVA of Table 6.18. Hence, more analysis of the experimental data is required.

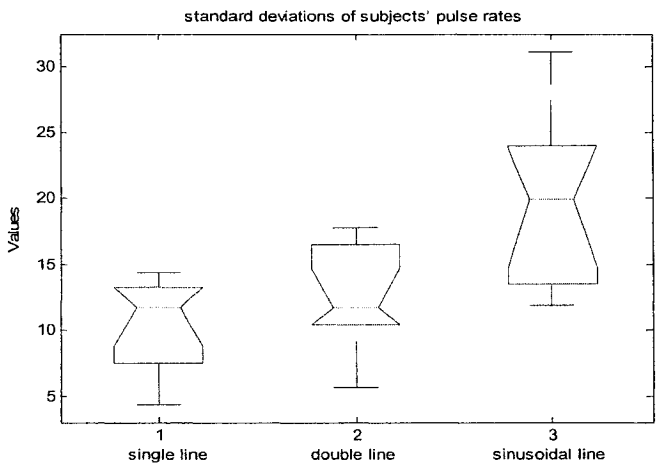

Figure 6.33 The boxplot of the standard deviations of subjects' pulse rates under single line, double line and sinusoidal line

Table 6.18 The analysis of variance of the standard deviations of subjects' pulse rates under three driving scenarios

Source of variation	SS	Degrees of freedom	MS	F_0	Critical F
Subjects	166.220	9	18.469	0.813	$F_{0.05,9,18}=2.460$
driving scenarios	469.134	2	234.567	10.325	$F_{0.05,2,18}=3.55$
Error	408.918	18	22.718		
Total	1044.272	29			

(3) Comparing the data of a single line and a double line

While comparing the standard deviations of the subjects' pulse rate under a single line and a double line, the experimenter obtains Table 6.19, which records the important statistics. The effect of the subjects is not noticeable because their F_0 is much less than the critical F, $F_{0.05,9,9}$. Thus, the effect of the difference between the subjects can be ignored. Moreover, the standard deviation of a subject's pulse rate is not sensitive to a single-line condition and a double-line condition because the F_0 of the experimental scenarios is much less than the critical F, $F_{0.05,1,9}$. Thus, statistically, a driver has the same standard deviation of pulse rate under single line and double line.

Table 6.19 The analysis of variance of the standard deviations of subjects' pulse rates under single line and double line

Source of variation	SS	Degrees of freedom	MS	F_0	Critical F
Subjects	120.0852	9	13.343	0.889	$F_{0.05,9,9} = 3.179$
Experiment scenarios	18.379	1	18.379	1.225	$F_{0.05,1,9} = 5.117$
Error	135.004	9	15.000		
Total	1948.904	19			

(4) Comparing the data of a double line and a sinusoidal line

Comparing the standard deviations of subjects' pulse rate under double line and sinusoidal line, the experimenter calculates the statistics recorded in Table 6.20. The standard deviation of the pulse rate under the sinusoidal line is statistically different from that under the double line because the F_0 of the experiment scenario is much larger than

the critical F, $F_{0.05,1,9}$. However, the effect of the subjects is not remarkable because their F_0 is less than the critical F, $F_{0.05,9,9}$.

Table 6.20 The analysis of variance of the standard deviations of subjects' pulse rates under single line and sinusoidal line

Source of variation	SS	Degrees of freedom	MS	F_0	Critical F
Subjects	105.502	9	11.729	0.316	$F_{0.05,9,9}=3.179$
Experiment scenarios	421.485	1	421.485	11.346	$F_{0.05,1,9}=5.117$
Error	334.323	9	37.147		
Total	861.340	19			

(5) Comparing the data of a single line and a sinusoidal line

When the standard deviations of subjects' pulse rate under single line and sinusoidal line are compared, the statistics are calculated and recorded in Table 6.21. The standard deviation of the pulse rate under a single-line condition is statistically different from that under a sinusoidal-line condition because the F_0 of the experiment scenario is much larger than the critical F, $F_{0.05,1,9}$. The effect of the subjects is small because their F_0 is less than the critical F, $F_{0.05,9,9}$.

Table 6.21 The analysis of variance of the standard deviations of subjects' pulse rates under double line and sinusoidal line

Source of variation	SS	Degrees of freedom	MS	F_0	Critical F
Subjects	311.2527	9	34.584	2.161	$F_{0.05,9,9}=3.179$
Experiment scenarios	263.837	1	263.837	16.484	$F_{0.05,1,9}=5.117$
Error	144.050	9	16.006		
Total	719.140	19			

(6) Summary

In summary, it can be seen that statistically a subject undergoes a larger standard deviation of pulse rate under the sinusoidal line than that under the double line and the single line. There is no difference between the standard deviations of his pulse rate under the single line and the double line. Hence, the extent to which a driver's pulse rate changes depends on the complexity of the driving scenario. A more complicated scenario induces more acute changes in the driver's pulse rate.

Chapter 7 Conclusions and future work

7.1 Contributions and conclusions

The present research aims at (1) developing a smart wheel that can monitor a driver's condition during daily driving and (2) investigating the relationship between the variance of a diver's pulse rate and the driving scenarios. Both of these are important in the field of achieving safe and comfortable driving.

Based on theoretical analysis, reasonable deduction and statistical data, monitoring a driver's condition is seen to be important for improving the safety and experience of driving. The literature reviews indicate that a driver's condition can be evaluated by measuring his physiological parameters. Next, the present research investigates the special requirements of the systems used to monitor a driver's condition and of the useful methods. The present research suggests that a smart wheel is a suitable approach for monitoring a driver's condition.

In the development of the smart wheel, different kinds of sensing methods are compared. To measure a driver's pulse wave and breathing wave, the PVDF film sensor is a suitable choice because (1) it has good sensing characteristics and (2) it is not sensitive to the driver's gripping force. However, the PVDF film sensor requires a special structure that can greatly increase the output of the sensor since the pulse wave and the breathing wave of a driver's palms are weak. To measure a driver's skin temperature, the analog semiconductor temperature sensor is selected because it has a quick response time and

good linearity across the range of a driver's skin temperature. To measure a driver's gripping force, the tactile piezo-resistive sensor is chosen because its structure is compact and it shows good sensitivity across the range of a driver's gripping force. Then, employing the sensors, the electronic system of a smart wheel is designed. It operates on the electrical power of a vehicle, consumes limited power, and has low cost. Moreover, considering the uncertain position of a driver's palm on the smart wheel during driving, the smart wheel requires a special structure and consists of 17 sensor groups. The design guarantees that a driver's palms remain in contact with at least one sensor group when gripping any position on the circular ring of the smart wheel. Then, a special software can determine which sensor group is being gripped and obtain the appropriate outputs. Thus, the smart wheel can reliably measure a driver's physiological parameters and can achieve good adaptability to modern vehicles. It shows a high cost-performance ratio and good engineering aesthetics and ergonomics.

By performing the experiments, the present research has verified the principle and performance of the smart wheel while measuring a driver's pulse rate. In addition, a driver's gripping force and vibration show a noticeable disturbance of the output of the PVDF film sensor. Thus, checking the amplitude of the output signal and appropriate filtering are very helpful in calculating a driver's pulse rate based on the pulse wave measured by using a smart wheel. The experiments of repeated measures design verify that the smart wheel has good accuracy under four conditions: (1) low gripping force and no vibration, (2) high gripping force and no vibration, (3) low gripping force and vibration, and (4) high gripping force and vibration. Moreover, the two-factor factorial

experiments indicate that a driver's gripping force is the main factor influencing the difference between the observations of a smart wheel and the manual method. However, the vibration has little effect on the difference. Thus, appropriate compensation for the gripping force is significant in improving the performance of the smart wheel.

While investigating the relationship between the standard deviation of a driver's pulse rate and the experiment scenarios, the present research utilizes the virtual reality system and the smart wheel. The virtual reality system provides a reasonable and inexpensive approximation to the actual circumstances because it employs the same physical theory of the actual world. The smart wheel can easily monitor a driver's pulse rate and does not disturb a driver's normal condition and behavior. The experiments of repeated measures design verifies that (1) a driver's pulse rate frequently changes under conditions using a single line, a double line and sinusoidal line maneuver, (2) a driver's pulse rate changes more frequently in the sinusoidal line than that in the single line and the double line because the sinusoidal line is more complicated. Hence, the variance of a driver's pulse rate has a close relationship with the driving scenarios.

In conclusion, the smart wheel developed in the present research can accurately and continuously measure a driver's physiological parameters during driving. It is an innovative and appropriate tool for achieving safety, comfort and convenience during driving. In addition, it is also useful in the research on driving and vehicles because it can eliminate the influence of experimental instruments on a driver. Using it allows more accurate results to be obtained.

7.2 Future work

The present research has designed the smart wheel and verified its performance by experimentation. In the future, work should be carried out to test the smart wheel in practical situations and to make necessary improvements. One of the important issues is to optimize the methods of processing signals such as filtering. Such optimization would allow the smart wheel to achieve a higher accuracy and a more stable performance.

REFERENCE

Andreeya, E., Aarabi, P., Philiastides, M.G., Mohajer, K., Emami, M., 2004, Driver drowsiness detection using multi-modal sensor fusion, Proceedings of SPIE - The International Society for Optical Engineering, v 5434, Multisensor, Multisource Information Fusion: Architectures, Algorithms, and Applications 2004, pp380-390.

Anliker, U., Ward, J.A., Lukowicz, P., Troster, G., Dolveck, F., Baer, M., Keita, F., Schenker, E.B., Catarsi, F., Coluccini, L., Belardinelli, A., Shklarski, D., Alon, M., Hirt, E., Schmid, R., Vuskovic, M., 2004, AMON: a wearable multiparameter medical monitoring and alert system, Information Technology in Biomedicine, IEEE Transactions on, Vol.8, Issue 4, pp415 – 427.

Austerlitz,H., 2003, Data acquisition techniques using PCs (second edition), Elsevier Science (USA).

Averty, P., Athenes, S., Collet, C., Dittmar, A., 2002, Evaluating a new index of mental workload in real ATC situation using psychophysiological measures, AIAA/IEEE Digital Avionics Systems Conference - Proceedings, v 2, pp7A41-7A413.

Backs, R.W., Lenneman, J.K., Wetzel, J.M., Green, P., 2003, Cardiac Measures of Driver Workload during Simulated Driving with and without Visual Occlusion, Human Factors, v 45, n 4, pp 525-538.

Ball, S.R., 2002, Embedded microprocessor system: real world design (third edition), Elsevier Science (USA).

Ballandras, S., Daniau, W., Martin, G., Berthelot, P., 2002, Wireless temperature sensor using SAW resonators for immersed and biological applications, Proceedings of the IEEE Ultrasonics Symposium, v 1, pp445-448.

Bettay,V., Cascettay, F., Sepe, D., 1997, An assessment of infrared tympanic thermometers for body temperature measurement, Physiological Measurement 18 (1997), pp215–225.

Blatties,C., 1998, Methods of temperature measurement, in physiology and pathophysiology of temperature regulation, World Scientific Publishing Co, pp273-279.

Brandt, T., Stemmer, R., Rakotonirainy, A., 2004, Affordable visual driver monitoring system for fatigue and monotony, Conference Proceedings - IEEE International Conference on Systems, Man and Cybernetics, v 7, 2004 IEEE International Conference on Systems, Man and Cybernetics, SMC 2004, pp6451-6456.

Brookhuis, K.A., Dick, D.W., 1993, Use of psychophysiology to assess driver status, Ergonomics, v 36, n 9, pp1099-1110.

Cacioppo, J.T., Tassinary, L.G., 1990, Inferring psychological significance from physiological signals, American Psychologist, 45(1), pp16-28.

Cheang, P.Y.S., Smith, P.R., 2003, An Overview of Non-contact Photoplethysmography, Proceeding of 1st Electronic Systems and Control Division Research Mini-conference, pp57-59.

Chi, Z.Y., Shida, K., 2003, A sensor structure for force vector measuring based on multifunctional sensing technique, Japanese Journal of Applied Physics, Part 2: Letters, v 42, n 7 B, ppL860-L862.

Cotton, D., Cranny, A., White, N., Beeby, S., Chappell, P., 2004, Design and development of intergrated thick-film sensors for prosthetic hands, Proceedings of the 7th Biennial Conference on Engineering Systems Design and Analysis - 2004, v 3, Proceedings of the 7th Biennial Conference on Engineering Systems Design and Analysis - 2004, pp573-589.

Cugini, P., Mammarella, A., Cardarello, C. M., Paoletti, V., Paradiso, M., Rosa, R.D., Pellegrino, A.M., Fontana, S., Dutto, L., Coda, S., Francesco, G.P., Bernardini, F., Curione, M., 2000, Circadian Rhythm of Heart Rate in Myotonic Dystrophy, Journal of Clinical and Basic Cardiology, 3(issue 3), pp181-186.

Da Silva, J.G., De Carvalho, A.A., Da Silva, D.D., 2002, A strain gauge tactile sensor for

finger-mounted applications, IEEE Transactions on Instrumentation and Measurement, v 51, n 1, pp18-22.

Dikkers, H.J., Spaans, M.A., Datcu, D., Novak, M., Rothkrantz, L.J., 2004, Facial recognition system for driver vigilance monitoring, Conference Proceedings - IEEE International Conference on Systems, Man and Cybernetics, v 4, pp 3787-3792.

Ding, X.H., Kuribayashi, K., Hashida, T., 2000, Development of a new type tactile sensor using micro electromagnetic coil for human robot, Proceedings of the International Symposium on Micro Machine and Human Science, pp181-187.

Dupuis,P., Eugène, C., 2000, Combined Detection of Respiratory and Cardiac Rhythm Disorders by High-Resolution Differential Cuff Pressure Measurement, IEEE Transactions On Instrumentation And Measurement,Vol.49, No.3, pp498-502.

Edgren,C.S., Radwin, R.G., Irwin, C.B., 2004, Grip Force Vectors for Varying Handle Diameters and Hand Sizes, Human Factors: The Journal of the Human Factors and Ergonomics Society, Vol.46, Iss.2, Summer 2004, pp244-251.

Eriksson, M., Papanikolopoulos, N.P., 2001, Driver fatigue: A vision-based approach to automatic diagnosis, Transportation Research Part C: Emerging Technologies, v 9, n 6, pp399-413.

Escudero, Z., Mai, M., SantaFe, A., 2003, Temperature Sensor for Medical Applications Based on Erbium Doped Optical Fiber, Annual International Conference of the IEEE Engineering in Medicine and Biology - Proceedings, v 4, pp3444-3445.

Fagergren, A., Ekeberg, O., Forssberg, H., 2000, Precision grip force dynamics: a system identification approach, IEEE Transactions on Biomedical Engineering, v 47, n 10, pp 1366-1375.

Fernando, K.L., Mathews, V.J., Varner, M.W., Clark, E.B., 2003, Robust estimation of fetal heart rate variability using Doppler ultrasound, IEEE Transactions on Biomedical Engineering, v 50, n 8, pp950-957.

Fraden, J., 1997, Handbook of modern sensors, American Institute of Physics.

Gajda, J., 2001, A new identification algorithm of the human respiratory system, Conference Record - IEEE Instrumentation and Measurement Technology Conference, v 2, 2001, pp784-789.

Gray, R.M., Goodman, J.W., 1995, Fourier transforms: an introduction for engineers, Kluwer Academic Publishers.

Hampson, K.M., Munro, I., Paterson, C., Dainty, C., 2005, Weak correlation between the aberration dynamics of the human eye and the cardiopulmonary system, Journal of the

Optical Society of America A: Optics and Image Science, and Vision, v 22, n 7, pp1241-1250.

Hasday, J.D., 1997, The influence of temperature on host defences, in Fever. Basic Mechanisms and Management, P.A. Mackowiak, Editor. 1997, Lippincott Raven: Philadelphia New York, pp 177-196.

Healey, J.A., Picard, R.W., 2005, Detecting Stress during Real-World Driving Tasks Using Physiological Sensors, IEEE Transactions on Intelligent Transportation Systems, v 6, n 2, pp156-166.

Helenic Institute of Transport, 2004, http://www.awake-eu.org/.

Hlimonenko, I., Meigas, K., Vahisalu, R., 2003, Waveform Analysis of Peripheral Pulse Wave Detected in the Fingertip with Photoplethysmograph, Measurement Science Review, Volume 3, Section 2, pp49-52.

Horng, W.B., Chen, C.Y., Chang, Y., Fan, C.H., 2004, Driver fatigue detection based on eye tracking and dynamic template matching, Conference Proceeding - IEEE International Conference on Networking, Sensing and Control, v 1, Conference Proceedings - 2004 IEEE International Conference on Networking, Sensing and Control, pp7-12.

Insurance Corporation of British Columbia, 2005, Traffic Collision Statistics(Police-attended injury and fatal collisions, British Columbia 2003).

Ishikawa, T., Watanabe, K., Nakamura, T., Okada, T., 2004, Unconstrained and noninvasive measurement of heartbeat by a pneumatic method for drivers, Proceedings of the SICE Annual Conference, SICE Annual Conference 2004, pp1727-1730.

Jacobs, J.L., Embree, P., Glei, M., Christensen, S., Sullivan, P.K., 2004, Characterization of a novel heart and respiratory rate sensor, Annual International Conference of the IEEE Engineering in Medicine and Biology - Proceedings, v 26 III, Conference Proceedings - 26th Annual International Conference of the IEEE Engineering in Medicine and Biology Society, EMBC 2004, pp2223-2226.

Jahn, G., Oehme, A., Krems, J.F., Gelau, C., 2005, Peripheral detection as a workload measure in driving: Effects of traffic complexity and route guidance system use in a driving study, Transportation Research Part F 8 (2005), pp255–275.

Jedrzejewska-Szczerska, M., Hypszer, R., 2004, White-light interferometric temperature sensor for biomedical diagnostic, Proceedings of SPIE - The International Society for Optical Engineering, v 5505, Progress in Biomedical Optics and Imaging - Optical Methods, Sensors, Imaging Processing, and Visualization in Medicine, pp72-77.

Jiao, K., Li, Z.Y., Chen, M., Wang, C.T., 2005, Power spectral analysis of heart rate variability of driver fatigue, Journal of Dong Hua University (English Edition), v 22, n 1, pp11-15.

Ji, Q., Zhu, Z.W., Lan, P.L., 2004, Real-time nonintrusive monitoring and prediction of driver fatigue, IEEE Transactions on Vehicular Technology, v 53, n 4, pp1052-1068.

Jovanov, E., Raskovic, D., Hormigo, R., 2001. Thermistor-based breathing sensor for circadian rhythm evaluation, Biomedical Sciences Instrumentation, v 37, pp 493-497.

Katayama, T., Sakai, K., 1994, Fluctuation of capillary pulse as an index for driver's internal states, Proceedings of Vehicle Navigation and Information Systems Conference, pp11-14.

Katsis, C.D., Ntouvas, N.E., Bafas, C.G., Fotiadis, D.I., 2004, Assessment of muscle fatigue during driving using surface EMG, Proceedings of the IASTED International Conference on Biomedical Engineering, pp259-262.

Kim, C.J., Min, B.C., Chung, S.C., Min, B.W., Park, S.J., 2000, Study of autonomic responses due to the vehicle speed change, Proceedings of the XIVth Triennial Congress of the International Ergonomics Association and 44th Annual Meeting of the Human Factors and Ergonomics Association, 'Ergonomics for the New Millennnium', pp 200-203.

Knight, J.F., Schwirtz, A., Psomadelis, F., Baber, C., Bristow, H.H., Arvanitis, T.N., 2005, The design of the SensVest, Personal and Ubiquitous Computing, v 9, n 1, pp6-19.

Kroemer, K., 2001, Ergonomics: How to design for ease & efficiency (2nd edition), Prentice Hall, NJ.

Korpasa, D., Háleka, J., Chlupováb, L., 2003, Surface Artery Volume Pulse Wave Measurement –Verification of A New Method, Biomedical Papers, Vol147(2), pp181–184.

Kuriyagawa, Y., IM, H.E., Kageyama, I., Onishi, S., 2002, A research on analytical method of driver-vehicle-environment system for construction of intelligent driver support system, Vehicle system dynamics, Vol.37, No.5, pp339-358.

Lal S.K.L., Craig, K., 2001, A critical review of the psychophysiology of driver fatigue, Biological Psychology 55 (2001), pp173–194.

Lal, S.K.L., Craig, A., Boord, P., Kirkup, L., Nguyen, H., 2003, Development of an algorithm for an EEG-based driver fatigue countermeasure, Journal of Safety Research, v 34, n 3, pp321-328.

Lau, O.Y.E., Chwang, A.T.Y., 2000, Relationship between wrist-pulse characteristics and body conditions, Proceedings of the Fourteenth Engineering Mechanics Conference., CD-ROM 6, pp1-7.

Leng, H. and Lin, Y., 2005, Design and analysis of a tissue softness sensor, Integrated Design and Process Technology Symposium 2005.

Leng, H. and Lin, Y., 2005, Smart wheel: a novel device in driver condition monitoring, Conference Proceedings- IEEE International Conference on Industrial Technology (IEEE ICIT 2005), accepted.

Levander, M.S., 2004, Measurement and Evaluation of Body Temperature: Implications for Clinical Practice, Doctoral thesis, Linköping University.

Li, J.S., Bao, Z.W., 2003, Research on the Application of the Neural Network in Optical Fiber Temperature Sensor Probe Design Used in Medical Treatment, Proceedings of SPIE - The International Society for Optical Engineering, v 5254, pp202-207.

Liess, M., Hausner, M., Schilz, J., Lauck, G., Karagoezoglu, H., Ernst, H., 2004, Temperature radiation sensors for automotive climate control, Sensors, 2004, Proceedings of IEEE, vol.1, pp5-7.

Lin, Y., 2003, A Novel Interface Design Framework for Complex Work Domain: Function-Behavior-State Paradigm, Doctoral dissertation, Department of Mechanical Engineering, University of Saskatchewan.

Liu, S.H., Lin, C.T., Chao, W.H., 2004, The Short-Time Fractal Scaling of Heart Rate Variability to Estimate the Mental Stress of Driver, Proceedings of the 2004 IEEE International Conference on Networking, Sensing & Control, pp829-833.

Liu, Y.L., 2003, Engineering aesthetics and aesthetic ergonomics: Theoretical foundations and a dual-process research methodology, Ergonomics, v 46, n 13-14, pp 1273-1292.

Lorandi, L., Diong, B., Nava, P., Solis, F., Menendez, R., Ortiz, G., Nazeran, H., 2003, Parametric Sensitivity Analysis of Human Respiratory Impedance, Annual International Conference of the IEEE Engineering in Medicine and Biology - Proceedings, v 1, p 778-781.

Lu, H., Bai, J., Zhang, L., Wang, S., 2003, A Multi-Element Nonlinear Model of Human Circulatory-Respiratory System and its Application in high-G Study, Annual International Conference of the IEEE Engineering in Medicine and Biology - Proceedings, v 1, 2003, pp 387-390.

Macchi, M., Boulos, Z., Ranney, T., Simmons, L., Campbell, S.S., 2002, Effects of an afternoon nap on nighttime alertness and performance in long-haul drivers, Accident Analysis and Prevention, v 34, n 6, pp 825-834.

Mack, D.C., Kell, S.W., Alwan, M., Turner, B., Felder, R.A., 2003, non-invasive analysis of physiological signals (naps): a vibration sensor that passively detects heart and respiration rates as part of a sensor suite for medical monitoring, 2003 Summer Bioengineering Conference, pp11-12.

Mascaro, S.A., Asada, H.H., 2001, Photoplethysmograph fingernail sensors for measuring finger forces without haptic obstruction, IEEE Transactions on Robotics and Automation, v 17, n 5, pp 698-708.

Meigas, K., Kattai, R., Nigul, M., Lass, J., 2002, Comparison of Signals of Pulse Profile as Skin Surface Vibrations, PPG and Doppler Spectrogram for Continuous Blood Pressure Monitoring, Proceedings of the International Federation for Medical & Biological Engineering, Vol.3, pp. 510-511.

Mina, B.C., Chungb, S.C., Parka, S.J., Kima, C.J., Sima, M.K., Sakamotoc, K., 2002, Autonomic responses of young passengers contingent to the speed and driving mode of a vehicle, International Journal of Industrial Ergonomics, 29, pp187–198.

Montgomery, D.C., 2001, Design and analysis of experiments, New York : Wiley.

Moreno, F., Aparicio, F., Hernandez, W., Paez, J., 2003, A Low-cost Real-Time FPGA solution for driver drowsiness detection, IECON Proceedings (Industrial Electronics Conference), v 2, pp1396-1401.

MSI (Measurement Specialties Inc.), 1998, Piezo Film Sensors Technical Manual (Internet Version).

Nasoz, F., Ozyer, O., Lisetti, C.L., Finkelstein, N., 2002, Multimodal affective driver interfaces for future cars, Proceedings of the ACM International Multimedia Conference and Exhibition, 2002, pp319-322.

Nikonovas, A., Harrison, A.J.L., Hoult, S., Sammut, D., 2004, The application of force-sensing resistor sensors for measuring forces developed by the human hand, Proceedings of the Institution of Mechanical Engineers, Part H: Journal of Engineering in Medicine, v 218, n 2, pp 121-126.

Noel, J.B., Bauer J., Kenneth W., Lanning, J.W., 2005, Improving pilot mental workload classification through feature exploitation and combination: A feasibility study, Computers and Operations Research, v 32, n 10, Application of Neural Networks, p 2713-2730.

Norin, F., Wyon, D.P., 1992, Driver vigilance-the effects of compartment temperature, SAE Special Publications, n 916, Design and Performance of Climate Control Systems, pp7-11.

Ong, K.G., Dreschel,W.R., Grimes, C.A., 2002, Detection of human respiration using square-wave modulated electromagnetic impulses, Microwave and Optical Technology Letters, v 36, n 5, pp 339-343.

Ossberger, G., Buchegger, T., Schimback, E., Stelzer, A., Weigel, R., 2004, Non-invasive respiratory movement detection and monitoring of hidden humans using ultra wideband pulse radar, 2004 International Workshop on Ultra Wideband Systems; Joint with Conference on Ultra Wideband Systems and Technologies, Joint UWBST and IWUWBS 2004, pp 395-399.

Picard, R.W., 1997, Affective computing, Cambridge, Mass.: MIT Press.

Picard, R., Healey, J., 1997, Affective wearables, Proc. of the 1st Int'l Symposium on Wearable Computers.

Polychronopoulos, A., Amditis, A., Bekiaris, E., 2004, Information data flow in AWAKE multi-sensor driver monitoring system, IEEE Intelligent Vehicles Symposium, Proceedings, 2004 IEEE Intelligent Vehicles Symposium, pp902-906.

Pottinger, M.G., Marshall, K.D., Lawther, J.M., Thrasher, D.B., 1986. A review of tire/pavement interaction induced noise and vibration. In: Pottinger, M.G., Yager, T.J. (Eds.), ASTM STP929 The Tire Pavement Interface. ASTM, Philadelphia, pp. 183–287.

Putten, M.J.A.M., Putten, M.H.P.M., Putten, A.F.P., Pompe, J.C., Bruining, H.A., 1997, A Silicon Bidirectional Flow Sensor for Measuring Respiratory Flow, IEEE Transactions On Biomedical Engineering, Vol. 44, No. 2, pp205-208.

Rada, H., Dittmar, A., Delhomme,G., Collet, C., Roure, R., Vernet-Maury, E., Priez, A., 1995, Bioelectric and microcirculation cutaneous sensors for the study of vigilance and emotional response during tasks and tests, Biosensors & Bioelectronics 10 (1995), pp7-15.

Rothkrantz, L.J.M., Van Vark, R.J., Datcu, D., 2004, Multi-medial stress assessment, Conference Proceedings - IEEE International Conference on Systems, Man and Cybernetics, v 4, 2004 IEEE International Conference on Systems, Man and Cybernetics, SMC 2004, pp3781-3786.

Sato, I., Nakajima, M., 2004, Non-contact respiration monitoring system using fiber grating sensor, Proceedings of SPIE - The International Society for Optical Engineering, v 5603, Machine Vision and its Optomechatronic Applications, pp262-271.

Schagger, H., De Coo, R., Bauer, M.F., Hofmann, S., Godino, C., Brandt, U., 2004,

Significance of respirasomes for the assembly/stability of human respiratory chain complex I, Journal of Biological Chemistry, v 279, n 35, pp 36349-36353.

Seto, Y., Minegishi, K., Yang, Z., Kobayashi, T., 2004, Research on detection of braking reactions in emergency situations, Vehicle System Dynamics, v 41, n SUPPL., 2004, pp 784-790.

Sherebin, M.H., Sherebin, R.Z., 1990, Frequency Analysis of the Peripheral Pulse Wave Detected in the Finger with a Photoplethysmograph, IEEE Transactions on Biomedical Engineering, vol.37 No. 3, pp313 - 317.

Shikida, M., Shimizu, T., Sato, K., Itoigawa, K., 2003, Active tactile sensor for detecting contact force and hardness of an object, Sensors and Actuators, A: Physical, v 103, n 1-2, pp213-218.

Smith, P., Shah, M., Lobo, N.V., 2003, Determining Driver Visual Attention With One Camera, IEEE Transactions On Intelligent Transportation Systems, Vol. 4, No. 4, pp205-218.

Stec, B., Dobrowolski, A., Susek, W., 2004, Multifrequency Microwave Thermograph for Biomedical Applications, IEEE Transactions on Biomedical Engineering, v 51, n 3, pp 548-551.

Takanobu, H., Saito, S., Tsuboi, H., Miura, H., Naemura, K., 2004, Development of wearable heart rate counter, Proceeding of the 2004 the Eleventh World Congress in Mechanism and Machine Science, pp1321-1325.

Takao, H., Sawada, K., Ishida, M., 2004, Silicon smart tactile image sensor with pneumatically swollen single diaphragm structure, Proceedings of the IEEE International Conference on Micro Electro Mechanical Systems (MEMS), 17th IEEE International Conference on Micro Electro Mechanical Systems (MEMS): Maastricht MEMS 2004 Technical Digest, pp 846-849.

Tanaka, J., Ishida, S., Kawagoe, H., Kondo, S., 2000, Workload of using a driver assistance system, IEEE Conference on Intelligent Transportation Systems, Proceedings, ITSC, pp382-386.

Tejero, P., Choliz, M., 2002, Driving on the motorway: The effect of alternating speed on driver's activation level and mental effort, Ergonomics, v 45, n 9, pp 605-618.

TEKSCAN cooperation, 2004, Flexiforce® Sensors User Manual.

Thompson Lightstone & Co, 2003, 2003 Aggressive Driving Study.

Ugata, M., Kuroda, T., Imamizu, H., Yoshioka, T., Wada, Y., Kawato, M., 2004, The possibility of using forward models for multi-limb coordination: Examination of models

for grip-load force coupling in humans, Electronics and Communications in Japan, Part III: Fundamental Electronic Science, v 87, n 11,, pp 44-56.

Ugural, A.C., 1981, Stresses in plates and shells, McGraw-Hill Book Company.

Vandoren, A.H., 1982, Data acquisition systems, Reston publishing company,INC.

Vanoverschelde, C., Dubois, L., Thomy, V., Sozanski, J.P., Camart, J.C., Chive, M., Pribetich, J., 2001, Miniature sensor for measurement and control of temperatures by microwave radiometry in medical applications, IEEE MTT-S International Microwave Symposium Digest, v 3, pp155-158.

Wells, R., Greig, M., 2001, Characterizing human hand prehensile strength by force and moment wrench, Ergonomics, v 44, n 15, pp 1392-1402.

Yin, Y.M., Qian, J., Lu, J.F., Huang, Y., 2003, On the operation mechanism of the microwave sensor for measuring human heartbeats and respirations, Proceedings of IEEE Sensors, v 2, n 1, pp565-568.

Zuckerwar, A.J., Pretlow, R.A., Stoughton, J.W., Baker, D.A., 1993, Development of a piezopolymer pressure sensor for a portable fetal heart rate monitor, IEEE transactions on biomedical engineering, Vol 40, No.9, pp963-969.

APPENDIX A

At the beginning of each experimental design, a pair of statistical hypothesis is stated. For example, it is denoted that μ_1 and μ_2 are the means of the observations of subjects' pulse rate measured by using a smart wheel and by using manual method, respectively. There is a pair of hypothesis

$$H_0 : \mu_1 = \mu_2$$

$$H_1 : \mu_1 \neq \mu_2$$

Then, H_0 and H_1 are named the null hypothesis and the alternative hypothesis, respectively. For verifying the hypothesis, a test statistic of the observations is calculated. If the test statistic falls into the specified critical region of the test, the hypothesis H_0 is true. Otherwise, H_1 is true. The statistical test possibly produces two types of errors: type I error, which occurs when H_0 is rejected while H_0 is true, and type II error, which occurs when H_0 is not rejected while H_0 is false. Their probabilities

$$\alpha = P(type\ I\ error) = P(reject\ H_0 \mid H_0\ is\ true)$$

$$\beta = P(type\ II\ error) = P(do\ not\ reject\ H_0 \mid H_0\ is\ false)$$

And the power of the test

$$Power = 1 - \beta = P(reject\ H_0 \mid H_0\ is\ false).$$

α is named the significance level of the test.

APPENDIX B

Subjects' pulse rates measured by using manual method and smart wheel:

Subject No.	Factorial combination											
	Note: GF → gripping force; V → vibration.											
	Low GF + no V			High GF + no V			Low GF + V			High GF + V		
	(1)	(2)	(3)	(1)	(2)	(3)	(1)	(2)	(3)	(1)	(2)	(3)
1	65	66.055	1.055	64	65.324	1.324	64	64.865	0.865	65	64.198	0.802
2	62	62.037	0.037	62	60.909	1.091	63	61.321	1.679	60	61.539	1.539
3	62	61.959	0.041	61	60	1	62	61.692	0.308	61	62.882	1.882
4	70	69.478	0.522	67	64	3	69	67.546	1.454	70	68.293	1.707
5	71	68.342	2.658	73	71.655	1.345	72	71.066	0.934	72	70.284	1.716
6	67	66.332	0.668	69	66.506	2.494	68	66.833	1.167	69	71.717	2.717
7	66	70.073	4.073	67	64.975	2.025	68	66.828	1.172	68	68.108	0.108
8	70	70.707	0.707	69	70.408	1.408	71	70.051	0.949	70	67.826	2.174
9	75	76.191	1.191	75	69.211	5.789	74	71.362	2.638	74	74.074	0.074
10	65	64.838	0.162	68	66.337	1.663	65	64.891	0.109	68	67.717	0.283
11	62	61.53	0.47	61	61.929	0.929	62	61.692	0.308	62	61.78	0.22
12	67	67.787	0.787	69	67	2	69	70.755	1.755	70	72.277	2.277
13	71	69.482	1.518	70	68.718	1.282	70	70.874	0.874	71	70.476	0.524
14	65	64.398	0.602	66	68.063	2.063	68	67.168	0.832	69	68.293	0.707
15	75	74.257	0.743	75	76.531	1.531	75	75.811	0.811	74	77.387	3.387
16	71	70.076	0.924	70	66.506	3.494	71	72.449	1.449	72	64.894	7.106
17	69	66.366	2.634	68	65.306	2.694	67	67.447	0.447	67	69.61	2.61
18	72	70.474	1.526	74	72.444	1.556	73	71.949	1.051	74	70.769	3.231
19	73	72.081	0.919	74	75.372	1.372	74	70.647	3.353	73	74.419	1.419
20	68	69.347	1.347	67	67.977	0.977	69	72.086	3.086	67	72.351	5.351
21	70	67.005	2.995	71	68.078	2.922	71	65.509	5.491	72	70.649	1.351
22	84	82.62	1.38	81	82.2	1.2	83	81.174	1.826	80	79.581	0.419
23	75	73.816	1.184	75	71.725	3.275	76	74.186	1.814	76	75.064	0.936
24	69	67.337	1.663	72	72.164	0.164	71	70.647	0.353	72	69.036	2.964
25	66	63.104	2.896	64	66.66	2.66	64	65.882	1.882	65	68.17	3.17
26	59	57.308	1.692	63	62.785	0.215	61	60.417	0.583	62	60.396	1.604
27	67	66.6	0.4	69	64.236	4.764	67	63.317	3.683	68	65.625	2.375
28	60	61.307	1.307	60	62.834	2.834	62	62.469	0.469	63	62.245	0.755
29	55	54.639	0.361	55	57.868	2.868	56	57.143	1.143	56	58.292	2.292
30	74	75.626	1.626	74	74.11	0.11	74	72.727	1.273	75	73.267	1.733
	Note: (1) → Observation of manual method. (2) → Observation of smart wheel. (3) → |(1)-(2)|.											

APPENDIX C

Boxplot is a usual type of graph in statistical analysis. It produces a box and whisker plot for each group of observations. For example, there are ten observations, {38 42 55 48 39 41 43 44 32 37}, of which the boxplot is shown as follow:

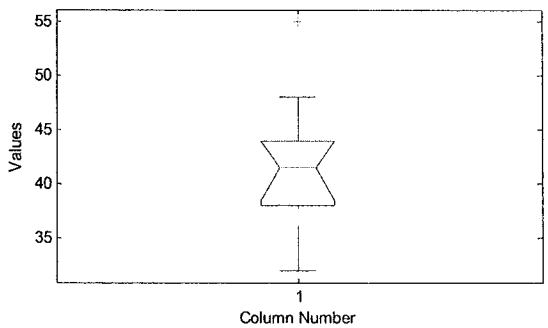

The important components of the boxplot include:

- The line located at the middle of the box indicates the median which is the center observation of the rearranged list of observations in ascending order. The median of the previous example is calculated as follows:
  (1) Arrange the data in ascending order {32 37 38 39 41 42 43 44 48 55}.
  (2) The median of the ten observations is the average of the 5th and 6th observations (41+42)/2=41.5.
- The notches of the box are a graphic confidence interval about the median.
- The lower and upper lines of the "box" are the 25th and 75th percentiles of the group of observations. Their values of the previous example are calculated as follows:
  (1) Arrange the data in ascending order {32 37 38 39 41 42 43 44 48 55}.

(2) The value of lower line is the median of the first half of the rearranged observations {32 37 38 39 41}, 38.

(3) The value of upper line is the median of the second half of the rearranged observations {42 43 44 48 55}, 44.

- The plus sign at the top of the plot is an outlier in the group of observations. It may be produced due to a data entry error, a poor measurement or a change in the measuring system.
- The "whiskers" (i.e., dash lines) extending above and below the box show the extent of the group of observations (excludes the outliers). The terminals of the upper whisker and lower whistle indicate the maximum and minimum of the group of observations, respectively.

APPENDIX D

Subjects' standard deviations of pulse rate in three driving scenarios

Subject No.	Driving scenarios		
	Single line	Double line	Sinusoidal line
1	13.0238	11.3871	24.0069
2	10.3722	10.3923	11.8924
3	14.3382	12.8062	19.7569
4	9.8641	17.7951	18.1590
5	7.5056	5.6862	20.0642
6	13.2759	11.8603	13.4071
7	13.2035	9.2871	13.5288
8	4.4347	17.7558	31.0859
9	5.6362	11.6103	25.1661
10	14.2373	16.4833	20.6376